# Progress In Interfacial Solar Steam Generation Using Low-Dimensional and Biomass-Derived Materials

Md. Nahian Al Subri Ivan[1a,b,#], Shuvra Saha [1a,#], Ahmed Mortuza Saleque[2], Safayet Ahmed[1a,b], Amrit Kumar Thakur[3a,b], Gongxun Bai[4], Zhang Miao[5], R. Saidur[6a,b], Yuen Hong Tsang[1a,b,*]

1a.) Department of Applied Physics and Materials Research Center, The Hong Kong Polytechnic University, Hung Hom, Kowloon, Hong Kong

1b.) Shenzhen Research Institute, The Hong Kong Polytechnic University, 518057 Shenzhen, Guangdong, People's Republic of China

2.) Department of Electrical and Computer Engineering, University of California, Davis, CA 95616, USA

3a.) Department of Mechanical Engineering, University of California, Merced, CA, 95343, USA

3b.) Department of Mechanical Engineering, KPR Institute of Engineering and Technology, Arasur, Coimbatore 641407, Tamil Nadu, India

4.) Key Laboratory of Rare Earth Optoelectronic Materials and Devices of Zhejiang Province, College of Optical and Electronic Technology, China Jiliang University, Hangzhou 310018, China

5) Department of Applied Biology and Chemical Technology and Research Institute for Smart Energy, The Hong Kong Polytechnic University, Hung Hom, Kowloon, Hong Kong

6a.) Research Center for Nano-Materials and Energy Technology (RCNMET), School of Engineering and Technology, Sunway University, Bandar Sunway, Petaling Jaya 47500, Selangor Darul Ehan, Malaysia

6b.) School of Engineering, Lancaster University, Lancaster LA1 4YW, UK

[#]) M.N.A.S.I. and S.S. equally contributed to this work

*.) Corresponding author: yuen.tsang@polyu.edu.hk

## Abstract

The pressing concern of escalating water scarcity has spurred the creation of advanced technologies, such as interfacial solar steam generation (ISSG), to tackle the challenge. ISSG employs solar energy for efficient water desalination and purification. This comprehensive review delves into various aspects of ISSG, primarily focusing on elucidating its mechanisms, optimizing substrate materials, implementing thermal management strategies, and exploring applications. The study dissects the intricate mechanism of ISSG, highlighting photothermal behaviors across different materials, including the significant role of nanoparticles in vapor generation. The impact of substrate composition and shape on solar evaporation efficiency is investigated, with multi-surface evaporators considered for environmental energy harnessing. To enhance performance, thermal management strategies, including innovative water transport paths for improved heat distribution, are assessed. Addressing key challenges like salt accumulation, biofouling, corrosion, and oil fouling, the review offers insights for issue mitigation. Practically, ISSG is spotlighted for its role in seawater desalination, wastewater treatment (e.g., dye and heavy metal removal), oil-water separation, and sterilization, extending its relevance across industries and healthcare. By comprehensively examining ISSG's mechanisms, substrate considerations, thermal strategies, and applications, this review advances its implementation as a transformative solution for global water challenges.

**Keywords:** Solar Energy; Interfacial Solar Steam Generation (ISSG); Desalination; Water Treatment; Low-dimension materials; Biomass

# Table of Contents


*1. Introduction ..... 4*

*2. Mechanism of ISSG ..... 7*

2.1. Photothermal Materials ..... 9

2.1.1. Plasmonic materials ..... 15

2.1.2. Semiconductor-based materials ..... 17

2.1.3. Carbon-based materials ..... 19

2.2. Structure of solar evaporators ..... 23

2.2.1. Single surface solar evaporator ..... 24

2.2.1.1. Thin single-surface solar evaporator ..... 24

2.2.1.2. Thick single-surface solar evaporators ..... 30

2.2.2. Multiple surface solar evaporator ..... 39

*3. Water transportation and thermal management techniques ..... 51*

*4. Salt rejection mechanism ..... 59*

4.1. Salt-ion diffusion ..... 60

4.2. Direct Salt-blocking by Janus structure ..... 61

4.3. Edge preferential salt crystallization ..... 63

4.4. Marangoni-driven salt removal ..... 64

*5. Corrosion resistance ..... 68*

5.1. Resistance against Acid/Alkali-based substance ..... 68

5.2. Resistance against Microbials ..... 70

*6. Anti-oil fouling ..... 75*

*7. Application ..... 76*

7.1. Seawater desalination ..... 78

7.2. Wastewater purification ..... 79

7.3. Oil-water separation ..... 80

7.4. Sterilization ..... 81

*8. Conclusion ..... 85*

*References ..... 88*

## 1. Introduction

Water remains a cornerstone of human civilization, its demand surging alongside population growth, agricultural expansion, and industrial development. Estimates project a staggering 55% increase in global water demand by 2050, exacerbating scarcity issues faced by nearly 4 billion people annually [1,2]. Access to safe drinking water remains a challenge for 2.2 billion individuals [3–5]. Seemingly, the solution lies in desalination, given that 97% of the Earth's water is saline[6]. Conventional desalination processes, be they thermal (such as Multi-effect Distillation (MED) and Multistage Flash (MSF)) or membrane-based (like Reverse Osmosis (RO)), require significant capital investment and accrue high operational energy costs [7,8]. Thermal systems face corrosion challenges and cost inefficiencies, while membrane-based technologies offer lower energy consumption but demand substantial capital investments. Despite advancements, desalination remains energy-intensive, with requirements ranging from 1.8 kWh/$m^3$ to 5.9 kWh/$m^3$ [9,10]. Such reliance on fossil fuels poses environmental risks. Harnessing solar energy for desalination emerges as an attractive alternative, given the Earth's immense solar resources annually [11].

Water evaporation through solar energy absorption, a natural hydrologic cycle phenomenon, suffers from poor efficiency due to water's limited light-absorbing capability [12]. Early attempts, such as black-painted reservoir bottoms, aimed to enhance solar absorption but resulted in inefficient vapor generation [12]. Researchers sought productivity enhancements by altering system parameters or designing new solar stills, yet systems with the absorber at the reservoir bottom achieved only 30% - 45% efficiency, suffering unnecessary heat loss [13–15]. The emergence of nanoscale photothermal materials introduced a revolutionary approach called volumetric water heating. Suspended solar absorbers, uniformly dispersed and close to water molecules, directly transfer heat, facilitating vapor generation [16–23]. This mechanism involves nanoparticle-induced localized heat generation or bulk fluid temperature rise, influencing evaporation rates tied to nanoparticle concentration in water [17,20,24–28].

Around 2014, the interfacial solar steam generation (ISSG) technique redirected solar energy concentration from the reservoir bottom to the air-water interface, enhancing evaporation efficiency by curbing heat loss [14,29]. Utilizing photothermal materials at this interface, ISSG systems either self-float or employ lightweight substrates, amplifying solar absorption [29]. Offering eco-friendly, electricity-independent water purification, ISSG holds promise for decentralized water plants, crucial for regions facing water scarcity and emergency supply needs [30]. This attention-grabbing technique finds relevance in water purification endeavors. This review stands out by offering a comprehensive perspective on Interfacial Solar Steam Generation (ISSG) that extends beyond the scope of previous reviews. Unlike earlier analyses that focused on specific types of evaporators or mechanisms [31–35], this article takes a holistic approach, delving into materials, engineering considerations, thermal regulation strategies, practical challenges, and diverse applications. By synthesizing advancements across multiple facets of ISSG technology, this review uniquely connects theoretical foundations to real-world implementation, distinguishing itself from prior works [31–35].

This comprehensive review not only contributes to the evolution of ISSG technology but also addresses critical gaps left by earlier analyses. By exhaustively compiling recent progress and offering integrated insights, it empowers the broader adoption of ISSG systems using low-dimension and biomass materials. The multifaceted analysis examines key factors ranging from photothermal nanostructures to device geometries and thermal regulation, providing a holistic perspective that propels ISSG's development using low-dimension materials and biomass materials. Additionally, this review stands out in its ability to address challenges inherent in ISSG systems, such as biofouling, salt accumulation, and thermal management. It goes beyond by highlighting ISSG's diverse applications, from desalination and wastewater treatment to oil-water separation and sterilization, showcasing its versatility across industries. In comparison to prior reviews that focused on specific aspects of ISSG, this comprehensive analysis connects materials, engineering, and applications. By advancing discourse on sustainable, energy-efficient water purification, this review acts as a catalyst for further technological advancements in ISSG, aiming to address urgent global water challenges.

In Summary, this comprehensive review article embarks on a thorough exploration of ISSG's multifaceted dimensions, delving into its intricate mechanisms, optimizing substrate materials, devising thermal management strategies, and unravelling its diverse applications. The underlying mechanisms of ISSG are meticulously dissected, shedding light on the photothermal behaviours exhibited by various materials. The pivotal role of nanoparticles in driving efficient vapor generation is scrutinized. In-depth analyses of substrate shape and composition uncover their contributions to elevated solar evaporation efficiency. The evaluation of multi-surface evaporators reveals their potential for maximizing environmental energy gains. To further elevate ISSG performance, a range of thermal management tactics are examined, including innovative water transport paths that facilitate optimal heat distribution, thereby ensuring sustained and proficient vapor generation. Crucially, this review addresses critical challenges inherent to ISSG systems, offering insights into the mitigation of issues such as salt accumulation, biofouling, corrosion, and oil fouling. In a practical context, the article underscores ISSG's far-reaching applications, highlighting its paramount role in seawater desalination as a sustainable remedy for the global freshwater scarcity crisis. Moreover, its versatility shines through in wastewater treatment scenarios, encompassing dye and heavy metal removal, thus contributing to essential environmental remediation efforts. ISSG's proficiency in oil-water separation and sterilization expands its relevance across diverse industrial and healthcare domains. By exhaustively examining ISSG's mechanisms, substrate considerations, thermal management strategies, and myriad applications, this review advances the discourse on sustainable, energy-efficient water desalination and purification. The amalgamated insights presented herein act as a catalyst, propelling the evolution of ISSG technology and empowering its widespread adoption as a transformative solution to the urgent global water challenges that lie ahead.

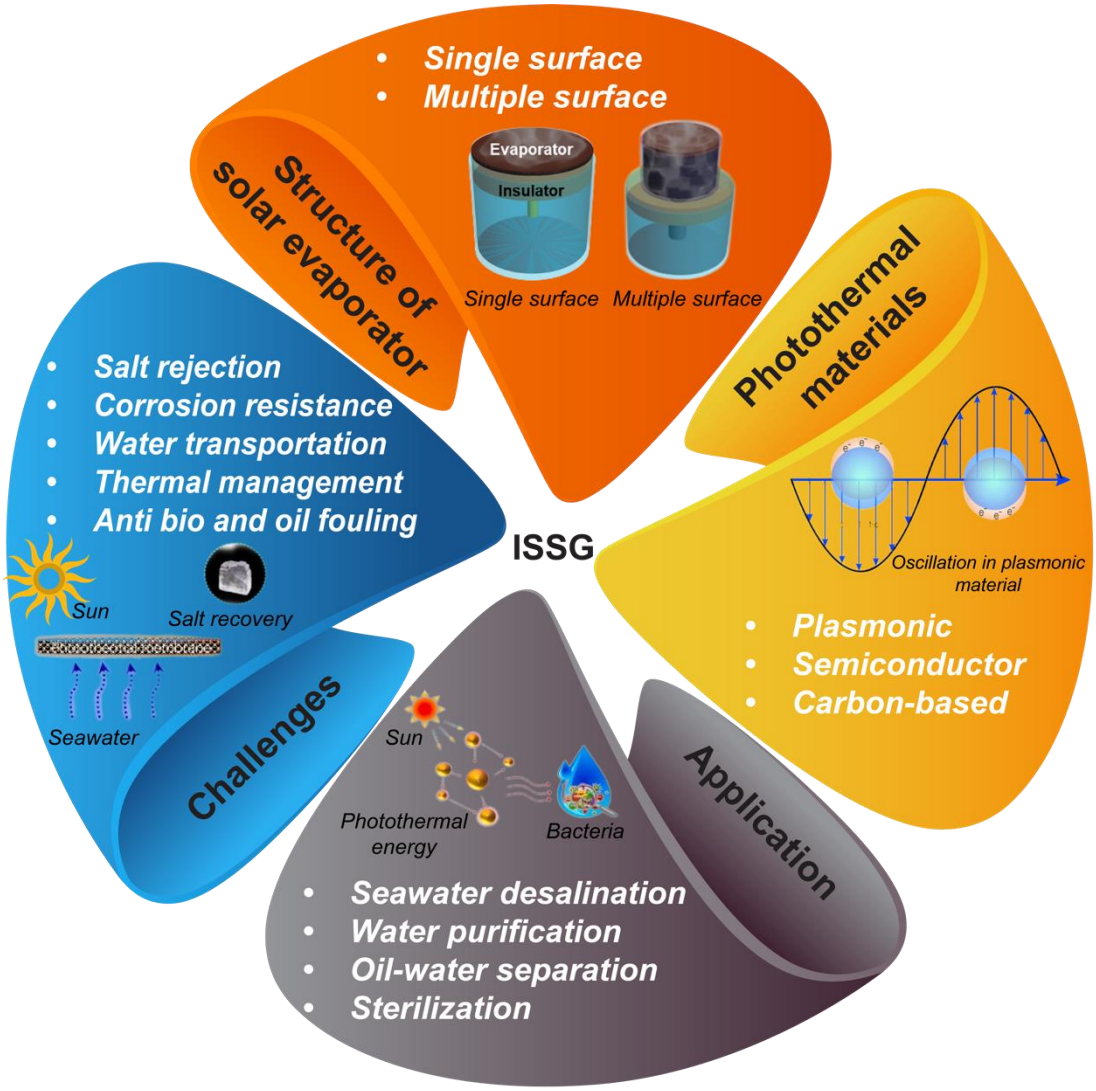


**Fig. 1.** Schematic illustration of the used materials, structure, challenges, and application of interfacial solar steam generation (ISSG) system.

## 2. Mechanism of ISSG

The ISSG technique utilizes a solar evaporator for harvesting solar energy and concentrating heat at air-water interface to generate vapor from seawater or wastewater. The generated vapor is then condensed to produce fresh water. The solar evaporator is the key component of the ISSG technique which is made by incorporating/coating/growing photothermal materials/layer on a suitable substrate.

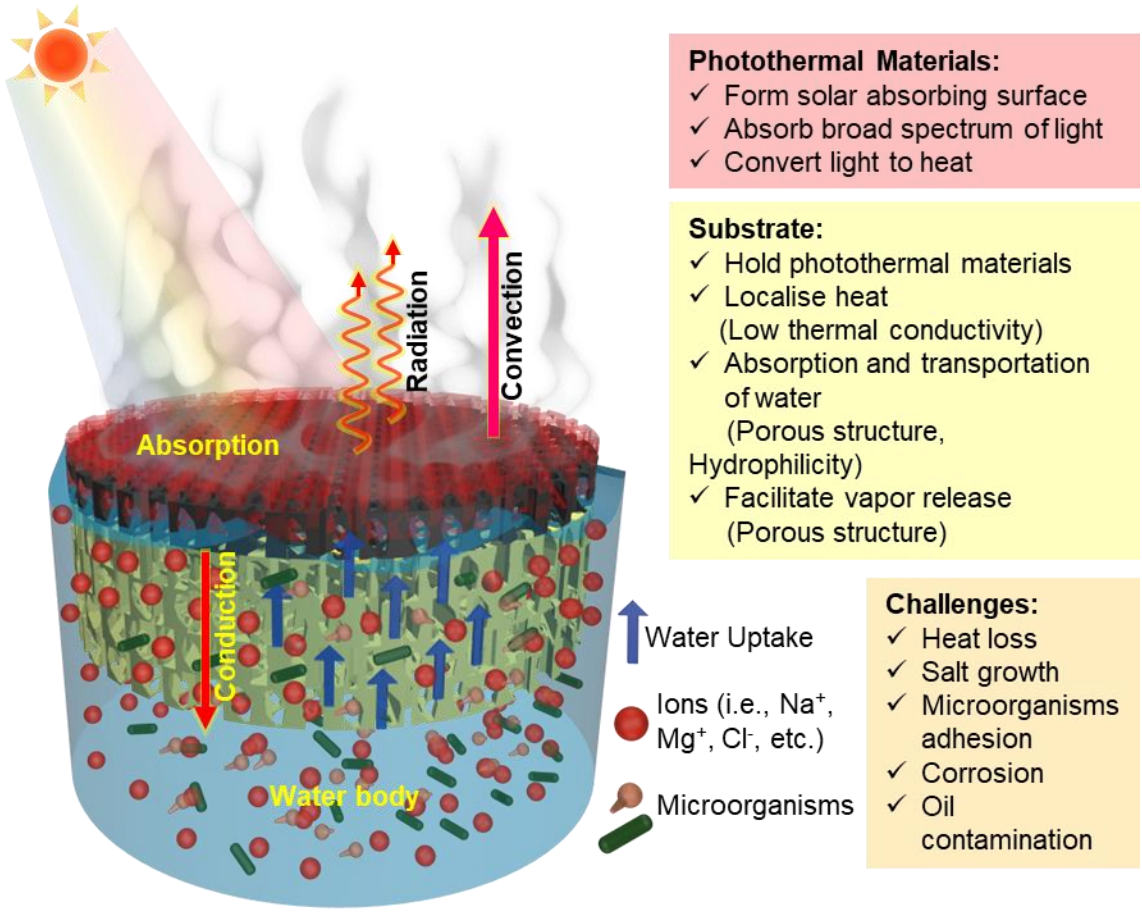


**Fig. 2.** Mechanism of ISSG.

For interfacial solar steam generation, the solar evaporator is placed on the top of the water body. It has two main functions; i) absorb sunlight, convert it to heat and concentrate the heat at a specific location, ii) absorb water and transfer it to a place where heat is localized for vapor generation (as shown in **Fig. 2**). Therefore, the performance of an efficient solar evaporator depends on its capability of (i) absorbing broad spectrum of light, (ii) converting light to heat by using photothermal materials, (iii) reducing heat loss by good thermal insulation system and localizing heat, (iv) absorbing water faster by hydrophilic surface and, (v) transporting tuned amount of water (by capillary effect) to the place where heat is localized. Reducing the vaporization enthalpy of water is another way of improving the performance of the solar evaporator. The vaporization enthalpy of water can be reduced by using hydrogel-based evaporator. Except these, literature shows that the water evaporation performance of a solar evaporator also depends on its shape and structure as they determine the light trapping and light absorbing capability of an evaporator from a different light incident angle and helps

to keep water evaporation rate high throughout the day. Moreover, the shape of an evaporator can also facilitate energy gain from the environment [36–38]. Therefore, for fabricating an efficient solar evaporator, the selection of appropriate photothermal material and substrate is very important. However, for practical implementation of the ISSG technique, the solar evaporator must have the capability to survive in a complex system like seawater and wastewater as they contain different types of salts, ions, and microorganisms. Therefore, the evaporator must have salt rejection capability, corrosion resistance property, and anti-biofouling capability. Hence in this review, the mechanisms of these properties of the evaporator are discussed in a separate section.

### *2.1. Photothermal Materials*

Photothermal conversion is a process of converting sunlight into heat. The material used for making the solar absorbing surface of the evaporator should have the capability of broadband absorption across the entire solar spectrum (0.25 – 2.5 μm) and high photothermal conversion efficiency [39,40]. Photothermal materials used for ISSG can be categorized as low dimensional materials and biomass derived materials. Low dimensional materials have at least one dimension in nanoscale and can be classified as 0D, 1D and 2D. Generally, the diameter of 0D materials is less than 10 nm. Nano particles with small diameter and quantum dots fall into this category. 1D nano materials generally have a linear structure with a diameter less than 100 nm. Nanotubes, nanorods, nanowires etc. are generally considered as 1D materials. On the other hand, nanoflakes, nanosheets etc. are known as 2D materials as their thickness is generally less than 100 nm. Graphene quantum dots (QDs) [41] and carbon dots [42,43] are some of the 0D photothermal materials used in the field of ISSG for preparing the evaporator. 1D and 2D materials like carbon nanotube (CNT) [44], $MnO_2$ nanorod [45], Titanium Oxide nanosheet [46], $Ti_3C_2$ nanosheets [47] etc. are also being used for preparing the solar absorbing layer of the evaporator. Sometimes to increase solar absorption, the combination of 0D, 1D and 2D photothermal materials are used to prepare the evaporator. For example, Irshad et al. utilized carbon dot modified $MnO_2$ nanowire to prepare the solar

absorbing layer of the evaporator [48]. Li et al. utilized the synergistic photothermal effect of 0D $Ti_2O_3$ nanoparticles and 1D carbon nanotubes to evaporate water [49]. Similarly, Ma et. al utilizes the combination of 1D CNT with 2D MXene nanosheets to prepare the solar absorbing surface of the evaporator [50]. Saleque et al. prepared the solar absorbing layer of an evaporator using TiTe2 QD decorated 2D rGO [51]. Fan et at. Utilizes 0D perovskite oxide/2D MXene heterostructure to prepare a hydrogel and demonstrated the synergistic photocatalysis and photothermal effect for water purification [52]. Gao et al. prepare a photothermal catalytic gel using $TiO_2$/Ag nanofibers for simultaneous freshwater and hydrogen generation under natural sunlight where $TiO_2$ nanofibers act as photoredox material and Ag nanoparticles act as cocatalyst and plasmonic solar absorber [53]. The synthesis and processing of low dimensional materials are sometimes complex. Moreover, the fabrication process of low dimensional materials may get expensive due to the cost of materials and equipment. Different approaches are taken for preparing low dimensional photothermal material based solar evaporator as shown in **Fig. 3a**. Generally, low dimensional materials are synthesized separately and coated on a suitable substrate.

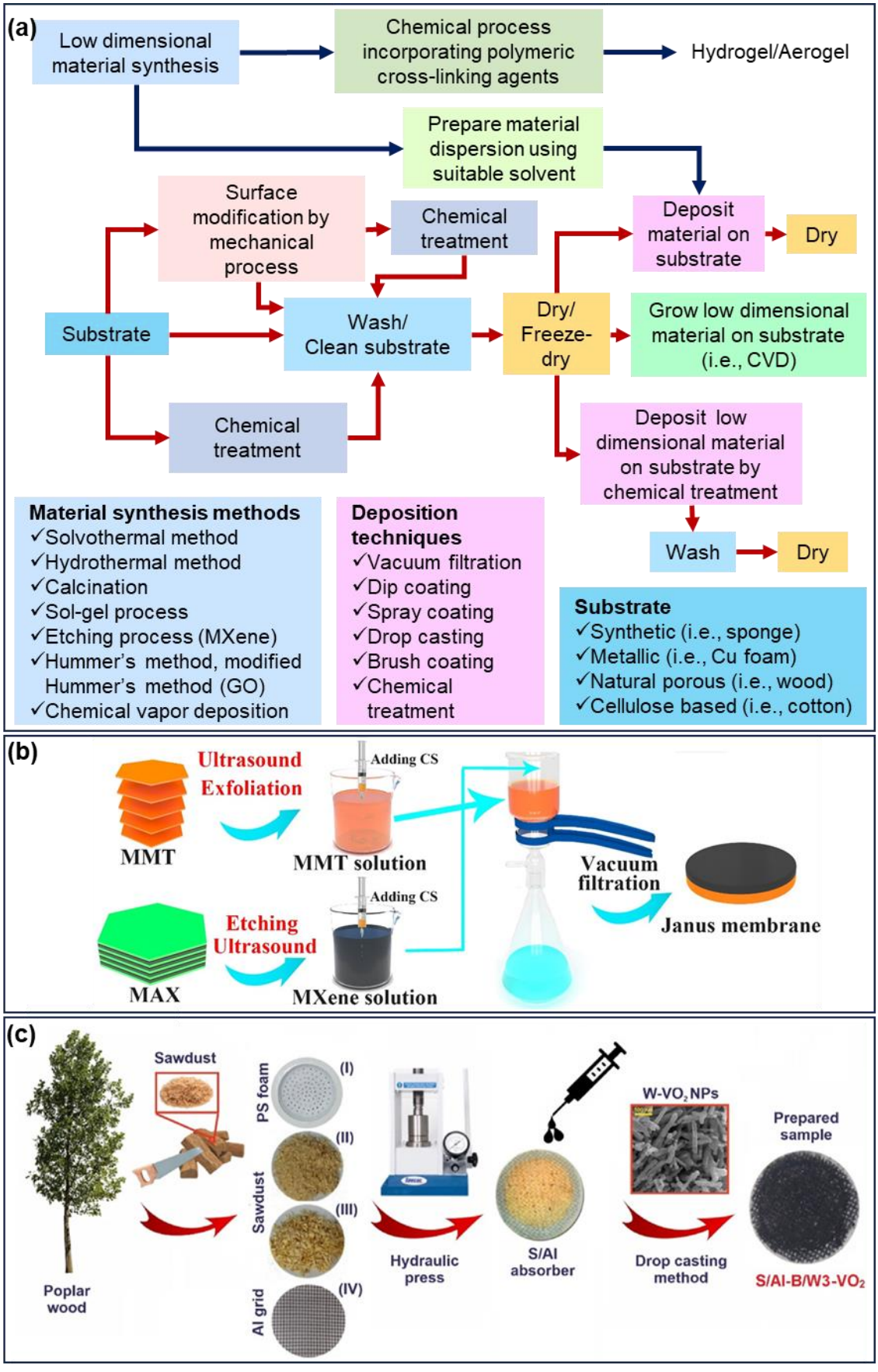


Fig. 3. Process of fabricating low dimensional photothermal material-based solar evaporator: (a) General steps of making solar evaporator using low dimensional photothermal materials.

(b) MXene deposition by vacuum filtration process [54]. Copyright 2022 Elsevier (c) W-$VO_2$ nanoparticles deposition by drop casting method to prepare solar evaporator [55]. Copyright 2022 Elsevier.

Normally drop casting [51,56], spray coating [57], dip coating [58,59], vacuum filtration [54,60] etc. are used for coating the substrate. For example, vacuum filtration method was used by Ai et al. to prepare Mxene/MMT nanosheets based Janus membrane for solar steam generation as shown in **Fig. 3b** [54]. Ghafurian et al. prepared a substrate using polystyrene, sawdust and aluminum grid and drop casted W doped $VO_2$ nanoparticles on it to prepare a solar evaporator as shown in **Fig. 3c** [55]. The low dimensional materials can also be deposited on substrate by chemical treatment method [61,62]. In some cases, these materials are grown directly on substrate [63,64]. In hydrogel-based evaporator, low dimensional materials are generally incorporated with polymeric materials to form the evaporator of desired shapes [65–67].

Biomass derived photothermal materials are found from naturally available animal and plant based organic materials. Carbonizing biomass is the most used technique for deriving photothermal carbon for solar evaporator. The process of making biomass derived photothermal carbon-based solar evaporator can be summarized by **Fig. 4a**. Generally, there are two ways of carbonizing biomass, i) surface carbonization and ii) complete carbonization. In the surface carbonizing process only the surface of the biomasses is carbonized to make solar absorbing surface, whereas in complete carbonization process the whole biomass is carbonized. Surface carbonization can be done by using flame [68], laser [69], hot plate [70] etc. Wang et al. partially carbonized freeze dried Enteromorpha by electric heating plate at 300 ºC to prepare a jellyfish like solar evaporator as shown in **Fig. 4b** [71]. Complete carbonization of biomass is generally conducted inside a vacuum chamber or non-reactive gas (i.e., N2, inert gas) filled chamber [72–74]. The complete carbonized biomass can be used directly as a solar evaporator [72,73], or they can be used with other substrate to prepare a solar evaporator [75,76]. Zhou et al. carbonized freeze dried *Pleurotus eryngii* at 800 ºC in Ar atmosphere to prepare a biomass based solar evaporator [74] as shown in **Fig. 4c**. Except carbonization, photothermal material can also be extracted from biomass. Recently, cuttlefish

ink has shown potential in the field of ISSG [77–79]. The ink contains natural melanin and shows broadband absorption of light. Moreover, it can be easily dispersed in water which makes it suitable for preparing hydrogel based solar evaporator. Bioderived photothermal materials are cheaper compared to low dimensional materials due to their availability in nature. The fabrication processes are also comparatively simple and cheap. Moreover, these materials can be used for making biodegradable and environmentally friendly solar evaporators. It is worth mentioning that the efficiency of the evaporator does not only depend on the photothermal materials. The type, structure, and shape of the substrate as well as the water transportation mechanism, thermal management system etc. are also the key factors for increasing the evaporation rate and efficiency of the evaporator. Therefore, bioderived photothermal material-based evaporators may show a higher evaporation rate than low dimensional photothermal material-based evaporators (Table 1 and Table 2). However, the lifetime of bioderived photothermal material-based evaporator may get reduced in complex systems like seawater and wastewater due to the presence of microorganisms. On the other hand, some low dimensional materials (nanoparticles like Ag, $TiO_2$, ZnO, CuO etc.) showed effectiveness against microorganisms (discussed in section 5) which makes them suitable for making antibiofouling evaporators. It's worth mentioning that the adhesion of low dimensional material to the substrate of the evaporator is very important as without proper adhesion there is a risk of secondary contamination (i.e., falling of nanoparticles) from evaporator to water. Falling of nanoparticles from the evaporator to water may cause due to ageing as well. If the ISSG system is not properly maintained, a large number of nanoparticles may get released to the environment and causes harm to the aquatic organisms and microorganisms [80,81] and may create negative impact to the environment in future. The lifetime of both types of evaporators (low dimensional material and biomass derived material) is very important. Low lifetime of evaporator may also increase the price of overall system in long run. It's very rare to find literature that only evaluates the lifetime of these two types of materials parallelly for ISSG application.

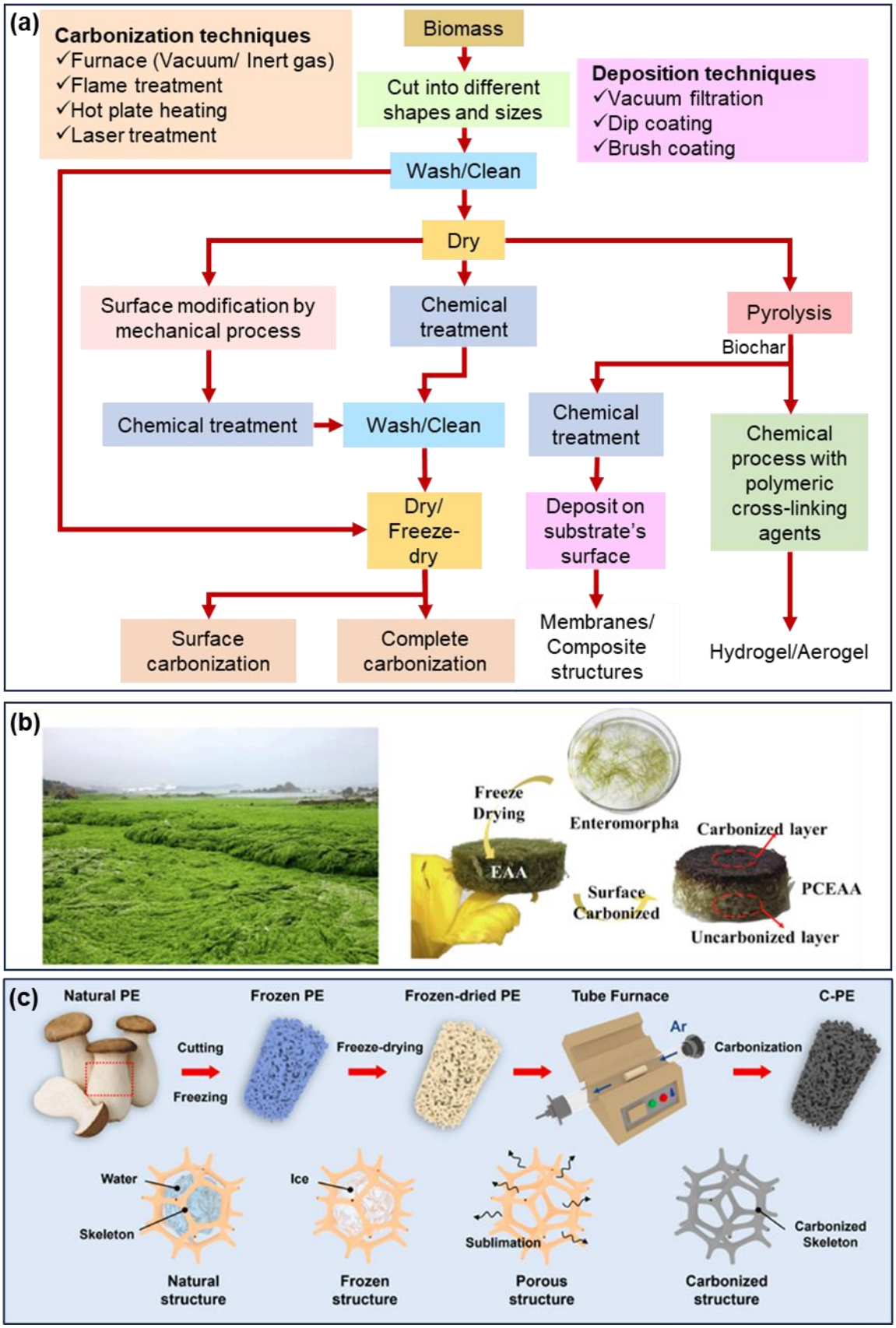


**Fig. 4.** Process of fabricating biomass derived carbon-based solar evaporator: (a) General steps of making solar evaporator using biomass derived carbon. (b) Process of making partial carbonized biomass (Enteromorpha) as solar evaporator [71]. Copyright 2022 Elsevier. (c)

Process of making completely carbonized biomass (*Pleurotus eryngii)* as solar evaporator [74]. Copyright 2023 Elsevier.

Therefore, it's very hard to assess these materials on the basis of lifetime for real time application and came into a direct conclusion for commercialization as the fabrication cost and cost of materials also controls the cost of the evaporator which determines its commercial feasibility.

The mechanism of photothermal conversion is not the same for all materials as different materials exhibit a different response to electromagnetic radiation (sunlight) due to their characteristic electronic or bandgap structure [40]. Generally, the photothermal conversion mechanism of the materials can be divided into three categories i.e., (i) Localized surface plasmon resonance, (ii) Electron-hole generation and relaxation, and (iii) Thermal vibration of molecules [40,82]. Depending on the photothermal mechanism, low dimensional materials can be categorized as plasmonic materials, semiconductor-based materials, and carbon-based materials. All biomass derived materials are basically carbon-based materials.

### 2.1.1. Plasmonic materials

Localized surface plasmon resonance (LSPR) is generally observed in some metallic nanomaterials such as gold, silver, copper, nickel, platinum etc. In the presence of light, if the frequency of the photon matches the natural metal surface electron frequency a resonant photon-induced coherent oscillation of charges occurs and causes LSPR effect [83]. If the plasmonic metal nanoparticles (NPs) are exposed to the light of their resonance wavelength, the photons are absorbed on the surface and cause the oscillation of electron gas. The excited electrons transfer to a higher energy level than the Fermi level and create hot electrons. Instead of radiative emission, if the decay of these hot electrons occurs through electron-electron scattering, the energy of the hot electron is redistributed and rapidly increases the surface temperature of metal NPs which is then transferred into the particle lattice through electron-phonon relaxation and later, cooling of nanostructure occurs by electron-phonon

coupling and phonon-phonon relaxation which causes heat dissipation to the surrounding medium (as shown in **Fig. 5a**) [40,82,84]. By this way the metal NPs absorbed sunlight, convert it to heat, and then dissipate heat to the surrounding through the vibration of lattice scattering and increases the temperature of the surrounding medium [40,84]. Depending on the structure and morphology of the nanoparticles the plasmonic resonance may occur at different regions of the electromagnetic spectrum [84]. For example, red-shift in localized surface plasmon may occur if the shape of a metallic nanoparticle (i.e., gold, silver, copper, etc.) is changed from spherical shape to rod-like shape [85]. Therefore, by changing the morphology of metallic nanoparticles the LSPR can be tuned from visible to near infrared frequency range. Plasmonic nanoparticles have strong light-absorbing capability around the LSPR peak, but their absorption spectrum is narrow. Du and Tang proposed to blend different gold nanofluids to achieve light absorption in both visible and near-infrared spectral regions at low concentrations of NPs [86]. A broadband absorptive metallic nanostructure prepared by physical vapor deposition of gold on an alumina nano porous template for a solar steam generation has been reported to show average measured absorbance of around 99% across the wavelength from 400nm to 10μm [87]. It should be noted that solar evaporators should have the capability of absorbing a broad spectrum of sunlight and hence sometimes the plasmonic nanoparticles are combined with carbon-based materials.

Shi et al. embedded plasmonic silver (Ag) nanoparticles in three-dimensional carbonized melamine foam and demonstrated the increase in light absorption in the visible region due to the inclusion of Ag nanoparticles and the prepared solar evaporator showed the photothermal efficiency of 102.99% under 1kW $m^{-2}$ solar illumination for pure tap water [88]. Goharshadi et al. demonstrated that wood coated with plasmonic Pd and Ag nanoparticles (NP) as top and bottom layer give highest evaporation rate (4.82 kg $m^{-2}$ $h^{-1}$) at 3 suns [89]. Ji et al. have used three different (Au, Ag, and Cu) metallic NP with carbon fibers to make three solar evaporators and demonstrated that the use of metallic NP increases water evaporation rate due to their LSPR effect [90]. Saad et al. used bimetallic plasmonic nano-shells composed of Ag and Cu

with sawdust-derived biochar to fabricate a solar evaporator that shows above 90% evaporation efficiency under 1 sun illumination [91]. Joo et al. demonstrated the use of metal-Si hybrid nano-wire structure (plasmonic Si nanowires) in solar steam generation application with water evaporation rate and efficiency of 1.12 kg $m^{-2}$ $h^{-1}$ and 72.8% respectively [92]. Different plasmonic metal nitrides like TiN, ZrN and HfN on nanoporous alumina substrate have shown efficiency of 78%, 88%, and 95% respectively [93]. In recent years MXene (i.e., $Ti_3C_2T_X$) has been utilized as a promising photothermal material in the field of solar steam generation [59,94]. Generally, MXene is hydrophilic in nature due to the presence of functional groups at its surface and shows the LSPR effect [40,95]. Except these, oxygen-deficient transition metal oxides (i.e., $WO_{3-X}$) also show an LSPR effect due to the presence of high charge carrier density [96].

***2.1.2. S***emiconductor-based materials

Semiconductor-based materials generally show electron-hole generation and relaxation effects. Under solar/light illumination, when these materials are excited by energy similar to their bandgap, electron-hole pairs are produced. The excited electrons have the tendency to return to the lower energy states by releasing energy. The excited electrons may release energy either in the form of a photon (radiative relaxation) or in the form of a phonon (non-radiative relaxation). If the energy is released by non-radiative relaxation, local heating of the lattice occurs, and a temperature distribution according to the optical absorption and surface recombination characteristics of the semiconductor materials is established [82]. The bandgap has an influence on the solar absorption (as shown in **Fig. 5b**) and photothermal conversion efficiency of semiconductor-based materials. Recombination of electron-hole pairs occurs easily in broad-bandgap semiconductors as most of the absorbed energy is released in the form of photons and hence decreases the photothermal conversion efficiency [40]. Hence, semiconductor materials with small bandgap have potential in the field of solar steam generation. Li et al. mentioned the ultra-narrow bandgap (≈ 0.1 eV) of $Ti_2O_3$ that gives it the

advantage of absorbing a broad spectrum of light and fabricated a three-dimensional $Ti_2O_3$ based aerogel that generated steam at 1.31 kg $m^{-2}$ $h^{-1}$ and showed photothermal conversion efficiency of 81.7% under 1 sun [97]. Another cost-efficient, narrow bandgap (0.45 eV) semiconductor; $CuFeSe_2$ nanoparticles decorated on wood substrate has shown solar thermal efficiency of 86.2% under 5 kW $m^{-2}$ illumination [98]. A spectrum-tailored solar harnessing aerogel composed of defect-rich semiconductor $HNB_3O_8$ nanosheets and polyacrylamide framework has been reported to perform both photochemical solar energy conversion utilizing high-energy ultraviolet photon and photothermal solar energy conversion using low energy visible-near infrared photon [99]. Semiconductor material, $MoS_2$ has been reported several times in the field of solar steam generation application in nanosheet form [100–102]. Except that a $NiV_{14}$ based hybrid semiconductor confined in a mesoporous glass has been reported to show water evaporation efficiency of 111.4% under 6 suns [103]. Sometimes to narrow the bandgap, semiconductor materials are doped with plasmonic metal nanoparticles as a plasmonic metal has its own heating effect and can reduce the bandgap of semiconductor materials effectively [96]. Huang et al. demonstrated the use of bifunctional Au@$TiO_2$ core-shell nanoparticle films for seawater evaporation application [104]. Sun et al. demonstrated Au-CuS (metal-semiconductor) gyroid structured material for solar steam generation and achieved the highest evaporation efficiency of 88.8% under 1sun [105]. Song et al. fabricated a solar evaporator (which evaporates water at 1.3 kg $m^{-2}h^{-1}$ with 73% conversion efficiency under 1 sun) by coating delignified wood with $Fe_3O_4$ semiconductor material [106]. $Fe_3O_4$ is very cost-effective and has narrow bandgap (≈ 0.8 eV) which gives it the capability of absorbing a broad spectrum of light [106]. Zahmatkesh et al. fabricated a solar evaporator by coating poplar wood with Au and $Fe_3O_4$ NPs [107]. By using the synergistic effect of broad light absorbing capability of $Fe_3O_4$ NPs and surface plasmon in Au NPs the evaporator showed an evaporation efficiency of 88.7% under 3 sun.

### *2.1.3. C*arbon-based materials

Generally, carbon-based materials and organic materials shows the effect of thermal vibration of molecules where heat is generated by lattice vibration caused by absorption of light energy [82]. Carbon-based materials demonstrate strong sunlight absorption capability due to their conjugated structure [39]. In a conjugated structure the neighboring π-electrons overlap or π-bond interact with p-orbital electrons; which redistributes electron cloud density in the system and causes a conjugation effect [39,40]. The hyperconjugation effect occurs when the electrons of a σ-bond interact with the adjacent empty or partially filled p-orbital [39,40]. The materials possessing conjugation or hyperconjugation effect show strong absorption of light in the near-infrared region as these effects accelerate the mobility of electrons [40]. The absorption of energy from light excites the electrons in the π-orbital and the excited electrons jump to the π*-orbital and release energy as heat while returning to the ground state. If the number of π bonds increases, the energy gap between the HOMO (highest occupied molecular orbital) and LUMO (lowest occupied molecular orbital) decreases. Carbon-based materials, especially graphene-like allotropes could have many conjugated π bonds which may cause the excitation of electrons by almost every wavelength of the solar spectrum and thus several π- π* transition occurs [82]. The electron absorbs light and jumps from HOMO to LUMO if the energy from light complements an electronic transition within the molecule and later these excited electrons are relaxed by electron-phonon coupling, for which energy is transferred from the excited electrons to the vibrational modes throughout the atomic lattices and causes a rise in materials temperature (as shown in **Fig. 5c**) [108] Several carbon-based materials like graphene [109], graphene oxide [110], reduced graphene oxide [111], carbon black [112–114] carbon nanotubes (CNT) [115] are reported to have photothermal conversion capabilities. Hierarchical graphene foam grown via plasma-enhanced chemical vapor deposition has been reported to show broadband enhancement, omnidirectional absorption of sunlight, and high solar vapor conversion efficiency (over 90%) for seawater

desalination [116]. A micro-structured graphene-based membrane shows the nature of self-adaptability in response to changing environments by displaying high water evaporation rate change under low sunlight and low water evaporation rate change under intense sunlight [117]. Xue et al. demonstrated the possibility of electricity generation due to water evaporation from the surface of a variety of nanostructured carbon materials [118]. Except this, the use of carbon nanotube (CNT) for solar vapor generation has been demonstrated by preparing a bi-layered material with a top self-floating hydrophobic carbon nanotube membrane and a bottom hydrophilic microporous silica substrate; that shows solar thermal conversion efficiency of 82% [115]. CNT is very popular for its excellent light-absorbing and photothermal conversion capability. However, the fabrication procedure makes this material costly. Multiwalled CNT (MWCNT) is comparatively cheaper than Single-walled CNT and can be used for fabricating efficient solar evaporators. Zhang et al. fabricated an evaporator using graphene oxide (GO), and CNT that shows an evaporation efficiency of 90.1% under 1sun [119]. Li et al. utilized $Fe_2O_3$ decorated CNT on wood to prepare a solar evaporator that generates steam at 1.42 kg $m^{-2}$ $h^{-1}$ with 87.2% evaporation efficiency under 1 sun [120]. Carbon black is amorphous and has excellent UV stability. Ge-Zhang et al. fabricated a wood-based evaporator using MWCNT and carbon black (CB) nanoparticles as a coating.[121] The MWCNTs/ carbon black coating exhibited an absorption efficiency of nearly 97.5% ad proved to be suitable for solar steam generation applications. Reduced graphene oxide (rGO) is a also very good light absorber and a very commonly used material in the field of ISSG [122–126]. Cheng et al. fabricated an rGO membrane using rGO and filter paper that shows very good optical absorption and with a very little amount of rGO (0.76 g $m^{-2}$) the evaporation rate reached 0.9 kg $m^{-2}h^{-1}$ under 1 sun [127]. Wang et al. fabricated a solar evaporator using rGO with polyurethane that exhibited solar photothermal efficiency of nearly 81% at a light density of 10 kW $m^{-2}$ [128].

Carbonizing biomass is another way of making cheap and efficient solar evaporators. Generally, natural biomasses (i.e., wood, daikon, lotus seedpod, etc.) have unique porous structures and excellent water-absorbing capability. Carbonization is done on biomasses to

attain a graphitic carbon layer to absorb a broad spectrum of sunlight. The graphitic layer on the carbonized biomass can be identified by Raman spectra as it gives a G band around 1580 $cm^{-1}$ and a D band around 1350 $cm^{-1}$ which are corresponding to the characteristic feature of

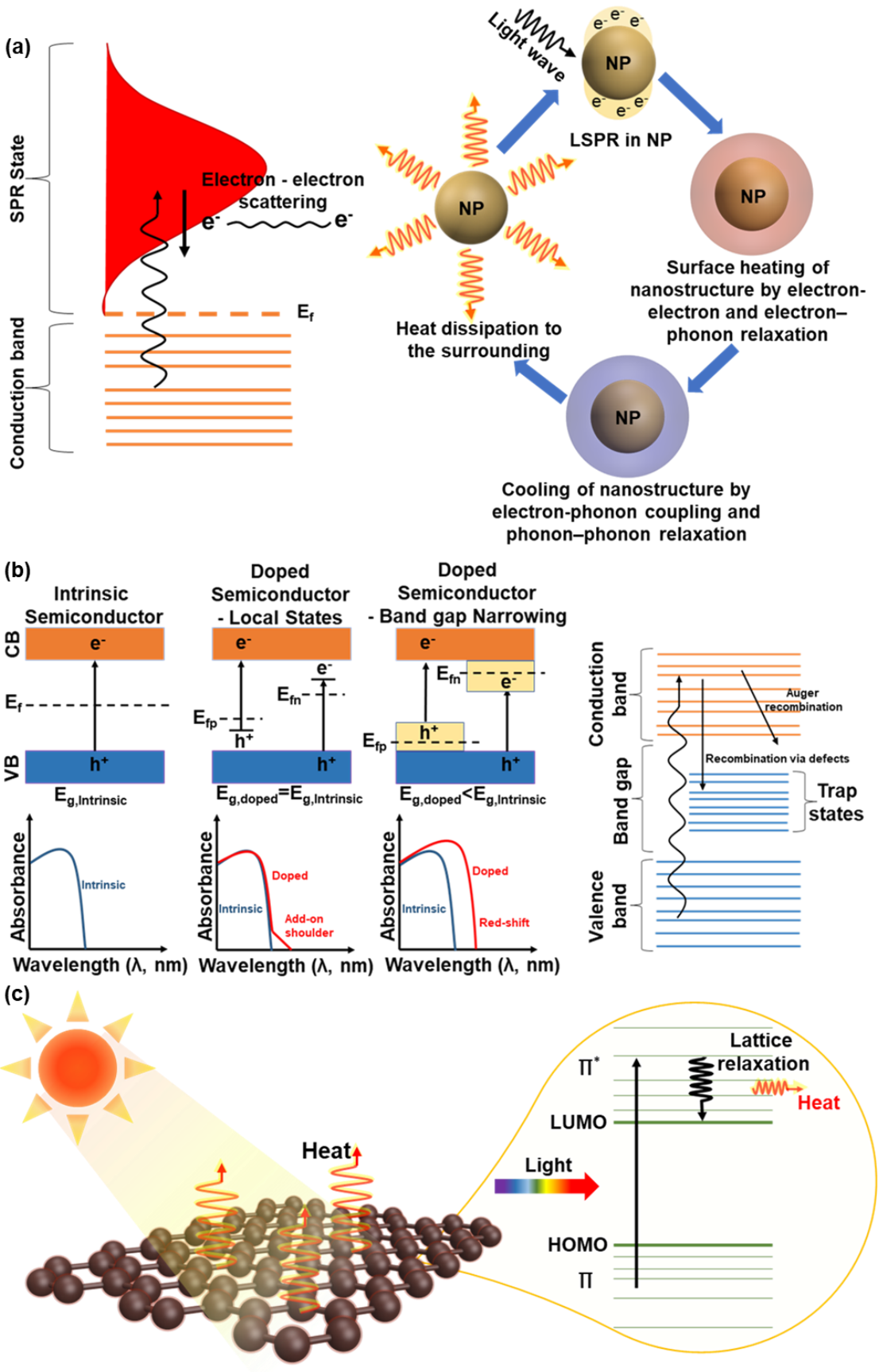


**Fig. 5.** Photothermal conversion mechanism. (a) LSPR mechanism in plasmonic metal nanoparticles showing the cyclic photothermal conversion [129]. Modified and used with

permission from Dove Medical Press Ltd. (Copyright 2018 Dove Medical Press Ltd). (b) Broadband absorption and photothermal mechanism of semiconductor-based materials [130]. Copyright 2020 American Chemical Society(c) Photothermal conversion mechanism of carbon-based materials [39]. Copyright 2021 Elsevier.

graphitic layer and disordered carbon or defective graphitic structures [131]. As mentioned earlier two different approaches are observed while carbonizing biomasses i) surface carbonization and ii) complete carbonization. In the surface carbonization technique, only the surface of the biomasses is carbonized. Xue et al. prepared a solar evaporator by carbonizing the wood block using an alcohol flame [132]. Jang et al. utilized a $CO_2$ laser to carbonize the surface of basswood and make a graphitic carbon layer to absorb sunlight [133]. To make a solar evaporator, Yu et al. utilized hot plate at 600 ºC to carbonize the surface of the wood substrate [134]. Complete carbonization is relatively complex as in this process the biomasses are carbonized in the presence of $N_2$ or inert gases or inside vacuum chamber. However, the complete carbonization technique is suitable for taking advantage of the complex natural structure of biomasses to evaporate water. Sun et al. carbonized sunflower head [131], Yuan et al. carbonized Platanus fruit [36] to make solar evaporators of unique shapes and demonstrated their effectiveness in evaporating water. Except these carbonized mushroom [135], daikon [136], carrot [137], corncob [138], algae [139] etc. are also reported for solar steam generation applications.

### *2.2. Structure of solar evaporators*

The structure of a solar evaporator has a significant impact on its efficiency, water transportation speed, water evaporation rate, and salt rejection capability [140–144]. As mentioned earlier an efficient solar evaporator performs two key tasks: first, it absorbs a broad spectrum of sunlight at the solar absorbing surface, converts it to heat, and localizes the heat in a certain area to reduce heat loss and second, it absorbs water from the bulk water body and moves it to the area where heat is concentrated. The effectiveness of the whole process depends on the efficiency of photothermal materials and the structure of the evaporator. Sometimes the structure of the evaporator depends on the structure of the substrate, where

the photothermal materials are deposited or grown and sometimes it depends on the fabrication process of the evaporator. Absorbing solar energy and converting it to heat is the main task of photothermal materials whereas holding the photothermal materials, concentrating the heat in a specific area, absorbing a tuned amount of water, and transferring it to the heated area is the task of the supporting substrate. The vapor release path also depends on the porosity of the supporting substrate. Based on the thickness of the solar evaporator, they may be divided into two categories: 2D structures and 3D structures. The 2D structures are normally made of various membranes [145–148], papers [127,149,150], and fabrics[151–153], while the 3d structures are constructed using different types of foams [154,155], hydrogel or aerogel [156,157], bio-derived materials (i.e., wood) [158], ceramic fiber wool and stainless-steel mesh [149], etc. However, the structures of the solar evaporators are not limited to their thickness. Some recent studies showed that the structure plays an important role in improving the performance of the evaporator throughout the day by harvesting sunlight from different light incident angles. These types of evaporators have multiple surfaces for solar absorption and vapor release. Moreover, some of these evaporators showed energy gain from the environment due to their unique structures. Depending on the number of effective light harvesting and vapor release surfaces of solar evaporators, they can be classified as i) Single surface solar evaporators, ii) Multiple surface solar evaporators.

### *2.2.1. Single surface solar evaporator*

Single-surface solar evaporators generally have only one major surface for absorbing sunlight and releasing vapor. The other surfaces are generally kept covered with insulating material or remain underwater and do not play a significant role in absorbing sunlight and releasing vapor. Depending on the thickness of these evaporators they can be classified as thin single-surface solar evaporators and thick single-surface solar evaporators.

#### *2.2.1.1. Thin single-surface solar evaporator*

A typical thin single-surface evaporator requires a supporting material that helps the solar evaporator float on water as shown in **Fig. 6a**. The supporting material also provides thermal

insulation between the absorber and bulk water and helps to reduce heat loss by conduction from the solar evaporator to water. For transporting water to the evaporator, 1D or 2D water transport path can be used for such kind of system. However, some supporting material with porous structure (i.e., sponge, foam) may also have the capability of transporting water. Several, types of photothermal materials have been used to fabricate this type of solar absorber such as metallic NPs, metal oxides, semiconductor-based materials, carbon-based materials, etc.[149]. Most investigated substrates are PTFE (Polytetrafluoroethylene) membrane, Polyvinylidene fluoride (PVDF), cotton, carbon fabrics and paper etc.[149].

**Polytetrafluoroethylene (PTFE) membrane**

One of the most popular substrates for fabricating thin single-surface solar evaporators is PTFE membrane. PTFE membrane possesses characteristics like acid-alkali resistance properties, mechanical strength, flexibility, and thermostability which make it suitable for constructing solar evaporators [159]. Chang et al. fabricated a thin single-surface solar absorber by coating metallic $MoO_2$ nanospheres on hydrophilic PTFE membrane using an in situ solvothermal deposition method, that has a water evaporation efficiency of 91% under 1 sun illumination [159]. This evaporator can work in harsh environments like acid, base solutions, and high-concentration seawater. Chang et al. also fabricated a solar evaporator by using flow through method to deposit a thin layer of solar absorbing hydrophobic $W_{18}O_{49}$ mesocrystal on a PTFE substrate that showed water evaporation efficiency of 82% under 1 sun [146]. For making membrane-based evaporators generally photothermal materials are deposited on the substrate by different filtration methods or by coating. Jiang et al. developed a solar evaporator by spray coating MoS2/LaF3/PDMS ink onto a commercial PTFE membrane that can provide 1.76 kg $m^{-2}h^{-1}$ water evaporation rate and 91% light-to-heat conversion efficiency under 1 sun with good thermal stability [160]. Lu et al. made an evaporator by coating molybdenum oxides hierarchical nanostructure on hydrophilic PTFE membrane which achieved an evaporation rate and efficiency of 1.255 kg $m^{-2}h^{-1}$ and 85.6% under 1 sun respectively [161]. Hydrophobic PTFE membranes can also be used as a

substrate of a solar evaporator [162,163]. Polydopamine (pDA) can be used to increase the hydrophilicity of the solar evaporator as it contains abundant hydrophilic catechol and amine functional groups [162]. pDA is also known for its good biocompatibility, high photothermal conversion efficiency and broad light absorption capability [164].

**Polyvinylidene fluoride (PVDF)**

Another popular material for fabricating thin solar evaporators is Polyvinylidene Fluoride (PVDF) membrane. PVDF membrane demonstrates good mechanical strength, chemical resistance, and thermal stability [165] which makes it an excellent substrate for fabricating solar evaporators. PVDF membrane can be either hydrophobic or hydrophilic. In recent times, many PVDF membrane-based thin surface evaporators have been investigated [147,166–170]. In order to create a membrane-based evaporator, photothermal materials can either be combined with PVDF solution [167] or directly deposited on a PVDF filter membrane through filtration [147]. Another approach for creating a thin single-surface solar evaporator using a PVDF is electrospinning. Moreover, PVDF membrane has piezoelectric properties that can be utilized for power generation in addition to steam generation. Huang et al. employed a solution casting method to fabricate PVDF/Graphene membrane (a membrane-based evaporator) for simultaneous vapor and electricity generation [171]. The evaporator generated water at the rate of 1.2 kg $m^{-2}h^{-1}$ with 84% efficiency. Because of Graphene addition, PVDF crystal is transformed from the α-phase to the piezoelectric self-assembly β-phase and hence this PVDF/Graphene membrane is also capable of giving an output voltage of 2.6 V and energy density of 2.11 $Wm^{-2}$ for 1 Hz simulated waves. For preparing a membrane-based solar evaporator, Tessema et al. prepared a solution mixing $CsxWO_3$@g-$C_3N_4$, DMF and PVDF and spun it into fiber membranes which showed an evaporation efficiency of 95.4% [170]. Electrospinning method was also adopted by Chen et al. to make a Janus PPy-$SiO_2$@PAN/F-$SiO_2$@PVDF-HFP membrane-based evaporator that delivered solar energy utilization efficiency of approximately 92.2% [168]. Huang et al. adopted a relatively complex fabrication method to make PDMS/CNT/PVDF membrane-based evaporator of productivity 1.43 kg $m^{-2}h^{-}$

[1]; where electrospinning method was applied to construct the bottom PVDF layer, spray coating to make the middle CNT layer and dipping method to make the top PDMS layer [169].

**Paper**

Paper has also been used as a substrate to make thin-film solar evaporators with good performance. The strong hydrophilicity and low thermal conductivity of filter papers make them suitable substrates for fabricating an evaporator [172]. Zhang et al. have developed a GO-CNT/paper membrane evaporator that shows high evaporation rate of 2.1 kg $m^{-2}$ $h^{-1}$ under one sun illumination [119]. By adhering CTGS film to the surface of conventional A4 printing paper, Shan et al. created CTGS/Paper membrane solar evaporator and under 1 sun illumination, this evaporator showed water evaporation rate and efficiency of 1.53 kg $m^{-2}h^{-1}$ and 95.9%, respectively [173]. Using the vacuum filtration method, Cheng et al. fabricated an rGO composite membrane with filter paper and developed a simple composite-enhanced system (CES) that achieved an evaporation rate and efficiency of 1.37 kg $m^{-2}h^{-1}$ and 85.6% respectively under 1 sun [127]. They have used a polyurethane foam (for heat insulation) beneath the rGO membrane and cut the membrane in flower shape to fold it around the foam for creating water transport path as shown in **Fig. 6b**. The SEM image of blank filter paper **(Fig. 6c (i,ii))** and rGO membrane **(Fig. 6c (iii,iv))** shows the change in morphology of filter paper before and after rGO coating. From the thermal distribution shown in **Fig. 6d**, it's clear that the system with insulator (CES) reduces heat loss from evaporator to water and only the top surface was heated due to solar illumination. Zhang et al. deposited polymerized Polypyrrole (PPy) on the surface of a filter paper to fabricate a black membrane that showed a high solar-to-vapor conversion efficiency of 95.6% under 4 sun irradiation [172]. To create an integrated evaporation device (maximum thermal conversion efficiency of 88.1% under 1 sun), Guo et al. loaded filter paper with a CNT-based solution using a spin coating procedure and sprayed polyurethane foam at one side of the membrane and solidified it [150].

**Cotton fabric**

Cotton fabric (CF) is a type of natural polysaccharide porous material with great stability and hydrophilicity, and it has numerous uses in the textile industry. It is possible to manufacture CF on a wide scale at a reasonable cost and can be reused after washing repeatedly [174–177]. Therefore, the salts deposited on the evaporator during desalination can be easily removed if the photothermal materials are bonded strongly with cotton fabric. In addition, it is possible to modify the cellulose-made CF with some nanomaterials and react with oxidizing agents [175]. Due to these qualities, Cotton fabric is another suitable substrate for making thin single-surface evaporators. By dipping cotton cloth in a carbonized carrot powder dispersion and dropping Nafion on one side, Qin et al. created a Janus hybrid evaporator for solar steam generation that exhibits an evaporation rate of 1.88 kg $m^{-2}h^{-1}$ for clean water and 1.52 kg $m^{-2}h^{-1}$ for seawater under one sun [178]. Wang et al. fabricated a MXene/CNT/Cotton fabric multi-layer evaporator by dip coating cotton fabric in MXene and CNT solutions repeatedly that exhibited evaporation rates of 1.35 kg $m^{-2}h^{-1}$ for water and >1.16 kg $m^{-2}h^{-1}$ for textile wastewater under 1 sun illumination [177]. Li et al. constructed a fabric utilizing electro-spraying PVDF-HFP on one side of the cotton fabric which showed tunable water delivery (TWD) property and then dip-coated the constructed fabric with carbon black dispersion to make a solar evaporator that can float on water with the help of **cotton fabric** wrapped Polystyrene (PS) foam (as shown in **Fig. 6e**) and showed vapor conversion efficiency and evaporation rate of 88.9% and 1.33 kg $m^{-2}h^{-1}$ respectively [153]. Here the cotton fabric around the PS foam worked as a water transport route. The surface morphologies of Cotton fabric, TWD fabric and coated TWD fabric are shown in Fig. **6f**. From the thermal image (**Fig. 6g**) it can be said that only one surface was heated due to solar illumination. The use of PS foam not only serves as a support to keep the thin evaporator afloat in water but also serves to physically isolate the photothermal conversion layer from bulk water to reduce heat loss [151,175]. Qi et al. also utilized PS foam as support material to hold a multi-layer cotton fabric (MWCNTs-COOH/BN-PDA/CF) based evaporator on water and used cotton yarns as water

supply channels and the system shows evaporation rate of 1.55 kg $m^{-2}h^{-1}$ under 1 sun [151]. Xiong et al. fabricate a flexible and washable solar evaporator by chemically depositing hierarchical $MnO_2$ nanosheets on cotton fabric that exhibited a water evaporation rate of 1.40 kg $m^{-2}h^{-1}$ with a photothermal conversion efficiency of 87.48% under 1 sun illumination [175]. Chen et al. synthesized NiFe2O4-NiAl-LDH-ACC by incorporating activated carbon cloth (ACC) and using a hydrothermal method and demonstrated its application as a solar evaporator [152]. A cheap solar evaporator (cost< \$1 per $m^2$) was prepared by Gao et al. by capturing candle soot using wet cotton fabric [179].

Apart from these activated pulverized coal-based membrane (APC) derived from activated pulverized coal and filter membrane [180], self-assembled $Fe_3O_4$@C film [181], rGO/PS@PSf and CB/rGO/PS@PSf fabricated by coating rGO/PS and CB/rGO/PS microspheres on polysulfone (PSf) membrane [145], etc. are also can be considered as single surface thin solar evaporator.

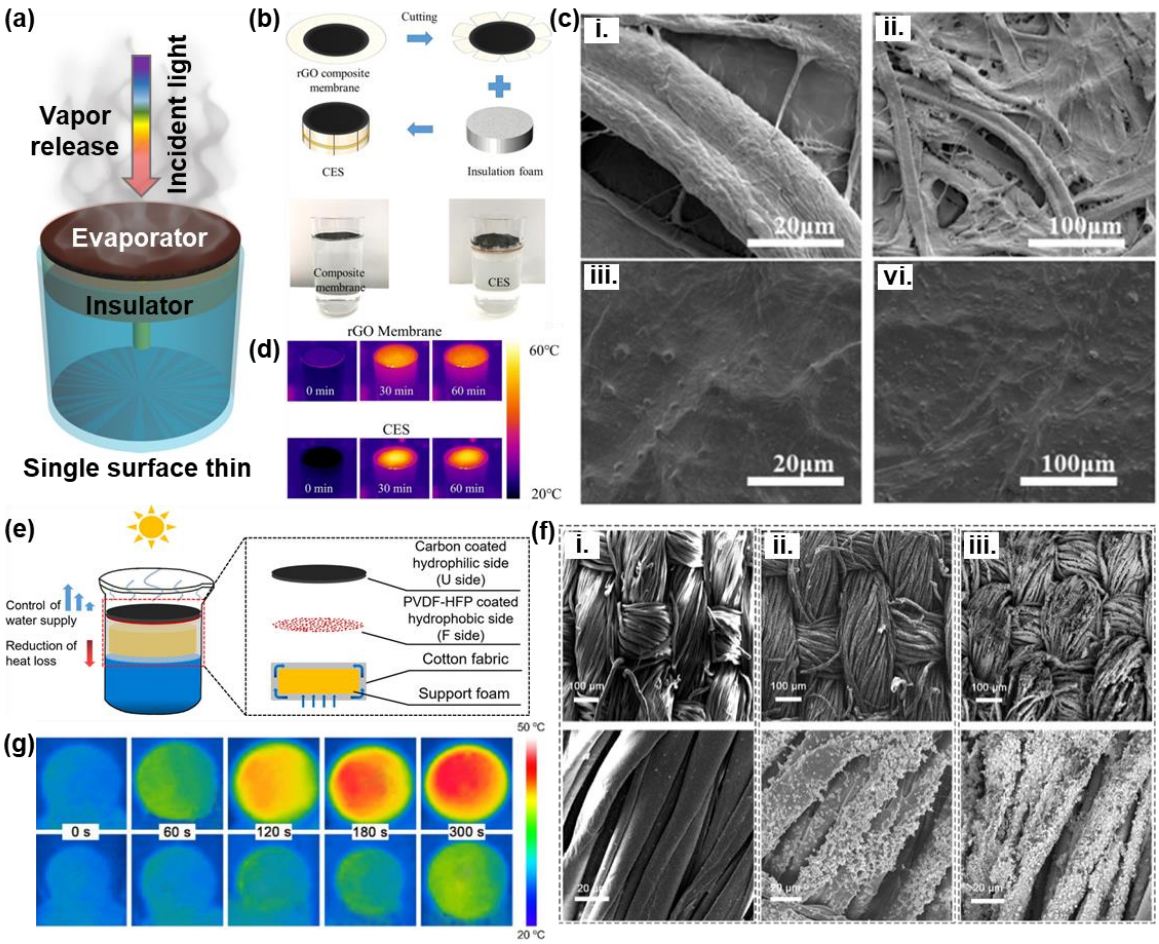


**Fig. 6**. Single-surface evaporator (Thin): (a) Schematic illustration of the concept of thin single-surface evaporator. (b) Schematic of the composite enhanced system (CES) using rGO composite membrane with insulation and a digital image showing the self-floating capability of the evaporators; (c) SEM image of (i-ii) blank filter paper and (iii-iv) rGO membrane; (d) IR image showing temperature distribution of RGO membrane and CES [127]. Copyright 2019 Elsevier. (e) Schematic illustration of thin single surface evaporator on support foam (f) SEM image of (i) cotton fabric, (ii) tuneable water delivery fabric (TWD) and coated TWD fabric; (g) thermal image showing temperature distribution of thin fabric based single surface evaporator [153]. Copyright 2019 American Chemical Society

### *2.2.1.2. Thick single-surface solar evaporators*

Normally the thick solar evaporators are fabricated using porous materials like different types of sponges, foam, wood, etc. Porous materials are generally used to transport water at the heat-localized area of the evaporator by capillary action. Moreover, porous structures have the capacity to trap light, store heat, and reduce heat loss. Generally, in the case of single-surface thick evaporators, only one surface floats above the water and participates in light absorption and vapor release as shown in **Fig. 7a.**

**Wood**

Wood has a natural hierarchical porous structure and through its natural microchannels wood can transport water by capillary force. Naturally wood can absorb water. Moreover, wood is a good heat insulator and has excellent thermal stability, floatability, and biocompatibility which makes it an excellent substrate for fabricating solar evaporators. Wood, however, does not effectively absorb light, which results in a low photothermal conversion for heating water [182]. To maintain the internal microchannels for water transportation, wood is generally cut horizontally to its growth direction for making solar evaporators. Wood-based evaporators are often prepared by following two approaches: (1) carbonization, and (2) photothermal materials insertion. Yang et al. deposited polydopamine (PDA) and Ag nano particles on natural wood by immersing a wood block in chemical solutions to a depth of 2 mm [183]. The prepared evaporator showed fast photothermal response due to the synergistic photothermal effect between PDA and Ag nanoparticles (as shown in **Fig. 7b)** and showed high evaporation rate of 1.58 kg $m^{-2}$ $h^{-1}$ under 1 sun. Song et al. fabricated a single-surface solar evaporator by decorating a thin layer of $Fe_3O_4$/polyvinyl alcohol (PVA) on a delignified wood surface that demonstrated an evaporation rate of 1.3 kg $m^{-2}$ $h^{-1}$ and conversion efficiency of 73% [106]. The delignification technique improved the wood structure's ability to transmit water while reducing thermal conductivity and heat loss. Carbon nanotubes decorated delignified wood and natural wood were employed by Yuming et al. for solar evaporation [184]. They discovered that under ambient sunshine, the interfacial solar steam generation efficiency of carbon nanotube-delignified wood is 20% higher than carbon nanotube-natural wood. The evaporation efficiencies of carbon nanotube-delignified wood and carbon nanotube-natural wood were 73% and 60%, respectively, and were 12% and 18% higher than those of wood alone. This increase in efficiency occurs as after the delignification process, the cell walls develop enormous micropores that speed up water transportation to the top surface and facilitate evaporation. After carbonizing different types of wood with varying thicknesses and utilizing them for solar evaporation, Jia et al. concluded that though decreasing thickness

increases evaporation rate, it increases heat loss as well due to a decrease in thermal confinement ability [185]. Yu et al. utilizes hot plate carbonization technique to prepare wood based solar evaporator of different thicknesses and claimed that thickness of 22 mm can provide highest evaporation rate of 6.89 kg $m^{-2}h^{-1}$ under 5 sun with an efficiency of 87.7% [134]. To make a self-regenerating solar evaporator Kuang et al. drilled some holes in a wood substrate and carbonized one surface to absorb sunlight, which demonstrated an efficiency of about 75% under 1 sun when placed on 20 wt% NaCl concentrated salt solution [186]. Xue et al. carbonized wood by alcohol flame and claimed that incomplete combustion of alcohol facilitates the deposition of carbon nanoparticles on flame-treated wood (shown in **Fig. 7c**) and hence increased its light absorption capability [132]. The prepared flame-treated solar evaporator showed high solar thermal efficiency (nearly 72% under 1 sun). The top and cross-sectional view (**Fig. 7c (iii, iv)**) show the porous structure and internal microchannels of flame treated wood. The SEM images (**Fig. 7c (v and vi)**) show the apparently deposited carbon nanoparticles on the inner walls surface and the morphology of deposited carbon nanoparticles. From the IR image shown in **Fig. 7d** it can be said that heat is localized on the top surface of the evaporator. In order to create a solar evaporator that can operate for a long time in saline water, Jang et al. employed a $CO_2$ laser to create a graphitic carbon layer on the surface of basswood [133]. Kim et al. created a low-cost photo absorber utilizing used coffee grounds and coated it on wood to make a solar evaporator [184]. The photo absorber successfully absorbed 91% of sunlight. With excellent photothermal and antifouling capabilities, the ball-milled activated waste coffee grounds-wood evaporator demonstrated an evaporation rate of 1.45 kg $m^{-2}$ $h^{-1}$ under 1 sun. By carbonizing a longitudinal wood surface, Liu et al. created a solar evaporator of reverse-tree design [184,187]. In a reverse tree design, a wood substrate is achieved by cutting the natural tree parallel to the growth direction and water transportation occurs through the pits of the natural microchannels rather than vessels and tracheid of wood. The evaporator showed a solar-to-thermal efficiency of 89% under 10 suns because of the broad-band sunlight absorption by carbonized surface and the low heat conductivity of longitudinal wood [187]. Luo et al. demonstrated the efficiency of various

carbon-based photothermal materials coated wood in generating vapor [188]. Ghafurian et al. prepared solar evaporators by incorporating different wood surface treatment techniques like laser treatment, carbonization and gold coating [189]. Huang et al. prepared an evaporator based on laser-induced graphene wood [190]. This evaporator was made up of three layers: a bottom layer of super hydrophilic laser-induced graphene for rejecting lipophilic organic molecules, a middle layer of wood for water transfer, and a hydrophobic top layer of laser-induced graphene for preventing salt accumulation. The bottom layer of laser-induced graphene contains oxygen functional groups, which greatly lessen bacterial biofouling and wood decay. In addition, several plasmonic metallic nanoparticles (i.e., Pd, Pt, Ag, Au, etc.) and semiconductor-based photothermal material (i.e., black $TiO_2C$, NiO, $WO_{3-x}$ nanorod, $MoS_2$, u$FeSe_2$, etc.) coated wood substrates have been reported in the field of interfacial solar steam generation [89,98,134,191–193]. Similar to wood substrates, several other bioderived substrates (i.e., bamboo, jute stick, etc.) have been utilized to prepare solar evaporators by incorporating both carbonization and photothermal material insertion techniques [194–196]. Sheng et al. made a plasmonic bamboo solar evaporator by decorating the cross-sectional surface of the bamboo with metallic Pd nanoparticles [195]. Because of the plasma effect, this plasmonic bamboo displayed a significant light absorption capability with a solar energy conversion efficiency of 87% under the intensity of 10 suns.

**Sponge**

Different types of sponges are used to make thick single-surface solar evaporators due to their porous structure and capability of absorbing water. Polyurethane (PU) sponge is considered a very good thick substrate for fabricating solar evaporators as it has a porous structure with many mass transfer channels and low thermal conductivity. Photothermal materials can be either coated on sponges or incorporated during the fabrication of sponges to make a solar evaporator. One of the potential materials to fabricate sponge-based solar evaporators is Polydimethylsiloxane (PDMS) for its high flexibility and thermal stability [197]. Wang et al. made a Janus, single surface thick solar evaporator by first by dip coating a polyurethane (PU)

sponge in PDA solution and then coating PDMS on the top layer of the PDA/PU sponge [197]. This evaporator exhibits a water evaporation rate of 1.2–3.1 $kgm^{-2}h^{-1}$ (under 1 to 2.5 sun) with a high solar conversion efficiency (above 90%). Due to the hydrophobic nature of PDMS, the hydrophobicity-induced interfacial layer (top layer) above the water surface functions as an effective light absorber, photothermal converter, and salt rejector, while the hydrophilic bottom layer (PDA/PU) is responsible for effective heat localization and continuous water supply. By embedding porphyrin/aniline-based conjugated microporous polymers on PU sponges using a dip coating approach, Shi et al. created conjugated microporous polymer sponges, which exhibit a seawater evaporation rate and solar thermal conversion efficiency of 1.33 kg $m^{-2}h^{-1}$ and 86.3% respectively [198]. Tsang's group prepared a thick multiple-surface solar evaporator in which a PU sponge is used as a supporting substrate to keep the evaporator floating on water and to induce faster water transportation to the top surface of the evaporator [114]. This evaporator provided a water evaporation rate and efficiency of 1.3 kg $m^{-2}h^{-1}$ and 78.5% respectively under 1 sun. A thermal-responsive PDMS/CNT-PNIPAM sponge was fabricated by Cai et al. which demonstrated seawater evaporation rate of 1.66 kg $m^{-2}h^{-1}$ under 1 sun [199]. Through thermo-controlled reversible switching wettability, this single-surface, smart sponge-based evaporator can achieve oil directional transport and automatically control desorption. Moreover, effective, and continuous evaporation was produced by the synergistic combination of high light-to-heat conversion capacity and superior salt resistance. Apart from these, several other sponges (i.e., commercial sponge [200], carbon sponge [201], lignocellulose-based sponge [202] etc.) have been reported for constructing solar steam generating devices. Recently, nature-derived loofah sponge has also gained attention for fabricating bio-derived solar evaporators due to its fibrous structure, low thermal conductivity, cost-effectiveness, and biocompatibility [203,204].

**Foams**

Foams are often considered as outstanding substrates for fabricating solar evaporators due to their microporous structure, low cost, chemical stability, and low thermal conductivity. A

hierarchical graphene foam was fabricated by Ren et al. by using Ni foam as substrate and growing a vertical graphene nanoplate array on the substrate by plasma-enhanced chemical vapor deposition growth method, which exhibited solar vapor conversion efficiency above 90% for seawater desalination [116]. Nickel foam [205] and copper foam [206] are generally used as supporting substrates for photothermal materials due to their strong structure and cost-effectiveness. Gao et al. synthesized one dimensional CuO nanowire and two-dimensional graphdiyne on copper foam for solar steam generation application which shows photothermal conversion efficiency of 91% [206]. The Cu foam act as a supporting structure and the CuO nanowires were responsible for solar absorption whereas the graphdiyne traps light by its structure and further increases the broadband light absorption capability of the solar absorbing surface by its intrinsic narrow bandgap. Except these for having special features like porous structure, mechanical, chemical, and thermal stability monolithic polymer-based foam has also been used as a substrate for solar evaporators [155,207,208]. He et al. utilized a polypyrrole (PPy) coated monolithic porous foam to evaporate water [209]. The evaporator can float on water keeping only one surface at air water interface as shown in **Fig. 7f**. The thermal image **Fig. 7g** also shows that heat is concentrated only on the top surface of the evaporator. Chen et al. fabricated durable monolithic polymer foam that shows an evaporation rate and efficiency of 1.1687 kg $m^{-2}h^{-1}$ and 80.5% respectively under 1 sun [155]. In addition to these, bio-derived foam [210,211], melamine derived foam [212] are also used for fabricating thick solar evaporators.

**Hydrogels and Aerogel**

Solar evaporator prepared by using polymeric material-based substrates like hydrogels [213–217] and aerogels [157,218–223] shows very high evaporation rate due to their super hydrophilicity, porous structure, and increased exposed surface area of evaporation [122,125,215,224–230]. In most cases, photothermal materials are incorporated with polymeric materials to produce hydrogel and aerogel-based thick solar evaporators. The presence of hydrogel in water generates three types of water due to polymer-water interaction,

which are known as free water, bound water, and intermediate water. Hydrogels create strong bond with water molecules by their polar functional groups (present in their hydrophilic polymeric chain) and create bound water (BW), intermediate water (IW) adjacent to bound water, and free water (no interaction with polymer chains). Compared to bulk water, less energy is required for the IW (as it interacts with fewer water molecules) to escape from the liquid surface by breaking the hydrogen bond [231,232]. Therefore, hydrogel-based solar evaporators may give a higher evaporation rate by reducing the enthalpy of vaporization of water. The amount of generated IW in the presence of hydrogel can be detected by Raman spectra [233,234]. Generally, The Raman peak appear near 3475 $cm^{-1}$ and 3570 $cm^{-1}$ for weakly Hydrogen bonded IW [234]. The proportion of IW, BW, and free water can also be measured from DSC measurement [233,235]. The equivalent evaporation enthalpy can be estimated by comparing the mass loss of water with mass loss of water in the presence of hydrogel under the same environmental condition (i.e., humidity, temperature) for the same surface area under the same power input (generally dark evaporation rate is measured) by the following equation [235–237].

$$U_i = \Delta H_w \times m_w = \Delta H_{wh} \times m_{wh} \quad (1)$$

Where $U_i$ = Power input, $\Delta H_w$ = Evaporation enthalpy for bulk water, $\Delta H_{wh}$ = Evaporation enthalpy of water in the presence of hydrogel, $m_w$ = Dark evaporation rate for bulk water, $m_{wh}$ = Dark evaporation rate for water in the presence of hydrogel

Zhou et al. prepared a hydrogel for wastewater treatment utilizing polyvinyl alcohol (PVA) and polystyrene sulfonate (PSS) to create a framework of two different polymeric chains and activated carbon as photothermal material which showed an evaporation rate of 3.86 kg $m^{-2}$ $h^{-1}$ with an energy efficiency of nearly 92% under 1 sun [235]. Xu et al. prepared a solar evaporator by utilizing starch as a cost-effective bio-hydrogel substrate and carbon nanotube as photothermal materials that shows an evaporation rate and efficiency of 2.77 kg $m^{-2}$ $h^{-1}$ and 88% under 1 sun [235]. Saleque et al. constructed a light-trapping textured bio-hydrogel using

agar-agar powder that generates seawater evaporation rate of 2.851 kg $m^{-2}h^{-1}$ with an efficiency of 91.17% under 1 sun illumination [238]. Except these Mao et al. fabricated a cryotropic hydrogel-based evaporator that shows the presence of 67% intermediate water content and a very high evaporation rate of 3.59 kg $m^{-2}h^{-1}$ under 1 sun illumination [239]. Aerogels are also very popular in the field of solar evaporators due to their porous structure, hydrophilicity, very low density, and low thermal conductivity. Gu et al. fabricated an integrated photothermal non-toxic aerogel with chitosan as a base and carbonized pomelo peel as solar absorbing material to make a solar evaporator that gives an evaporation rate of 1.78 kg $m^{-2}h^{-1}$ under 1 sun illumination [157]. Wen et al. fabricated a polypyrrole-based Janus aerogel for solar steam generation utilizing PVA as a base (for forming aerogel structure) which shows evaporation rate and efficiency of 1.68 kg $m^{-2}h^{-1}$ and 94.7% under 1 sun due to the reduced vaporization enthalpy [240].

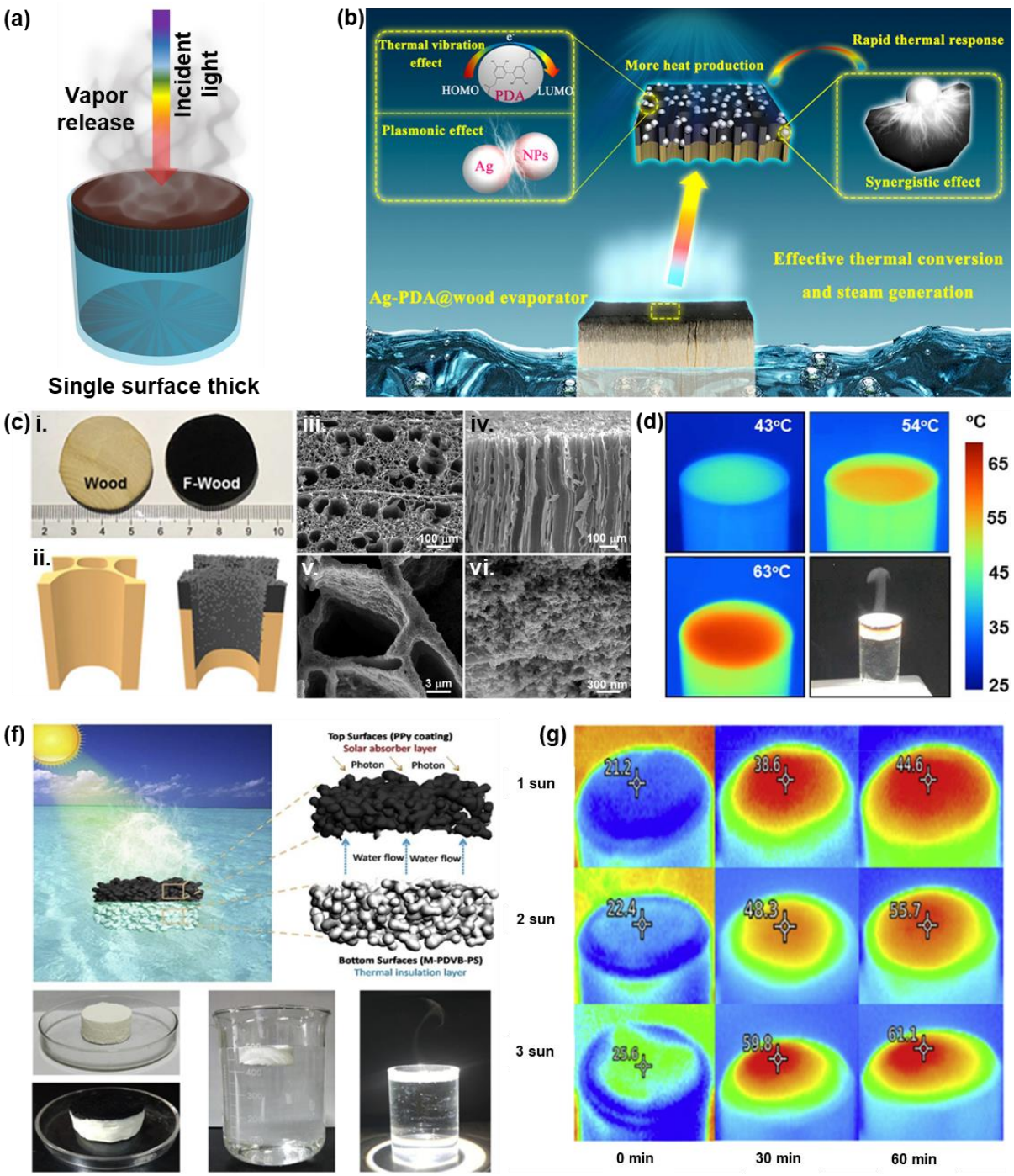


**Fig. 7.** Single surface evaporator (thick): (a) Schematic illustration of thick single surface evaporator (b) Schematics showing the synergistic photothermal effect of Ag nanoparticles and PDA coated on thick wood substrate[183]. Copyright 2020 American Chemical Society. (c) Flame-treated wood as a single surface thick evaporator (i) digital image of flame-treated wood (ii) Schematic inner structure of flame-treated wood, SEM image of (iii) top, (iv) cross-sectional and (v) inner pores of flame treated wood (vi) morphology of deposited carbon nanoparticles and (d) thermal image of the evaporator under different solar illumination [132]. Copyright 2017 American Chemical Society. Schematics of (f) polypyrrole-coated monolithic porous foam for ISSG with a digital image showing its self-floating capability and (g) thermal image showing the temperature distribution of this thick single surface evaporator at different solar irradiation [209]. Copyright 2019 Elsevier.

### *2.2.2. Multiple surface solar evaporator*

Multiple surface solar evaporators are generally fabricated using thick substrates. The substrate materials are similar to single-surface solar evaporators. The only difference is that, in the case of multiple surfaces, a significant area of the solar evaporators is kept above water as shown in **Fig. 8a**. Therefore, a large surface area (for spherical structures) or more than one surface area (for structures like cylindrical, conic, bar, etc) contributes to absorb energy and release vapor. The whole vapor releasing area can be divided into two regions or surfaces: hot solar absorbing region/surface and comparatively cool environmental energy gain region/surface. These types of evaporators can track the sun and absorb light from a broad range of light incident angles. The evaporation rate in the presence of these evaporators is higher for their high evaporation area index ($EAI$). $EAI$ can be denoted as the ratio of the total evaporative surface area to the projected ground area [241,242].

$$EAI = \frac{Total\ surface\ area}{Projected\ area} \quad (2)$$

Hence, for a multiple-surface cylindrical solar evaporator the $EAI$ can be calculated as

$$EAI = \frac{\pi\frac{d^2}{4} + \pi dh}{\pi\frac{d^2}{4}} = 1 + \frac{4h}{d} \quad (3)$$

Where, $d$ = diameter and $h$ = effective height of the cylinder. Hence by increasing the height of the cylinder, the $EAI$ can be increased which will lead to a higher evaporation rate. Finnerty et al. demonstrated that by increasing $EAI$ of an evaporator from 1 to 70, the evaporation rate can be increased from 1.8 kg $m^{-2}h^{-1}$ to 34.7 kg $m^{-2}h^{-1}$ [241]. It should be noted that an Increase in $EAI$ or increase in height not only increase vapor generation but also increases the Dark evaporation rate (as shown in **Fig. 8b and 8c**). Multiple surface solar evaporators of unique shapes have more area for releasing vapor and can harvest energy from the environment (**Fig. 8g**) and use that energy for vapor generation. Researchers have denoted this phenomenon as energy gain [37,38]. In multiple surface evaporator the temperature of the top surface is often higher than the side surface and most of the time the temperature of the side surface remains close to/lower than environmental temperature (**Fig. 8d, 8e**). The temperature

of the side surface decreases with increasing height and the environmental energy gain increases as shown in **Fig. 8e** and **Fig. 8f**. During the evaporation of water, the light of same intensity may not reach to every surface of the multiple-surface evaporator. Moreover, some areas of the evaporator may remain under shade, which can be considered as unexposed areas. The unexposed area is more obvious for multiple surface evaporators while light is projected on the evaporator from different angles as shown in **Fig. 8h**. Study shows that [114] the temperature of the unexposed area is lower than the environmental temperature as shown in **Fig. 8i**. This happens as the heat absorbed from the environment is used for evaporating water which reduces the surface temperature of light unexposed areas. Energy loss ($Q_{loss}$) to the environment from the hot surface and energy gain ($Q_{gain}$) from the environment at cold surface can be calculated by following equations [37,38] :

$$Q_{loss} = -A_h h(T_h - T_a) - \varepsilon\sigma A_h(T_h^4 - T_a^4) \quad (4)$$

$$Q_{gain} = -A_c h(T_c - T_a) - \varepsilon\sigma A_c(T_c^4 - T_a^4) \quad (5)$$

Here,

$A_h$ = Area of the hot region of the evaporating surface, $A_c$ = Area of the cold region of the evaporating surface, $T_h$ = Average temperature of the hot region of the evaporating surface, $T_c$ = Average temperature of the cold region of the evaporating surface, By adding $Q_{loss}$ and $Q_{gain}$ the overall heat loss or heat gain can be calculated.

Hence, creating multiple surface evaporators is a very effective strategy to increase the evaporation rate and efficiency of solar evaporator throughout the day [36,114,213,243–246]. Tang et al. achieved a low latent heat for a solar evaporator by regulating the hydrophilicity of the surface of burnt wood and make a multiple surface evaporator by tuning the height of the cylindrical shaped wood-based evaporator above the water surface [247]. The side surface of the evaporator contributed to the evaporation process by harvesting environmental energy for which the evaporation rate reached up to 3.91 kg $m^{-2}$ $h^{-1}$. Xu et al. reported an interesting all-in-one polymer sponge composite multiple surface evaporator for

simultaneous ISSG based desalination and electricity generation [246]. They made PVA (polyvinyl alcohol) sponges compounded with poly (3,4- ethylenedioxythiophene):poly(styrene sulfonate) and carbon nanotubes. This sponge composite had a hierarchical porous structure and demonstrated high light absorption as well as strong anti-salt fouling capability. Because of the increased evaporating surface area and the low evaporation enthalpy, this evaporator showed a high evaporation rate of 6.8 kg $m^{-2}$ $h^{-1}$ and an excellent evaporation efficiency of 94.9% under one sun. Moreover, a steady voltage of 117.8 mV is produced by the high-flux, directional saltwater flow caused by evaporation via the ionic channels of the sponges. Wang et al. fabricated a multiple surface evaporator utilizing an interpenetrating network sponge (a chitosan/gelatine-based sponge incorporated with melanin-coated titania hollow nanospheres) from natural polymer chitosan and gelatine for solar-driven wastewater treatment [248]. Due to the presence of hydrophilic hierarchical vertical channels in the sponge, the evaporator showed excellent water transportation capability. Moreover, the evaporator showed antibacterial properties for the formation of biofilm. Li et al. developed a central hollow cylinder of reduced graphene oxide (RGO) foam with radially and vertically oriented channels for effectively evaporating and purifying water using ISSG technique [244]. The channels with radial orientation transport water and transfer heat in radial direction in order to utilize the heat accumulated by the central hole of the foam, whereas the channels with vertical orientation facilitate transportation of water to the top surface of the evaporator. The foam's central hole accelerates the evaporation of water by accumulating more heat, and the newly formed inner sidewall that results from the hole can absorb additional thermal energy from the environment in a similar way to the foam's outer sidewall due to the surface cooling effect of the water evaporation. Because of these factors, this multiple-surface RGO foam evaporator produced a high solar steam generation rate of 2.32 kg $m^{-2}h^{-1}$ with an excellent energy conversion efficiency of 120.9% under 1-sun illumination. Anukunwithaya et al. demonstrated a bio-based thick multiple surface sponge evaporator (aerogel) with a tunable porous structure fabricated with chitosan (CS), agarose (Aga) and multiwalled carbon

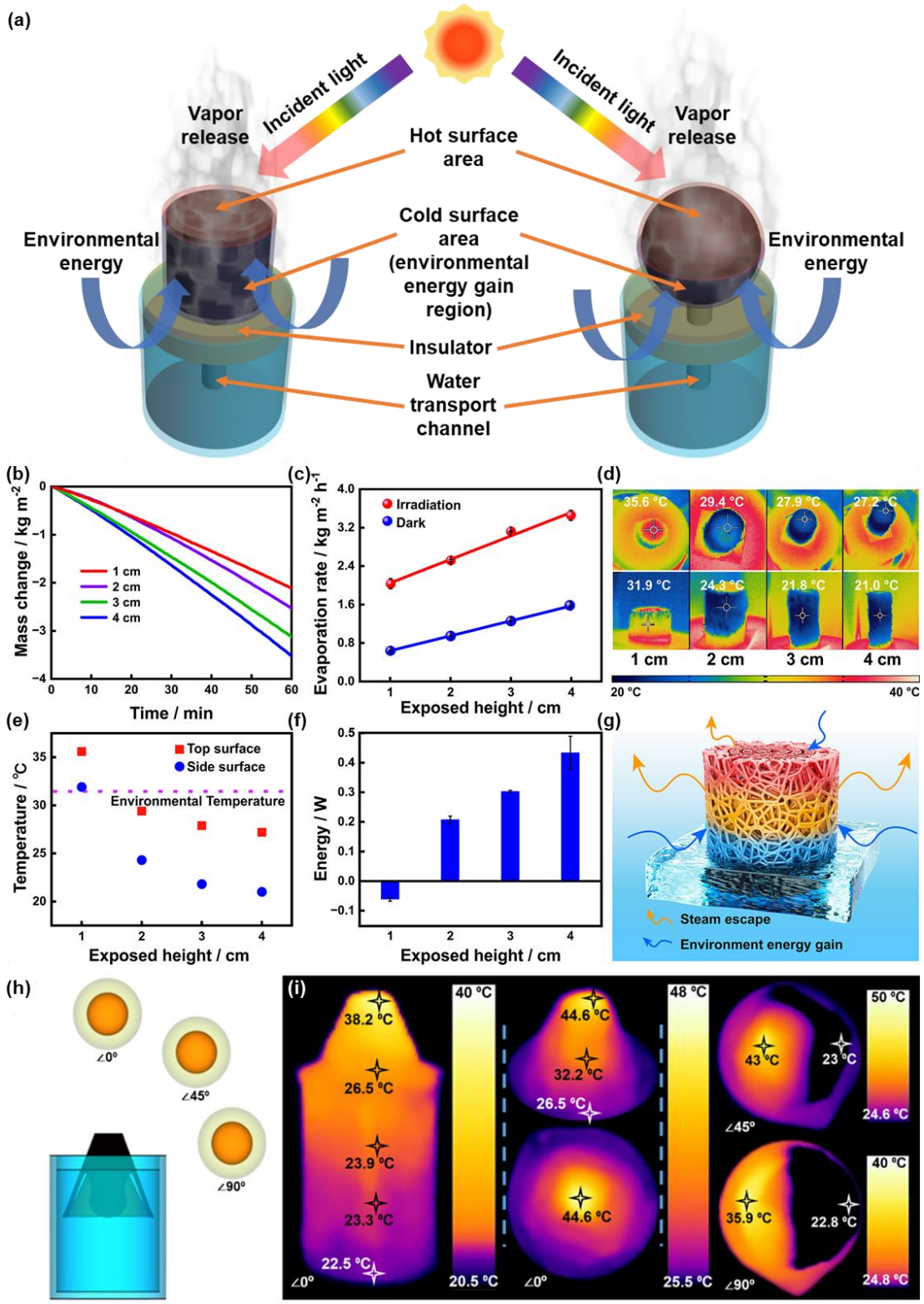


**Fig. 8:** Multi-surface evaporator: (a) Schematics showing the hot surface and cold surface of the evaporators. With different heights of the evaporator (b) mass change over time (c) evaporation rate under dark and 1 sun (d) IR image showing temperature distribution (e) temperature of sidewall and the top surface (f) net input energy (g) schematics showing energy gain and steam escape [249]. Copyright 2023 American Chemical Society. For different light incident angles (h) Schematics showing light absorption by evaporator (i) thermal image showing temperature distribution [114].Copyright 2022 American Chemical Society.

nanotubes (MW) [250]. The sponge evaporator was constructed by applying mechanical blending followed by freeze-casting and drying, yielding a monolithic aerogel structure. By varying the CS to Aga ratio, the pore structures of the sponge can be tuned. Moreover, they have tested the performance of the solar evaporator for both single-surface and multiple-surface structures by adjusting the height of the device above the water reservoir surface. The evaporator showed excellent evaporation rates of 2.24 kg $m^{-2}h^{-1}$ and 3.07 kg $m^{-2}h^{-1}$ for 30 mm and 60 mm height respectively which are beyond the theoretical limit for conventional 2D evaporators. However, they have also demonstrated that salt accumulation increases with the increase in height of the evaporator above water. Chen et al. fabricated a multiple-surface hydrogel bar using an industrial carbon nanotube and polyacrylamide for solar steam generation and demonstrated a maximum evaporation rate of 62.26 kg $m^{-2}h^{-1}$ for a 25 cm long bar [242]. They have demonstrated that the evaporation rate can be increased to 72.28 kg $m^{-2}h^{-1}$ by increasing the bar size to 35 cm long and by introducing a downward water supply where instead of capillary force, gravitational force is used to push water through the hydrogel bar. They have further demonstrated that if multiple bars are utilized, a proper distance is required to be maintained between two bars for efficient utilization of thermal energy from the environment or else the evaporation rate will decrease. For multiple bar system the maximum evaporation rate of 12.22 kg $m^{-2}h^{-1}$ was obtained.

Table 1: Performance comparison of different low dimensional photothermal material-based solar evaporators.

| Photothermal material | Substrate | Efficiency (%) | Evaporation rate (kg $m^{-2}h^{-1}$) | Solar irradiation (1 sun = 1 $kWm^{-2}$) | Type of water | Claimed behavior | Absorbance (%) | Structure of the evaporator | Ref. |
|---|---|---|---|---|---|---|---|---|---|
| $WO_{3-x}$ Nanorod | Natural wood | 82.5 | 1.28 | 1 Sun | Seawater | Plasmonic | 94 | Single surface (Thick) | [193] |
| rGO/$Cu_{7.2}S_4$ | Poly (vinyl alcohol)/Polyacrylamide (PVA/PAM) hydrogel | 96.65 | 2.19 | 1 Sun | Seawater | Plasmonic + Carbon | - | Multiple surface | [122] |
| $LaNiO_3$ | Cellulose membrane | 96 | 2.3 | 1 Sun | Seawater | Metallic | - | Multiple surface | [251] |
| Au−CuS Nps | Helical networks of gyroid photonic crystals from the wing of butterfly | 88.8 | 1.54 | 1 Sun | Water | Plasmonic | - | Single surface (Thin) | [105] |
| SiO2/MXene (nanosheets) | Hydrophilic poly(tetrafluoroethylene) (HPTFE) membrane | 85.6 | 1.53 | 1 Sun | Distilled Water | Plasmonic | 93 | Single surface (Thin) | [148] |
| Ternary Pt/Au/$TiO_2$ (nanoparticles) | Wood | 90.4 | - | 10 Suns | Water | Plasmonic | - | Single surface (Thick) | [192] |
| MXene and protonated g-$C_3N_4$ nanosheets | Natural latex foam | 93.5 | 1.85 | 1 Sun | Water | Metallic | 93 | Single surface (Thick) | [252] |
| GO/MXene ($Ti_3C_2Tx$) | Polytetrafluoroethylene (PTFE) | 90.7 | 1.27 | 1 Sun | Water | Carbon + Metallic | - | Single surface (Thick) | [253] |
| MXene ($Ti_3C_2Tx$) | Kapok fiber | 90.4 (water) 82.87% (oily wastewater) | 1.47 (water) 1.40 (oily wastewater) | 1 Sun | Water/oily wastewater | Metallic | 97 | Single surface (Thick) | [254] |
| Ag@MXene ($Ti_3C_2Tx$) | Polyacrylonitrile | 92.4 | 2.08 | 1 Sun | Water | Metallic | 93 | Single surface (Thin) | [255] |
| MXene ($Ti_3C_2Tx$) | Cellulose Acetate fiber-based cigarette filter | 132.9 | 3.38 | 1 Sun | Water | Metallic | 97 | Multiple surface | [256] |
| MXene($Ti_3C_2Tx$) /CNT | Cotton fabric | 88.2 | 1.35 (water) | 1 Sun | Water and textile | Carbon + Metallic | 93.5 | Single surface (Thin) | [177] |

| | | | | | | | | | |
|---|---|---|---|---|---|---|---|---|---|
| | | | 1.16-1.27 (textile Wastewater) | | wastewater | | | | |
| MXene ($Ti_3C_2Tx$) | Montmorillonite (MMT) gel | 93.7 | 1.36 | 1 Sun | Seawater | Metallic | >94 | Single surface (Thick) | [257] |
| MXene ($Ti_3C_2Tx$) | Montmorillonite (MMT) | 84.86 | 1.22 | 1 Sun | Water | Metallic | 84 | Single surface (Thin) | [258] |
| MXene ($Ti_3C_2Tx$) | Polyimide | 81 | 14.4 | 4 Sun | Water | Metallic-plasmonic | - | Multiple surface | [259] |
| MXene ($Ti_3C_2Tx$) | Cellulose | 85.8 | 1.44 | 1 Sun | Water | Metallic-plasmonic | 94.1 | Single surface (Thin) | [260] |
| MXene ($Ti_3C_2Tx$) | Cellulose | 90.7 | 2.71 | 1 Sun | Water | Metallic-plasmonic | 97 | Multiple surface | [228] |
| MXene ($Ti_3C_2Tx$) | Cellulose Acetate | 86.7 | 1.33 | 1 Sun | Water | Metallic | 93.2 | Single surface (Thin) | [261] |
| MXene ($Ti_3C_2Tx$) | Cellulose Acetate | 92.1 | 1.47 | 1 Sun | Seawater | Metallic | - | Single surface (Thin) | [262] |
| MXene ($Ti_3C_2Tx$) | Polypropylene (PP) filtration membrane | 94.3<br>91.7 | 1.67<br>14.52 | 1 Sun<br>10 Sun | water | Metallic plasmonic | 96 | Single surface (Thin) | [263] |
| MXene ($Ti_3C_2Tx$) | wood | 88 (for combined solar and electrical energy input) | 1.624 (Higher than only 1 Sun light energy input) | 0.5 Sun light energy + 2.5 V electrical supply | water | Metallic | 99 | Multiple surface | [264] |
| $WO_{3-x}$ | Ni foam | 88 | 1.5 | 1 Sun | Seawater | Semiconductor | 95 | Single surface (Thick) | [265] |
| Vanadium dioxide, $VO_2$(M) nanoparticles | Poplar wood | 75.60 | 3.63 | 3 Sun | Caspian seawater | Semiconductor | - | Single surface (Thick) | [266] |
| $CuS/Sn_2S_3$ | Mixed cellulose ester (MCE) membrane | 82.93 | 1.42 | 1 Sun | Seawater obtained from Rose Bay Beach, Sydney, as well as a simulated wastewater containing organic dyes | Semiconductor | 92 (dry state)<br>98 (wet state) | Single surface (Thick) | [267] |
| Black $TiO_2$ ($BTiO_2$) | No substrate (PVDF binded film) | 77.14 | 1.16 | 1 Sun | Distilled water | Semiconductor | - | Single surface (Thin) | [268] |

| | | | | | | | | | |
|---|---|---|---|---|---|---|---|---|---|
| $CuFeMnO_4$ | Quartz glass fibrous (QGF) filter membrane paper | A net efficiency close to 100 | 2.04 | 1 Sun | Seawater (Red Sea) | Semiconductor | - | Multiple surface | [269] |
| Aluminophosphate | Wood | 90.8 | 1.423 | 1 Sun | Seawater | Semiconductor | 98 | Single surface (Thick) | [270] |
| $MnO_2$ nanowires | Chitosan | 90.6 | 1.78 | 1 Sun | Simulated sea water, water from Shahu Lake, Wuhan, China, Oil emulsions | Semiconductor | 94 | Multiple surface | [226] |
| D-$HNb_3O_8$ (Oxygen vacancy defect-rich $HNb_3O_8$ Nanosheets) | Polymeric Polyacrylamide (PAM) | 91 | 1.4 | 1 Sun | Water | Semiconductor | 90 | Single surface (Thin) | [229] |
| $Ti_2O_3$ nanoparticles | Cellulose membrane | Nearly 100 (Internal)<br>Nearly 92 (External) | 1.32 | 1 Sun | Seawater | Semiconductor | 92.5 | Single surface (Thin) | [271] |
| $CuFeSe_2$ nanoparticles | Wood | 86.2 | 6.6 | 5 Suns | Water | Semiconductor | 99 | Single surface (Thick) | [98] |
| Hybrid compound $[Ni(Phen)_3]$ $[V_{14}O_{34}Cl]Cl$ | Mesoporous glass | 111.4 | 14.38 | 6 Suns | Water | Semiconductor | - | Single surface (Thin) | [103] |
| CuS (thin films) | Mixed cellulose ester (MCE) membrane | 80 +- 2.5 | 1.12 | 1 Sun | Water | Semiconductor | 85 | Single surface (Thin) | [272] |
| CuO | Polyvinyl alcohol/ Chitosan (PVA/CS) | 87.1 | 2.14 | 1 Sun | Water | Semiconductor | 95 | Multiple surface | [230] |
| $Co_3O_4$@PDA-rGO (nanoparticles) | Commercial cellulose–cotton sheet | 107 | 3.71 | 1 Sun | Pure water | Semiconductor | 96.4 | Multiple surface | [125] |
| $MoS_2$/$LaF_3$/PDMS ink (PDMS: Polydimethylsiloxane) | Polytetrafluoroethylene (PTFE) membrane | 91 | 1.76 | 1 Sun | DI water | Semiconductor | - | Single surface (Thin) | [160] |

| | | | | | | | | | |
|---|---|---|---|---|---|---|---|---|---|
| $Co_3O_4/Ti_3C_2$ MXene composites | Non-woven fabric | 130.4 | 1.89 | 1 Sun | Pure water | Semiconductor | 94 | Multiple surface | [38] |
| rGO (reduced Graphene Oxide) | Filter paper | 85.6 | 1.37 | 1 Sun | water | Carbon | 88.3 | Single surface (Thin) | [127] |
| rGO/FeNi nanocomposites | Poplar Wood | 98.36 | 4.19 | 3 Sun | Seawater | Carbon | 96 | Single surface (Thick) | [126] |
| rGO | Mixed cellulose esters (MCE) membrane | 71.8 ± 3 | 2.282 g water evaporated in 30 mins | 4 Sun | water | Carbon | - | Single surface (Thin) | [273] |
| Chinese ink | Wood | 74 | 1.6 | 1 Sun | 3.5wt% NaCl solution | Carbon | >98 | Single surface (Thick) | [274] |
| $BiVO_4$-rGO composite | Hydroiodic acid-based hydrogel | 87 | 1.6 | 1 Sun | water | Semiconductor + Carbon | - | Single surface (Thick) | [275] |
| Melanin nanoparticles + rGO | Aerogel composed of Sodium Alginate | 93.9 | 2.64 | 1 Sun | water | Carbon | - | Single surface (Thick) | [276] |
| Carbon black nanoparticles | Polydopamine (PDA) coated non-woven fabric | 91.5 | 1.68 | 1 Sun | water | Carbon | 95.2 | Single surface (Thin) | [277] |
| Carbon Black | Cellulose/Alginate matrix | 90.6 | 1.33 | 1 Sun | water | Carbon | 97 | Single surface (Thick) | [225] |
| rGO | Polyurethane Foam | 81 | >11 | 10 Sun | water | Carbon | - | Single surface (Thick) | [128] |
| Carbon Black | Hyper-cross-linked polymer (HCP) [ C-[BzPy]Br-co-PhH] | 88.4 | 1.43 | 1 Sun | water | Carbon | 94 | Single surface (Thick) | [278] |
| GO | Polyacrylonitrile (PAN) | 92.63 | 2.27 | 1 Sun | water | Carbon | - | Multiple surface | [279] |
| rGO | Aerogel composed of 3-aminopropyltriethoxysilane (KH550)-modified hollow glass micro-spheres (HGM) | 89.13 | 1.4856 | 1 Sun | water | Carbon | 93 | Single surface (Thick) | [280] |
| rGO | Filter Paper fiber | 89.2 | 1.14 | 1 Sun | water | Carbon | - | Single surface (Thin) | [123] |
| Chinese ink | wood | 82.2 | 1.31 | 1 Sun | water | Carbon | ≈ 90 | Single surface (Thick) | [281] |

| | | | | | | | | | |
|---|---|---|---|---|---|---|---|---|---|
| Carbon black fiber | Polyester cotton | 98.6 | 1.48 | 1 Sun | water | Carbon | 97 | Single surface (Thin) | [282] |
| Carbon Black nanoparticles | Cloth composed of polymeric nanofibers | 83 | 1.24 | 1 Sun | Pure water | Carbon | 94 | Single surface (Thin) | [283] |
| rGO | Plant fiber sponge | 88.8 | 1.375 | 1 Sun | Seawater from the South China | Carbon | 95.5 | Single surface (Thick) | [284] |
| MnO2 Nanowire + reduced graphene oxide | Polypyrrole coated aerogel | 93.8 | 1.3542 | 1 Sun | Water | Semiconductor + Carbon | 100 | Single surface (Thick) | [285] |
| rGO | Spacer fabric | 86 | 1.4352 | 1 Sun | Water | Carbon | ≈ 88 | Single surface (Thick) | [286] |
| rGO | Melamine foam | 92.9 | 1.476 | 1 Sun | Water | Carbon | 95 | Single surface (Thick) | [124] |
| rGO | Polyester Fiber | 81 | 1.3578 | 1 Sun | Water | Carbon | 85 | Single surface (Thick) | [287] |
| rGO | Nickel foam | 83.4 | 1.33 | 1 Sun | Water | Carbon | 89 | Single surface (Thick) | [205] |
| Commercial ink | Filter paper | 85.8 | 1.25 | 1 Sun | Water | Carbon | 95 | Single surface (Thin) | [288] |
| rGO | Commercial cotton sheet | 178.6 | 7.6 (absolute evaporation rate) | 1 Sun | Water | Carbon | 97 | Multiple surface | [37] |
| Graphene Oxide (GO) | Carbonized aerogel composed of Polyvinyl alcohol (PVA) | 92 | 1.63 | 1 Sun | Water | Carbon | > 94 | Single surface (Thick) | [224] |

Table 2: Performance comparison of different biomass derived photothermal material-based solar evaporators.

| Photothermal material | Substrate | Efficiency (%) | Evaporation rate (kg $m^{-2}h^{-1}$) | Solar irradiation (1 sun = 1 $kWm^{-2}$) | Type of water | Claimed behavior (plasmonic/ metallic/ semiconductor) | Absorbance (%) | Structure of the evaporator | Ref. |
|---|---|---|---|---|---|---|---|---|---|
| Carbonized kelp | Fiber cotton | 84.8 | 1.351 | 1 Sun | Water | Carbon | 93 | Single surface (Thin) | [289] |
| Carbonized wood | wood | 87.7 | 6.89 | 5 Sun | Water | Carbon | 97 | Single surface (Thick) | [134] |
| Carbonized corncob | Corncob | ≈ 132 | 4.16 | 1 Sun | Water | Carbon | - | Multiple surface | [138] |
| Carbonized rice husk foam | Rice husk foam made of sodium dodecyl sulfate, 1-dodecanol and gum acacia | 71 | 1.0315 | 1 Sun | DI Water | Carbon | 92 | Single surface (Thick) | [211] |
| Carbonized corn straws | Citric acid treated Raw corn straws | 89.3 | 1.422 | 1 Sun | DI Water | Carbon | 96.5 (300 – 1000 nm) | Single surface (Thick) | [290] |
| Carbonized daikon | Fresh daikon | 85.9 | 1.57 | 1 Sun | Water | Carbon | 95.5 (visible) 93.5 (near Infrared) | Single surface (Thick) | [136] |
| Carbonized sawdust | Cellulose sponge | 91.5 | 0.967 kg/m2 (45 minutes) | 1 Sun | Water | Carbon | 96.8 | Single surface (Thick) | [291] |
| Carbonized potato | Ethanol treated potato slice | - | 3.18 | 1 Sun | Water | Carbon | - | Single surface (Thick) | [292] |
| Carbonized poplar wood | Poplar wood | 86.7 | 12.1 | 10 Sun | Water | Carbon | 92 | Single surface (Thick) | [185] |
| Carbonized Lotus Seedpod | Lotus Seedpod | 86.5 | 1.3 | 1 Sun | Water | Carbon | 98 – 99 | Single surface (Thick) | [293] |
| Carbonized Loofah Sponge | NaOH treated Loofah | 83.7 | 1.36 | 1 Sun | Water | Carbon | 84 | Single surface (Thick) | [294] |
| Fractal carbonized pomelo peels with Polypyrrole nanowires | Pomelo peels | 92.4 | 1.95 | 1 Sun | Water | Carbon | 98 | Single surface (Thick) | [295] |

| | | | | | | | | | |
|---|---|---|---|---|---|---|---|---|---|
| Carbonized rice straw powder and bacterial cellulose | Cellulose paper | 75.8 | 1.2 | 1 Sun | 3.5 wt% salt water | Carbon | 89.4 | Single surface (Thin) | [296] |
| Carbonized rice husk powder | Hydrogel composed of carbonized rice husk, Acrylamide, Methylenebisacrylamide and sodium dodecyl sulfate | 94 | 1.77 ± 0.05 | 1 Sun | 25 wt% salt water | Carbon | 93.4 | Single surface (Thin) | [297] |
| PAM treated carbonized bamboo leaves | Bamboo leaves | 91.9 | 1.75 | 1 Sun | Water | Carbon | 96.1 | Multiple surface | [298] |
| Carbonized beef bone | Beef bone | 80 | 1.82 | 1 Sun | Water | Carbon | 90.0–99.3 | Single surface (Thick) | [299] |
| Carbonized coconut fiber | Coconut fiber | 90.2 | 1.5 | 1 Sun | Water | Carbon | 87.3 | Single surface (Thick) | [300] |
| Carbonized platanus fruit | Platanus fruit | 81.3 | 2 | 1 sun | Water | Carbon | 95.4 | Multiple Surface | [73] |

## 3. Water transportation and thermal management techniques

For interfacial solar steam generation, it is very important to reduce heat loss to increase vapor generation efficiency and hence, thermal management techniques play an important role in this field. Sometimes, Heat loss depends on the type of water reservoirs. For example, the solar evaporator can be placed on the top surface of open water or on the top surface of a closed water reservoir like water tank [301]. If the water tank is designed with proper heat-insulating material, heat loss to open water from evaporator will be reduced and therefore, increase solar evaporation efficiency [301]. Almost all solar thermal evaporation systems utilized some form of thermal management system and in the case of floated solar evaporators, these systems can be classified as hydrophilic bilayer structures, structures with dedicated water transport channels, and hanging structures [301]. The bilayer structure uses two layers the top layer is used for the absorption of solar energy and the hydrophilic bottom layer is used for thermal insulation, transportation of water, and keeping the evaporator afloat on water [302]. In the case of a structure with a dedicated water transport channel, instead of using the whole bottom layer for water transportation, some independent wicks [303] or capillary tubes [123] are inserted through the floating heat insulator for water transportation, which reduces heat conduction to the water from underneath the floating structure and thus reduces heat loss. For hanging structures, the solar evaporator is kept hanging and the water is supplied to the evaporator from both sides of the hanging structure [301,304]. The air gap between the hanging structure and the water works as an insulator, which reduces heat loss. Therefore, it can be said that the thermal management technique is influenced by the type of water transport channels. Researchers have integrated 1D and 2D water channels into the structure of solar evaporators to limit heat conduction loss and boost photothermal conversion efficiency [228,305–307]. Therefore, in general the water can be supplied to the evaporators in 3 different ways: i) by direct water contact (**Fig. 9a**) ii) 1D water transport route (**Fig. 9b**) and iii) 2D water transport route (**Fig. 9c**).

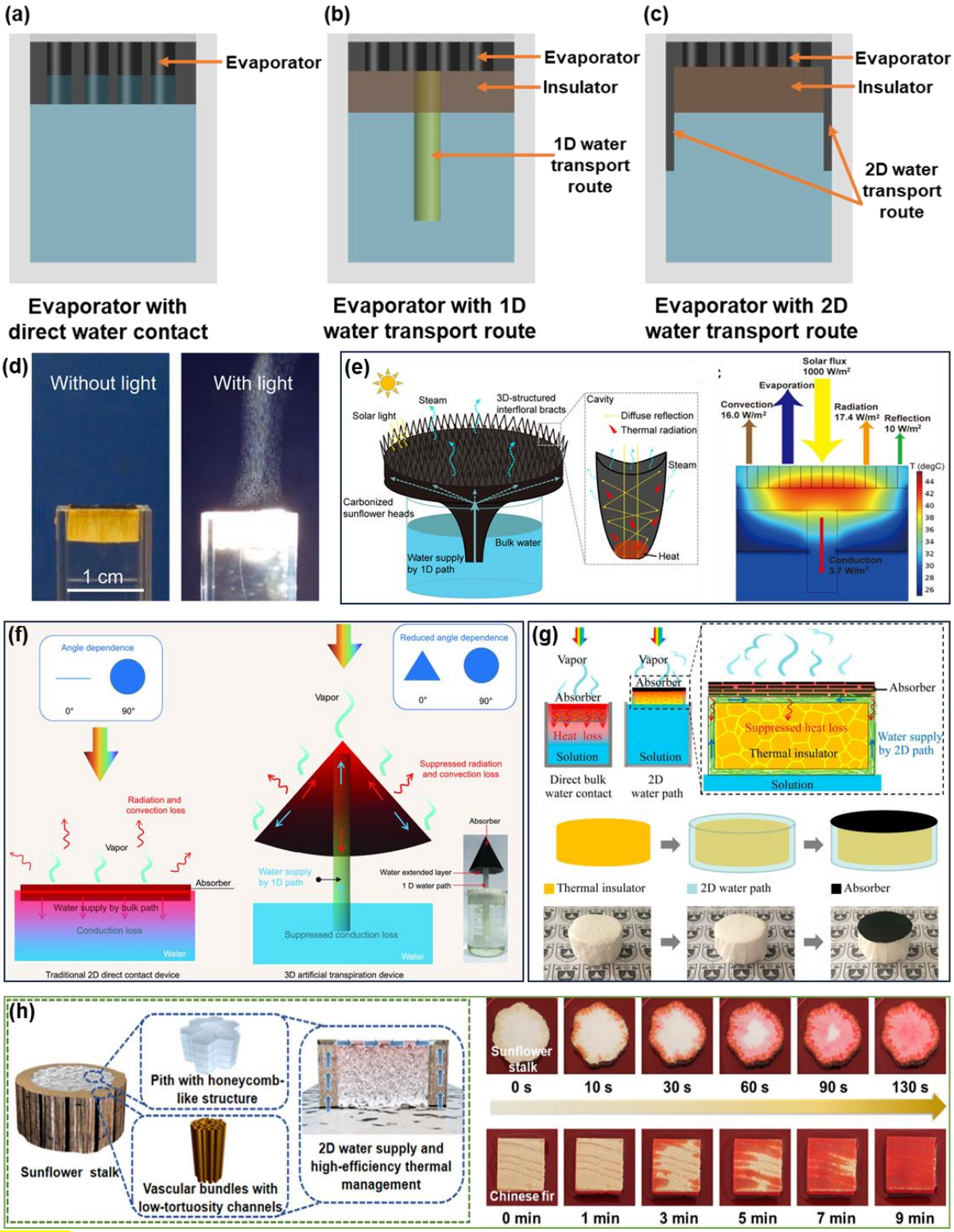


**Fig. 9.** Water transport path and thermal management system. Schematic illustration of evaporator with (a) direct water contact (b) 1D water transport route (c) 2D water transport route. (d) Wood based evaporator with direct water contact [110]. Copyright 2017 American Chemical Society. (e) Schematics of carbonized sunflower heads with 1D water transport route showing the heat losses [131]. Copyright 2020 American Chemical Society (f) Solar evaporator with 1D water transport route [308]. Copyright 2017 Oxford University Press (g) evaporator with 2D water transport route with associate thermal management system

[309]. Copyright 2023 National Academy of Science (h) Solar evaporator with 2D water transport route from sunflower stalk [310]. Copyright 2021 American Chemical Society

The performance of the solar evaporator can be influenced by selecting a proper water transport system. Sometimes for having the advantage of low thermal conductivity of the supporting substrates, some thick solar evaporators (i.e., wood-based evaporators, sponge/foam-based evaporators) are placed directly on the water as shown in **Fig. 9d**. The thermal conductivity of the substrate determines the conductive heat loss from the evaporator to bulk water during ISSG. A substrate with low thermal conductivity ensures heat localization in a specific area by reducing heat loss from the hot surface of the evaporator and hence it is a very important parameter. The thermal conductivity of a substrate depends on its moisture content. For instance, the thermal conductivity of a flame-treated wood was recorded as 0.33 W $m^{-1}$ $K^{-1}$ and 0.54 W $m^{-1}$ $K^{-1}$ for dry and wet conditions [132]. For basswood, the thermal conductivity was claimed to be 0.26 W $m^{-1}$ $K^{-1}$ during dry conditions, which increases to 0.46 W $m^{-1}$ $K^{-1}$ when it becomes wet [133]. A substrate is considered suitable to place directly on water if its thermal conductivity is low. Therefore, sometimes sponge (thermal conductivity nearly 0.644 W $m^{-1}$ $K^{-1}$) based solar evaporators are also placed directly on the water [199]. It is worth to be mentioned that the thermal conductivity of water is nearly around 0.6 W $m^{-1}$ $K^{-1}$ [132,133,199]. However, heat loss by conduction from the evaporator to bulk water cannot be entirely prevented if the solar evaporator is placed directly on the water, which leads to a reduction in evaporation efficiency [307].

Therefore, to increase the efficiency it is better to keep the solar evaporator separated from direct contact with bulk water by a heat insulator and to introduce 1D and 2D water transport path for transferring water from bulk water body to solar evaporator. 1D water transport path is inspired by nature, where a plant absorbs water using its roots and supplies it to its leaves through a confined water transport path. This strategy is followed for solar evaporators with a 1D water transport channel where a hydrophilic material surrounded by heat-insulating material is used to absorb water from the bulk water body and supply it to the evaporator. For

example, Li et al. fabricated a 3D hollow cone shape solar evaporator and for water transportation, they utilized a 6 cm long cotton rod supported by a polystyrene (PS) foam. The cotton rod was inserted through the PS foam (as shown in **Fig. 9f**) and the overall system demonstrated solar vapor efficiency above 85% under 1sun [308]. Sui et al. inserted a cotton strip through a PS foam to supply water to a carbon black coated flower-like sponge-based solar evaporator that demonstrated an evaporation rate of 2.31 kg $m^{-2}h^{-1}$ under 1 sun [311]. the PS foam acted as a support structure as well as a heat insulator. Some researchers have utilized the natural 1D water transport channel of natural biomass as a water transport route. For example, Sun et al. utilized the stalk of sunflower as a 1D water transport route (**Fig. 9e**) and demonstrated that a 3D structured solar evaporator can be prepared by carbonizing sunflower head and the prepared evaporator with 1D water transport route can evaporate water at 1.51 kg $m^{-2}h^{-1}$ rate under 1 sun [131]. Xu et al. utilizes the fibrous stripe of carbonized mushroom surrounded by supporting foam as a quasi-water transport channel to supply water to the carbonized mushroom-based solar evaporator [135].

For constructing a 2D water transport channel, a hydrophilic material is used to surround a heat-insulating material. PS foam is a very popular heat-insulating body for its low thermal conductivity (nearly 0.04 W $m^{-1}$ $K^{-1}$) [312]. Li et al demonstrated that if a thin solar evaporator is placed directly on the water the evaporation efficiency becomes poor [309]. To increase the efficiency, they have constructed a 2D water transport route by wrapping a PS foam with a hydrophilic cellulose-based material (as shown in **Fig. 9g**) to supply water to the thin evaporator (prepared by using graphene oxide as solar absorbing material) which demonstrated efficiency near 80% under 1 sun [309]. Zhang et al. also used PS foam as a heat-insulating material as well as a support structure and a microporous hydrophilic polyester as a 2D water path for a solar evaporator that demonstrated an evaporation rate of 1.48 kg $m^{-2}h^{-1}$ and solar energy conversion efficiency of 98. 6% under 1 sun [282]. Liu et al. utilized a cylindrical EPE (expanded polyethylene) foam as a heat-insulating body due to its low thermal conductivity of 0.026 W $m^{-1}$ $K^{-1}$ and utilized a hat shaped flame treated melamine foam to

cover it to form a 2D water transport path and the system displays efficiency up to 87.9% under 2 sun [313]. Peng et al. has wrapped a polyethylene-covered cellulose aerogel with a treated hydrophobic soot-coated cloth and hydrophilic pristine cloth bilayer to prepare a Janus solar evaporator with 2D water transport route for seawater desalination application [305]. Liu et al. demonstrated 2D water transport route in sunflower stalk based solar evaporator (**Fig. 9h**) [310]. Except these heat insulators incorporated water transport routes; some other water transport systems were investigated for ISSG where instead of transferring water from bulk water body to evaporator by capillary effect, water is injected to the evaporator in a controlled way which is sometimes commonly termed as injection based water transport system [314,315].

The measurement of heat loss by conduction, convection, and radiation is important for showing the effectiveness of the thermal management system. Moreover, it can be used to validate the evaporation efficiency of the ISSG system as reduced heat loss means a gain in evaporation efficiency.

**Heat loss by conduction:**

Energy loss due to heat conduction from the evaporator to water can be calculated using temperature gradient and Fourier's law.

$$q_{cond} = kA\frac{\Delta T}{L} \tag{11}$$

Where, $k$ is the thermal conductivity of water and $\frac{\Delta T}{L}$ is the temperature gradient. So, the percentage of conductive heat loss can be calculated using the following equation,

$$\eta_{cond} = \frac{kA\frac{\Delta T}{L}}{Aq_s} = \frac{k\frac{\Delta T}{L}}{q_s} \tag{12}$$

$q_s$ = Incident solar flux per unit area.

Thermal conductivity of the substrate (i.e., wood, foam etc.) or the heat insulating materials (used to separate the evaporator from direct contact with water) plays an important role to

localize heat at the top solar absorbing surface and reduce heat loss by conduction. The rate at which heat can transfer by conduction through a unit cross section area is known as thermal conductivity. Thermal conductivity varies from material to material and can be measured by laser flash method [316]. In this method, one side of the target sample is heated by instantaneous laser pulse and a detector is used to log the response of temperature on the other side to determine the thermal conductivity by the following equation,

$$\lambda = \alpha \rho C$$

Where, $\alpha =$ thermal diffusivity along a particular direction, $\lambda$ = thermal conductivity, $\rho =$ density and C is the heat capacity.

One of the most used techniques is steady state method where the sample is sandwiched between two quartz glasses and placed on the heating source [317,318]. This creates 3 interfaces, heating source-glass1, glass1-sample, and sample-glass2. The temperature differences between the interfaces are measured and by using Fourier equation thermal conductivity is measured.

$$Q = -\lambda \frac{dT}{dx}$$

Where, $Q$ is the heat transfer rate, $dT =$ temperature difference between the interfaces and $dx =$ distance difference or thickness. If the thermal conductivity and thickness of the quartz glass is known, the heat transfer rate ($Q$) can be calculated by measuring the temperature of heating source-glass1 and glass1-sample interfaces. Later, by using the temperatures of glass1-sample, and sample-glass2 interfaces the thermal conductivity of the target sample of known thickness can be calculated.

Except that thermal conductivity of a material may be calculated from the DSC curve by using following equation derived from Fourier's law: [319]

$$Q = \lambda \Delta T \frac{A}{L} \quad (6)$$

Here, $A$ is the cross-sectional area of the sample and $\frac{\Delta T}{L}$ is the temperature gradient.

Hence

$$\lambda = \frac{QL}{A\Delta T} \quad (7)$$

The heat required to maintain the temperature gradient can be found from the difference between DSC readings at two different temperatures ($T_1$and $T_2$).

$$Q = H_2 - H_1 \quad (8)$$

**Heat loss by convection:**

From Newton's law of cooling, the convective heat transfer loss from evaporator to air can be measured by,

$$q_{conv} = Ah(T_{ase} - T_a) \quad (9)$$

Here, $A$ = effective surface area (area above water) of the evaporation, $h$ = Convective heat transfer coefficient of air in natural convection, $T_{ase}$ = Average temperature of the effective surface of the evaporator, $T_a$ = Ambient temperature

The ratio of the energy losses caused by the convective heat transfer can be calculated by the following equation.

$$\eta_{conv} = \frac{Ah(T_{ase}-T_a)}{Aq_s} = \frac{h(T_{ase}-T_a)}{q_s} \quad (10)$$

**Heat loss by radiation:**

The energy loss due to thermal radiation from the surface of the evaporator can be calculated using Stefan-Boltzmann's equation:

$$q_{rad} = \varepsilon A\sigma(T_{ase}^4 - T_a^4) \quad (11)$$

Here, $\varepsilon$ = emissivity of the effective surface of the evaporator, which can be calculated using following equations:

$$\alpha = 1 - R(\lambda) - T(\lambda) = \frac{\int_{250}^{2500} I(\lambda)(1-R(\lambda))d\lambda}{\int_{200}^{2000} I(\lambda)d\lambda} \quad (12)$$

$$\varepsilon = 1 - \alpha = \frac{\int R(\lambda) P_{Sun}(\lambda) d\lambda}{\int P_{Sun}(\lambda) d\lambda} \quad (13)$$

Here, $\alpha$ =solar absorptance, $R(\lambda)$ is the reflectivity function of the sample at different wavelength, $I(\lambda)$ is the light intensity function of the solar spectrum at different wavelength and $T(\lambda)$ is the transmitivity function of the sample at different wavelength. For non-transparent sample $T(\lambda)$ can be considered 0.

The radiation loss rate can be calculated by:

$$\eta_{rad} = \frac{\varepsilon A \sigma (T_{ase}^4 - T_a^4)}{A q_s} = \frac{\varepsilon \sigma (T_{ase}^4 - T_a^4)}{q_s} \quad (14)$$

**Efficiency calculation**

In an ISSG system the materials with photothermal conversion capability are used to convert sunlight to heat energy. A part of the generated heat is used for producing water vapor and the rest is lost in the form of heat by conduction, convection, and radiation. Total solar thermal evaporation system efficiency can be calculated by [39]

$$\eta_{TST} = \eta_{ST}(1 - \frac{T_1}{T_2}) \quad (15)$$

Here, $\eta_{TST}$ = Total conversion efficiency, $\eta_{ST}$ = Sunlight to heat conversion efficiency, $T_1$ = Environment temperature, $T_2$ = Stable evaporation temperature.

$$\eta_{ST} = E_\alpha - E_R = \frac{C * \int d\lambda \alpha(\lambda) E_s(\lambda) - \int d\lambda \alpha(\lambda) E_B(\lambda, T_2)}{C * \int d\lambda E_s(\lambda)} \quad (16)$$

Here, $E_\alpha$ = Whole sunlight absorption, $E_R$ = Heat radiation loss, $E_s$ = Solar Irradiation, $E_B(\lambda, T_2)$ = Blackbody radiation at $T_2$, $C$ = Concentration factor,

The water evaporation rate, $m_e$ can be calculated by following equation:

$$m_e = \frac{m_h}{A} \quad (17)$$

Here, $m_h$ is mass loss of water per hour due to evaporation and $A$ is the area of evaporation surface.

$$\eta_{se} = \frac{m_l\,(H_{LV}+Q)}{E_{in}} \quad (18)$$

$$H_{LV} = 1.91846 * 10^6 * [T_e/T_e - 33.91]^2 \quad (19)$$

$$Q = c * (T_e - T_w) \quad (20)$$

Here, $m_l$ = net evaporation rate (kg/m$^2$),

$$m_l = m_e - m_d \quad (21)$$

$m_d$ = dark evaporation rate, $E_{in}$ = energy input of the incident light (kJ/m$^2$h), $H_{LV}$ = is the latent heat required for vaporization of water (J/kg), $T_e$ = is the average temperature of the solar evaporation surface while evaporating water, $Q$ = is the required heat for increasing the temperature of water, $c$ = is the specific heat of water (4.2 J/gK), $T_w$ = initial temperature of top surface

## 4. Salt rejection mechanism

One of the biggest challenges of utilizing ISSG for seawater desalination is the growth of salt crystal on the top of solar absorbing surface as salt crystals reflect light and reduce solar absorbing capability of the evaporator. Moreover, the salt crystals block the internal microchannels of the evaporators and affect water transportation. Hence, the accumulation of salt crystals on the evaporator surface reduces the performance of the solar evaporator significantly. Except that the growth of salt crystals may reduce the lifetime of the evaporator by cracking the microchannels of the evaporator. Therefore, for desalination application solar evaporators are designed in such a way so that the accumulated salt can be cleaned or removed effortlessly. Researchers have proposed different types of evaporators with different salt mitigation mechanisms to solve this issue.[320,321] Here some of the most commonly used salt mitigation mechanisms will be discussed.

### *4.1. Salt-ion diffusion*

Salt-ion diffusion mechanism or natural salt diffusion is one of the most commonly used techniques that depend on the microchannels and wettability of the substrate. During ISSG the salt concentration of water at the top surface of the evaporator starts to increase due to the vaporization of water at a higher rate in the presence of a light source, which gradually leads to the formation of salt crystals. For some evaporators, this salt formation process is slow, and in the absence of a light source when the vaporization of water stops, these salt crystals start to dissolve and get back to the bulk water by the microchannels of the evaporator. Zhu et al. demonstrated this kind of self-cleaning mechanism by fabricating a plasmonic wood-based solar evaporator [61]. They have demonstrated that the accumulated salt (after 8 hours of evaporation of saline water under 5 sun illumination) on the top surface of the evaporator dissolved back into the water within 16 hours while the system was kept in dark condition. A similar self-cleaning mechanism was demonstrated by Bian et al for a carbonized bamboo-based 3D solar evaporator, where the accumulated salt (after 8 hours of evaporation of saline water under 2 sun) dissolves back to water within 16 hours of no light condition due to efficient water absorption and transportation capability of the evaporator [322].The evaporator fabricated by Zhang et al. showed slightly better performance, where the accumulated salt crystals were removed completely from the top solar absorbing surface within around 10 hours due to the super wettability of the cellulose acetate/carbon black-based evaporator [323]. Tsang's group prepared a 3D solar evaporator using waste egg trays and tonner which has also shown a salt ion diffusion mechanism due to wettability and high mass water absorbing capacity of the evaporator [114]. Considering the practical scenario of day-night conditions, this mechanism works well. However, this kind of self-cleaning mechanism is slow and may cause a decrease in evaporation performance during long-time desalination in the presence of the sun. To solve this issue Kuang et al. designed a self-regenerating solar evaporator that can stop the growth of salt during the daytime by drilling some arrays of holes (diameter 1 mm) on the wood substrate [186]. The substrate has natural microchannels of nearly 12 μm

and 50 μm diameters with pits of 1 – 2 μm diameter on their walls. The drilled wood was carbonized to make a solar-absorbing surface. When the evaporator was kept on water, the water flux in the drilled channel was higher than the natural microchannels following the fourth-power relationship between the xylems channel radius and flow through a capillary tube [324]. Therefore, in the presence of light when the vaporization of seawater takes place, the salt concentration of water becomes higher inside natural microchannels than drilled channels which creates a lateral salt gradient. The natural microchannels of wood contain several natural pits on their walls which facilitate lateral salt exchange between the microchannels and drilled channels and later the salt goes back to bulk seawater using the drilled channel of large diameter. This evaporator demonstrated excellent performance while evaporating 20 wt% NaCl concentrated water under 1 sun and the evaporation performance remained stable for a long period (over 100 h) of continuous operation as no growth of salt was observed during that period. Ebrahimi et al. demonstrated that the self-cleaning of salt in the presence of drilled channels can enhance the cycle life of the solar evaporator from 3 cycles to 11 cycles [325]. Zhang et al. incorporated the same salt mitigation mechanism for their solar evaporator by drilling some holes in a wood substate and coating one surface with Chinese ink for absorbing sunlight [274]. The effectiveness of drilled hole is demonstrated in **Fig. 10a(i, ii and iii)**. For this evaporator, no growth of salt was observed during the vaporization of 3.5 wt% NaCl concentrated water under 1 sun after 2 hours of continuous operation [274].

### *4.2. Direct Salt-blocking by Janus structure*

Janus evaporators have at least two surfaces that show different affinities toward water. In most cases, the Janus evaporators have a hydrophilic bottom surface and a hydrophobic top surface. The hydrophilic surface is responsible for absorbing water and transporting it to the area where heat is localized, whereas the hydrophobic surface is responsible for absorbing sunlight and releasing vapor. The vaporization of water occurs at the hydrophobic-hydrophilic interface and as the hydrophobic surface is responsible for releasing vapor, the thickness of this surface is kept low to keep the heat conduction path and vapor escape route short [326].

The hydrophobic solar absorbing surface blocks the climbing of saline water to the top surface of the evaporator and keep it at the hydrophobic-hydrophilic interface whereas the bottom hydrophilic water absorbing surface pumps a huge amount of water from the bulk water body and keeps the salt dissolved inside the microchannels of the evaporator. Therefore, no growth of salt is observed for this type of evaporator while evaporating saltwater for a long period of time [320]. Generally, the solar absorbing surface of the evaporator is made hydrophobic by coating it with hydrophobic solar absorbing material (i.e., MWCNT, candle shoot etc.), or with hydrophobic modifier. For example, Lv fabricated a 3D Janus evaporator by using radish as a hydrophilic supporting substrate and MWCNT as photothermal materials, which shows resistance against surface salt accumulation while evaporating 20 wt% NaCl concentrated water for 10 consecutive days [327]. For making the hydrophobic solar absorbing layer they have coated the sliced freeze dried radish with a mixture that contains MWCNT (solar absorbing material) and poly(vinylidene fluoride-*co*-hexafluoropropylene) (a linker and hydrophobic modifier). A flexible Janus evaporator was fabricated by Wang et al., which demonstrated resistance against salt growth while continuously evaporating saline water for 7 days [328]. A Janus evaporator with a directional salt transfer structure was demonstrated by Gu et al. which evaporated 10 wt% NaCl concentrated brine for 5 continuous days with an evaporation rate of nearly 1.21 kg $m^{-2}h^{-1}$ under 1 sun [329]. They have spray coated the solar absorbing surface with silane to make it hydrophobic. After coating with silane the water contact angle between water and the silanized hydrophobic surface became 134.5º. It is worth mentioning that a surface can be considered hydrophobic, if the static contact angle between water and surface become higher than 90º [330]. Chen et al. demonstrated that a hydrophilic solar absorbing surface initially (up to 2 hours) provides a slightly high evaporation rate than a hydrophobic solar absorbing surface of Janus evaporator while evaporating 10 wt% NaCl concentrated water [331]. However, with time the performance of the hydrophilic solar absorbing surface becomes lower while the performance of the Janus evaporator remains stable. Moreover, after 8 hours of evaporation, the internal structure of the Janus evaporator shows no obvious deposition of salt in the upper region. To prepare the Janus evaporator,

they have coated the melamine foam with Poly(dimethylsiloxane) (PDMS) as a hydrophobic modifier and Graphite powder as solar absorbing photothermal material. Except this Janus evaporator can be fabricated by 3D printing using hydrophobic composite powder for making solar absorbing surface and hydrophilic composite powder for making water absorbing bottom part of the evaporator [332]. The effectiveness of Janus solar evaporator in stopping salt growth is demonstrated in **Fig. 10b(i and ii)**.

### *4.3. Edge preferential salt crystallization*

Edge preferential salt crystallization is another proven concept for removing salt from the top middle surface of the evaporator. In this type of design, salt crystallization occurs at the edge of the evaporator surface and then falls from the surface by itself due to the influence of gravity. This mechanism can be established in an evaporator by controlling the water transportation property. Xia et al. constructed this type of evaporator with controlled water transport property and showed that using this mechanism both salt and usable water can be harvested without declining the evaporation rate much (almost stable evaporation rate) for 600 hours of continuous operation [333]. They have demonstrated the effectiveness of using one inlet (water transport path) to crystallize salts at the edge of the evaporator. Following the same concept, a bioinspired synthetic tree was designed by Shao et al. which demonstrated a steady evaporation rate of 2.03 kg $m^{-2}h^{-1}$ and solar thermal efficiency of 75% for more than 60 hours of continuous operation [334]. They have demonstrated that instead of homogeneous salt crystallization, a salt ring of a certain diameter can form on the top of the solar absorbing surface, and by observing this phenomenon a suitable diameter for the solar evaporator can be determined so that the salt crystallized at the edge of the evaporator as shown in **Fig. 10c**. Li et al. proposed a PVA hydrogel based thick multi-surface solar evaporator with a conical frustum structure which shows a stable solar desalination performance in high-salinity brine by activating edge-preferential salt crystallization [217]. For a cylindrical structured evaporator, concentration of water movement is highest at the center and therefore, salt tends to accumulate on the top surface and blocks light absorption and hinders vapor release. But

in case of a conical frustum structure, the circular cross-sectional area continuously increases as water transports from bottom to top through the evaporator. As a result, brine on the center is spontaneously transported towards the edge, inducing a radial brine transport. As evaporation continues, the concentration of water transport on the edge increases with time which leads to salt accumulation on the edge of the top surface and later, the deposited salt spontaneously falls back into the water and redissolves. A thick multi-surface evaporator with 3D cup-shaped design was proposed by Shi et al. from which salt can be harvested as a byproduct and the proposed evaporator continuously vaporized 25 wt% NaCl concentrated brine for nearly 120 hours with almost no reduction in evaporation rate [335].

### *4.4. Marangoni-driven salt removal*

Marangoni-driven salt removal techniques often end up with edge preferential or localized salt crystallization. Marangoni flow can be established in the solar evaporators by designing it in such a way so that a temperature gradient can be created in the evaporator while evaporating saline water in the presence of sun. Hence this mechanism is suitable for 3D structure or multiple surface evaporator. Marangoni flow from lower surface tension area to higher surface tension area of the evaporator is driven by thermo-capillary and solute-capillary force [336]. To introduce Marangoni flow by temperature gradient-induced surface tension difference, Zou et al. designed a solar evaporator with 3D bridge-arched structure that showed the capability of salt rejection for 200 hours of continuous operation while evaporating 10 wt% saltwater [337]. In the demonstrated evaporator, the evaporation rate at the top of the bridge is higher than the bottom part of the bridge due to the temperature gradient. Therefore, the liquid film present at the top of the bridge has a higher salt concentration than the bottom part of the bridge and bulk water. However, due to Marangoni flow inside the liquid film, transportation of liquid occurs from top of the bridge (high temperature and low surface tension area) to the bottom of the bridge (low temperature high surface tension area) and remove salts from the top surface area. The effectiveness and the mechanism of Marangoni driven salt removal is

demonstrated in **Fig. 10d**. A biomimetic cone shaped 3D structured multi-surface solar evaporator with localized salt crystallization capability was demonstrated by Wu et al. where Marangoni flow facilitates water supplementation to the top of the evaporator where the evaporation rate is higher [338]. For this biomimetic 3D evaporator, liquid flow occurs from the bottom (liquid film temperature around 34.5 °C) of the evaporator to the top (liquid film temperature 21.3 °C) under 1 sun illumination and as the salt concentration of the apex liquid film is higher due to higher evaporation rate of water, crystallization of salt occurs at the top of the evaporator (as shown in **Fig. 10e**) which can be removed and collected easily. The proposed evaporator evaporated 25 wt% salt concentrated water with energy efficiency and evaporate of 96% and 2.63 kg $m^{-2}h^{-1}$ respectively, under 1 sun. Shao et al. demonstrated that Marangoni flow can drives away the salt from the solar absorbing surface area [339]. They have conducted a 20-hour long experiment which showed that during the first 4 hours the crystallization of salt hinders the capillary-driven water flow and causes further salt accumulation over a larger area. After 4 hours the salinity gradient causes surface tension gradient in the wick and activates Marangoni flow. Therefore, solutions with low salinity move forward and dissolve the salt and the crystallization of salt occurs further away from its initial position which leads to edge preferential salt crystallization. During 36 hours of continuous testing of the system, the salt accumulated and crystallized outside the device. Except these, Marangoni-driven salt rejection, Marangoni-driven salt migration and edge preferential salt crystallization in solar evaporators are demonstrated by the researchers [340][341].

Except these salt removal mechanisms, sometimes new mechanism or combinations of two mechanisms are demonstrated for salt removal. Xia et al. proposed a cylindrical solar evaporator of ultra-high salt tolerance of 300 g $L^{-1}$ that demonstrates self-regenerating capability by self-rotation [342]. In this solar evaporator, salt starts to crystalize on the top of the evaporating surface during the vaporization of saline water. While a certain amount of salt is accumulated, an imbalance between gravity and buoyancy occurs which leads to self-rotation of the evaporator on water that facilitates the evaporator to remove salt from its

evaporating surface. Ivan et al. demonstrated that combining two different salt mitigation mechanisms (natural hole induced salt ion diffusion and direct salt blocking by thin hydrophobic solar absorbing surface) in an evaporator can facilitate stable evaporation performance while evaporating highly salt concentrated (20 wt% NaCl) water under high solar irradiation (up to 3 sun) [196].

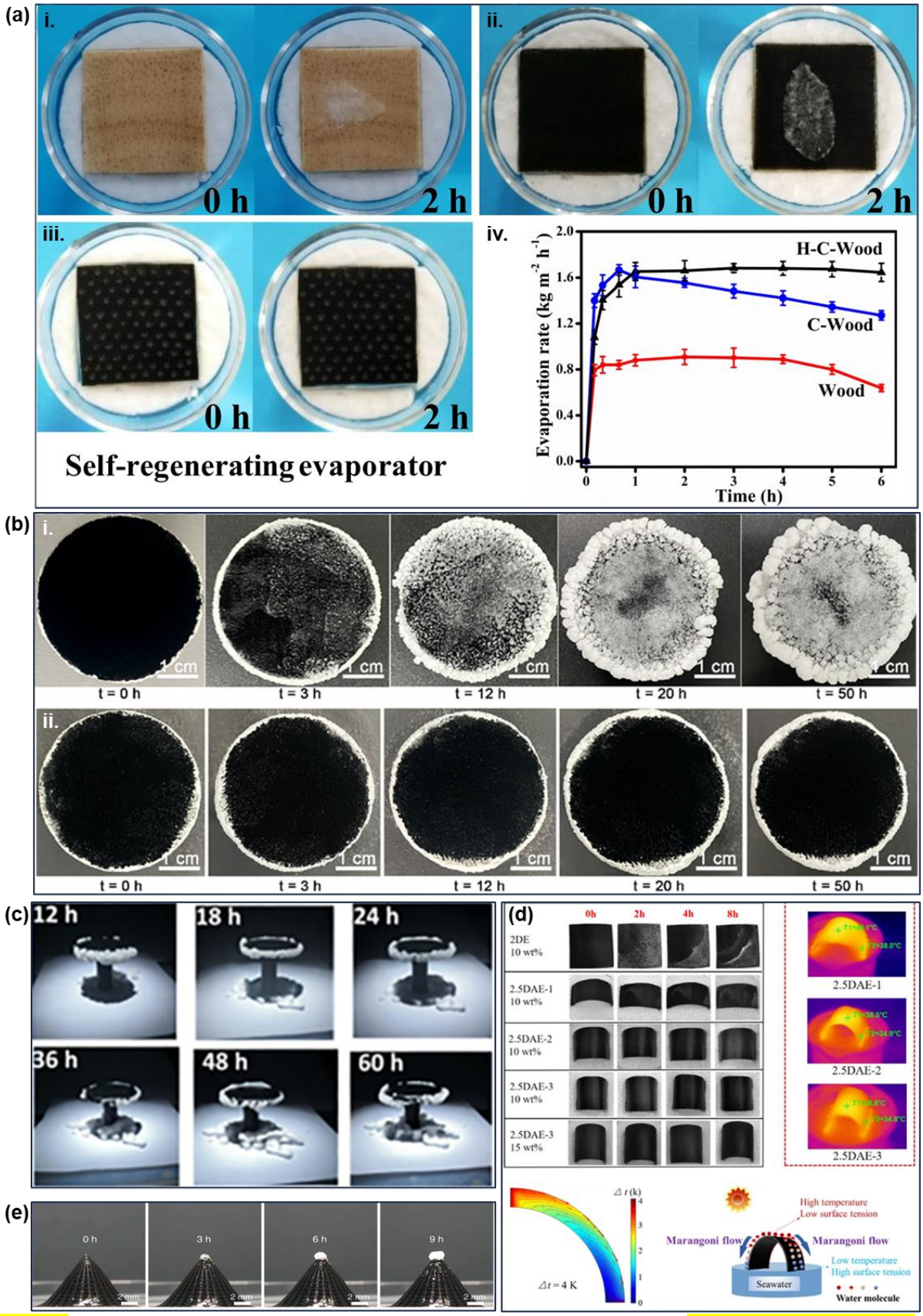


**Fig. 10.** Salt removal and localized salt crystallization mechanisms. (a) Salt diffusion facilitated by drilled hole: (i-ii) growth of salt (iii) no salt growth due to drilled hole [274]. Copyright 2020 Elsevier. (b) Effectiveness of Janus evaporator in blocking the growth of salt on the top of

evaporating surface: (i) hydrophilic surface, (ii) hydrophobic surface of Janus structure [332]. Copyright 2023 American Chemical Society (c) Edge preferential salt crystallization, keeping the evaporating surface free from salt growth and producing salt as biproduct [334]. Copyright 2020 John Wiley & Sons Australia, Ltd. (d) Effectiveness of Marangoni driven salt removal, and its mechanism (schematics) [343]. Copyright 2022 Elsevier. (e) Marangoni driven water flow from bottom to top, where evaporation flux is higher, resulting in localized salt crystallization [338]. Copyright 2020 the authors, Springer Nature.

## 5. Corrosion resistance

The seawater and wastewater are complex systems which may contain many microbes as well as acid and alkali-based substances that can deteriorate the performance of the evaporator by corroding its structure. Salt corrosion is also required to be considered while using evaporators for desalination. To solve these issues, materials of strong acid and alkali resistance, as well as salt resistance, can be used as substrates for the evaporator. Sometimes the coating of photothermal materials may have corrosion resistance properties. Some photothermal nanoparticles show the capability of stopping the growth of bacteria and hence can be used to construct a solar evaporator with anti-biofouling capability.

### *5.1. Resistance against Acid/Alkali-based substance*

Materials like Copper and Nickel etc. can be used as substrates for solar evaporators to provide resistance against corrosion, as these materials are known for their mechanical strength and corrosion resistance properties. Dong et al. chemically treated the surface of the copper foam to fabricate a corrosion-resistant copper-based membrane for efficient solar steam generation [344]. Li et al. fabricated a solar evaporator by utilizing porous nickel mesh as substrate with CNT as photothermal material for removing dye molecules and heavy metal ions from wastewater [345]. Sun et al. prepared a 3D porous NiAl substrate for fabricating a corrosion-resistant solar evaporator [346]. Carbon nanotube was deposited on the substrate by chemical vapor deposition technique to increase its light absorbing capability. The proposed intermetallic compound-based structure demonstrated resistance against salt, strong acid, and strong alkali solution. Moreover, the evaporator shows a high light absorption rate of 94.4% and a high evaporation rate of 2.41 kg $m^{-2}h^{-1}$ under 1 sun irradiance. Fu et al.

utilizes hierarchical porous metallic glass for its corrosion-resistant property to fabricate a solar evaporator that demonstrates a high evaporation rate and efficiency of 1.72 kg $m^{-2}h^{-1}$ and 94.2% respectively under 1 sun [347]. Li et al. demonstrated the effectiveness of carbon-coated glass fiber cloth as a corrosion-resistant solar evaporator [348]. To demonstrate the corrosion resistance property of the evaporator against strong acid and alkali 2 samples were prepared using carbon-coated glass fiber cloth. One sample was exposed to 0.2 M $H_2SO_4$ while another was exposed to 0.2 M NaOH solution. The Acid-treated and alkali-treated samples respectively retained 90% and 95% of the original sample's evaporation performance. To prevent salt corrosion a silicate-based solar evaporator composed of a polypyrrole-modified commercial sand core and basalt fiber was proposed by Zhang et al. which shows an evaporation rate and efficiency of 1.26 kg $m^{-2}h^{-1}$ and 85.9% respectively under 1 sun [349]. The presence of basalt fiber protects the solar evaporator from salt corrosion. Jin et al. prepared a washable nonwoven photothermal cloth composed of polymeric nanofiber as a supporting substrate and carbon black nanoparticles as light-absorbing material for solar steam generation purposes which has corrosion-resistant properties against acid alkali organic solvent and salty water [283]. Polyamide 6 graphene oxide (PA6-GO) membrane is highly stable and has strong alkali and acid corrosion resistance and hence Xu et al. fabricated a solar evaporator by decorating PA6-GO membrane with gold nanoparticle by vacuum filtration for solar steam generation [350]. A photothermal wood was prepared by He et al. by immersing wood substrate in tannic acid aqueous solution followed by a ferric sulfate solution [351]. A sample of photothermal wood (Poplar-Ta-$Fe^{3+}$) was treated with an acid solution of pH 2 and an alkaline solution of pH 12 for 24 hours. No change in color was observed for the prepared evaporator which demonstrates the acid and alkali resistance properties of the prepared evaporator. Yan et al. fabricated a super hydrophilic carbon nanofiber membrane for solar desalination of seawater considering the inherent anti-acid and anti-alkali corrosion properties of carbon nanofiber [352].

### *5.2. Resistance against Microbials*

Some micro-organisms present in seawater have the capability to adhere themselves with solar evaporators and this issue may limit the use of evaporators in practical application [353]. These micro-organisms and their metabolites can hamper the water transport channel of the evaporators. Moreover, with time the growth rate of these micro-organisms increases and later reduces the performance of the evaporator by reducing its light absorbing capability. Hence it is required to design solar evaporators with anti-biofouling capability. To demonstrate the anti-biofouling property of an evaporator, generally two types of bacteria (gram-positive, Staphylococcus aureus (*S. aureus*) and gram-negative, Escherichia coli (*E. coli*)) are used. Except that adhesion resistance of protein, chlorella, diatoms to the evaporator are also tested. Nanostructured metallic oxides like $TiO_2$, ZnO, CuO etc. are very well-known for their antibacterial property. $TiO_2$ nanoparticles are very well known for their stability and excellent photoactivation properties. In the presence of light, the photogenerated electrons and holes produced by $TiO_2$ nanoparticles facilitate the production of reactive oxygen species (ROS) which can effectively destroy the bacteria [354,355]. Moreover, in no light condition $TiO_2$ can change the permeability and morphology of the bacterial cell wall which leads to alteration of bacterial osmotic balance [354][355]. Hence inclusion of $TiO_2$ nanoparticles in solar evaporator can effectively stop the growth of bacteria. Mehrkhah et al. fabricated a solar evaporator by coating rGO and $TiO_2$ on poplar wood and demonstrated that a nanocomposite composed of rGO and $TiO_2$ in 1:2 weight ratio has high antibacterial activity [355]. Wang et al. incorporated ZnO nanoparticles in solar evaporator and mentioned its effectiveness in stopping the growth of bacteria as ZnO nanocrystals can produce ROS even in dark conditions [356][357]. ROS is very effective against bacterial growth. Hence photothermal materials capable of producing ROS are used for fabricating solar evaporators. To prepare a 3D solar evaporator with anti-biofouling capability Li et al. utilized aggregation-induced-emission active molecule (AIE-luminogens) as photothermal materials that can produce ROS in the presence of the sun [358]. CuO nanoparticles show a bactericidal effect by damaging the bacterial cell membrane [359].

Therefore, the inclusion of CuO nanoparticles in the solar evaporator can stop the growth of bacteria [230]. Positive Cu ions released by CuO nanowire mesh can integrate themselves with the negative cell membrane of bacteria that leads to the leakage of intracellular substances and later causing the death of bacterial cells and hence Xu et al. fabricated a solar evaporator using CuO nanowire mesh which demonstrated evaporation efficiency of 84.4% under 1 sun and stopped the growth of both *E. coli* as well as *S. aureus* effectively [360]. $TaTe_2$ quantum dots have an affinity for the sulfur proteins present in the bacterial DNA which makes it effective against both *E. coli* and *S. aureus.* Tsang's group fabricated a light trapping textured bio-hydrogel incorporating $TaTe_2$ quantum dots and reduced graphene oxide (rGO) and demonstrated the effectiveness of $TaTe_2$ quantum dots against bacterial growth [238]. In recent years, some photothermal MXenes based anti-biofouling solar evaporators have been reported [255,260,361]. MXene (i.e., $Ti_3C_2T_X$) is considered to be a highly effective bacteriostatic agent as it can stop the growth of bacteria. The rough and sharp edges of $Ti_3C_2T_X$ sheets can cause physical stress on bacteria which leads to membrane damage and the formation of $TiO_2$ can impose oxidative stress on bacteria which also ensures long time antibacterial activity [260]. Huang et al. fabricated a laser-induced graphene wood-based solar evaporator and demonstrated that the oxygen functional groups present in the laser-induced graphene can minimize bacterial biofouling and protect the wood from decaying [190]. Ag nanoparticles are very well-known photothermal material in the field of ISSG due to their LSPR mechanism and antibacterial property [362,363]. Ag nanoparticles can release positive Ag which can be absorbed by bacteria that leads to damage of bacterial DNA. Moreover, after damaging one bacterium positive Ag ion attack the next bacteria and hence it has long-lasting antibacterial effect [363]. Except these, many solar evaporators with anti-biofouling capability have been reported in the field of ISSG [183][364,365]. Peng et al. fabricated a hydrogel consisting of polypyrrole, sulfobetaine methacrylate (SBMA), and [2-(methacryloyloxy)-ethyl] trimethylammonium chloride (METAC) for solar steam generation and demonstrated the capability of composite P(SBMA-co-METAC) hydrogel to repeal both gram-positive and gram-negative bacteria, algae (chlorella) and proteins (FITC-BSA) [353]. They have demonstrated

that by increasing PSBMA segment in hydrogels the proteins adsorption can be decreased. They have also demonstrated that increasing PSBMA segment (SBMA segment is higher in $S_{10}M_0$ than $S_0M_{10}$) can decrease chlorella adhesion in hydrogel (as shown in **Fig 11e**). Wen et al. developed a Zwitterionic hydrogel-coated floater for solar steam generation which shows resistance against both *S. aureus* and *E. coli as well as* protein (FITC-BSA) and diatom (*Navicula parva*) [366]. They have shown that the presence of ZCB (Zwitterionic PolyCBAA) reduces the growth of *E. Coli* significantly as shown in **Fig. 11d**. The antibacterial activities of specific materials can be demonstrated by exposing the solar evaporators with and without those specific materials to bacterial suspension for a certain time period and taking the SEM images (as shown in **Fig. 11a**). Another way can be co-culturing bacteria in the presence of the specific antibacterial materials or agent and cultivate this experimental group in agar plate under suitable environmental condition (temperature 37 °C) for a certain period and compare it with the control experimental result where the bacteria was cultured without exposing it to the specific antibacterial agent (control group). After the cultivation, the antibacterial ration can be obtained by counting the colonies of bacteria using the following equation [353],

$$\text{Antibacterial ration}(\%) = \frac{CN_C - CN_E}{CN_C} * 100 \quad (22)$$

Here $CN_C$, and $CN_E$ represents the statistical colony numbers of the controlled group and experimental group respectively.

The bio-adhesion of protein test is generally conducted by incubating the samples of evaporator (with and without antibiofouling agent) with FITC-BSA solution under dark. The adhesion of protein can be observed by relative fluorescence intensities. The sample capable of resisting the adhesion of proteins demonstrates week fluorescence intensity (as shown in **Fig. 11b**) [353,366]. Except these the samples can be co-incubated with diatom as well as chlorella to demonstrate the effectiveness of the evaporator against the adhesion of such microbials. In these cases, optical image/ optical microscopy image is utilized to count the

adhered diatoms (**Fig. 11c**) and algae (**Fig. 11e**) to evaluate the antibiofouling property of the evaporator [353,366].

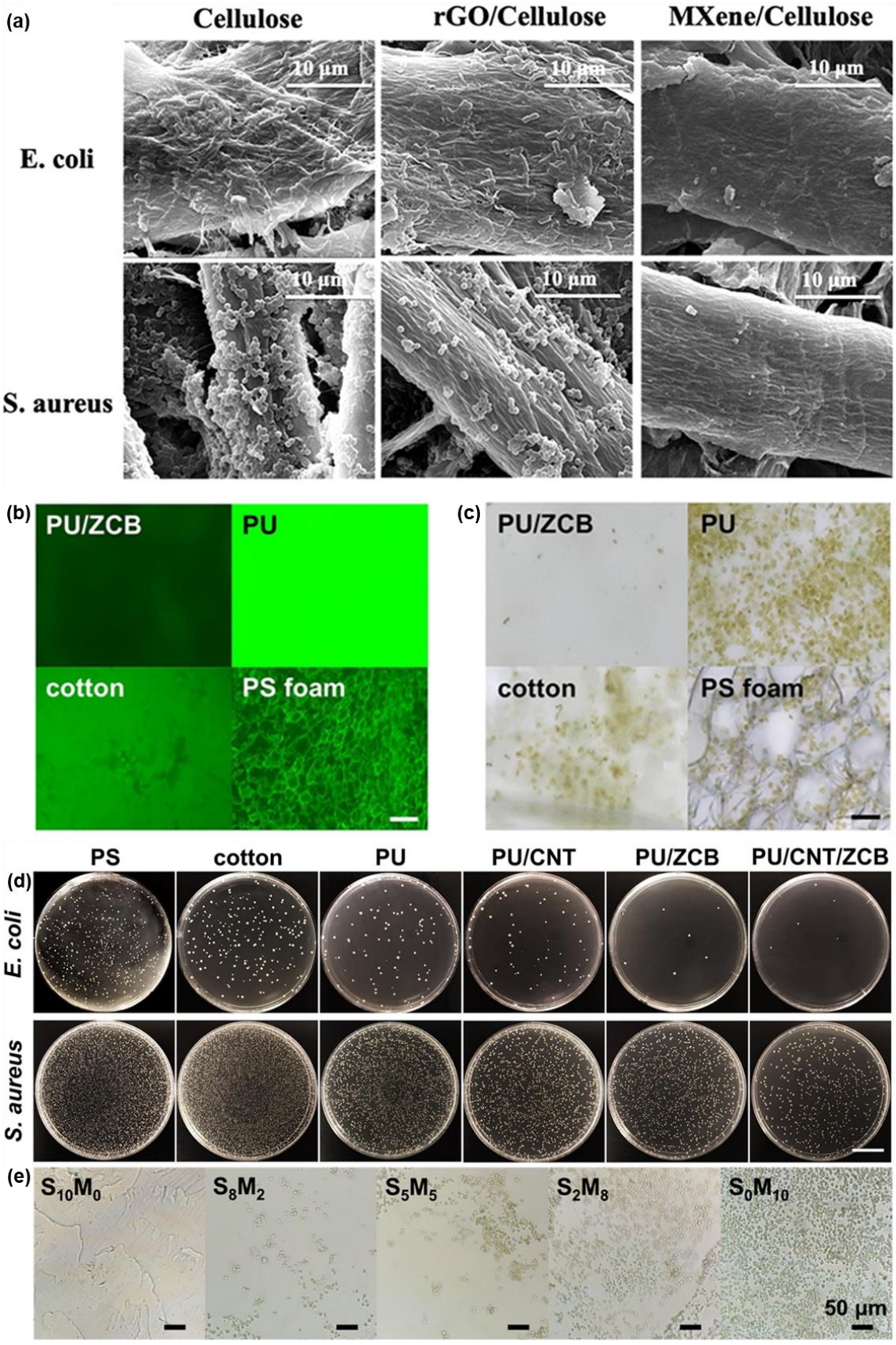


**Fig. 11.** Antibiofouling property. (a) SEM image showing the effectiveness of MXene in preventing bacterial adhesion [260]. Copyright 2019 American Chemical Society. (b) Protein (FITC-BSA) adsorption of various surfaces shown by fluorescence microscopy images,

demonstrating the effectiveness of ZCB (Zwitterionic PolyCBAA) to prevent protein adhesion [366]. (c) Optical image showing the effectiveness of ZCB to prevent diatom adhesion [366] (d) optical image demonstrating the effectiveness of CNT/ZCB in preventing bacterial adhesion [366]. Copyright 2021 Elsevier. (e) Optical microscopy image demonstrating the effectiveness of the evaporators (with different monomer ratio SBMA/METAC) in preventing chlorella adhesion [353]. Copyright 2022 American Chemical Society.

## 6. Anti-oil fouling

From different studies, it has been observed that in most cases researchers have evaluated the performance of solar evaporators in evaporating different dye contaminated, heavy metal ion-contaminated water (as model wastewater) and seawater or saline water (as simulated seawater). From a practical point of view, due to many unwanted accidents, oil is spilled into the sea from ships and oil extraction stations. Also, oily wastewater from industries eventually ends up in the sea. If the evaporator does not have the oil rejection capability, the surface of the photothermal materials may be contaminated and in the worst case, the water transport channels may get blocked and eventually the evaporation performance may degrade over time and make the evaporator unusable or inefficient. Therefore, it is also crucial for solar evaporators to have anti-oil fouling capability. Recently, different methods have been utilized for adding oleophobic properties to ISSG devices [141,226,253,254,351,367–370]. Generally, the ISSG evaporator is made oleophobic by coating the surface of the substrate with polymer solutions that contain functional nanoparticles with oil-repellent capability. Chen et al. fabricated a solar evaporator by carbonizing the mixture of basalt fiber and tissue paper [369]. Despite giving a high energy conversion efficiency for water, this non-oleophobic evaporator showed only 26% energy conversion efficiency in oily water [369]. Chen and group then made oleophobic modification by spray coating the surface of the substrate with a polymer solution (Polydiallyl dimethylammonium chloride (PDDA) - sodium perfluorooctanoate (PFO) / $SiO_2$ suspension in ethanol). PDDA-PFO polymer can be synthesized by reaction between PDDA and PFO in water at room temperature. The presence of fluorinated groups as well as carboxyl and quaternary ammonium groups in PDDA-PFO polymer helps to make the coating oleophobic and super hydrophilic [224,367,369]. This modified evaporator showed a very high

energy conversion efficiency of 81% in oily water [369]. Xia et al. chemically surface coated fluorine and $Al_2O_3$ nanoparticles to fabricate a super hydrophilic and oil repellent solar evaporator [367]. Once the evaporator is coated for oleophobic modification, its hydrophilicity and oil separation capability are checked using wettability and oleophobic tests. Normally, droplets of water and n-hexadecane are placed on the evaporator's surface and contact angle is measured to evaluate its water absorption and oil separation respectively. Xia et al. conducted an oleophobic test by placing a drop of n-hexadecane on the treated surface of the evaporator. Because of coating with oil repellent fluorine and $Al_2O_3$ nanoparticles, the surface had a contact angle of $139^0$ with n-hexadecane and consequently the solar energy conversion efficiency of the evaporator increased from 48% to 79% [367]. In oily wastewater, the bottom surface of the evaporator which is in contact with water, may be fouled by oil droplets and water absorption can be hindered drastically due to blockage of water transport channels through pores. He et al. applied an underwater oleophobic test to verify the performance of their Tannic acid and $Fe^{3+}$ treated wood evaporator in different oil emulsified water [351]. The underwater soybean oil and crude oil contact angles of the evaporator surface were measured as $162^\circ$ and $158^\circ$ which proved the oleophobic property. Except that, Wu et al. designed a suspended membrane multiple surface evaporator where only a small area with oleophobic property is kept under water keeping the evaporating and environmental energy consuming area above water [371]. This prevents oil volatilization as the heating surface is not in direct contact with the oily wastewater. Earwood et al. demonstrated that $TiO_2$ coating on basalt membrane improves the anti-crude oil fouling property [368].

## 7. Application

ISSG technique is suitable for seawater desalination as well as wastewater purification application. Recent studies show the effectiveness of solar evaporators in removing salts, dyes, heavy metal ions and oils from contaminated water. Moreover, the steam generated from solar evaporators can also be used to sterilize medical equipment. Except these the application of ISSG was also observed for combined hybrid applications like simultaneous

water and hydrogen production, water and electricity generation etc.[372]. Wang et al. propose a system for simultaneous steam and electricity generation by utilizing salinity gradient and temperature gradient between evaporation surface and bulk water, induced by interfacial evaporation [373]. They propose to integrate thermogalvanic cell and reverse electrodialysis into an interfacial solar evaporation system to harvest electrical energy and their system generates vapor at the rate of 1.4 kg $m^{-2}h^{-1}$ and electricity of 1.11 $Wm^{-2}$ simultaneously under 1 sun illumination. The use of Thermoelectric (TE) module is another way of using temperature gradient for electricity generation. Ren et al. incorporated TE module with solar evaporator ($MnO_2$-decorated cotton cloth) to generate electricity and vapor simultaneously [374]. Zhu et al. prepared a solar evaporator by coating CNT/cellulose nanocrystals nanocomposite on a PDMS sponge for water evaporation with an efficiency of 87.4% under 1 sun and by adding a thermoelectric module beneath it they demonstrated the potential of electricity generation [375]. Moreover, by incorporating photocatalytic material with ISSG, hydrogen (H2) generation can be increased. For example, Guo et al. demonstrated that photocatalytic H2 production can be boosted by constructing a photothermal-photocatalytic system [385]. They have carbonized the surface of natural wood (biomass-derived photothermal carbon) for solar vapor generation and spin-coated CoO nanoparticles (low dimensional photocatalytic material) as a photocatalyst on carbonized wood for H2 production. Han et al. carbonized the surface of pretreated pine wood for vapor generation and loaded $TiO_2$ on a carbonized layer by brush painting method for H2 production [386]. They have claimed that that vapor generated by photothermal carbonized wood creates a solid/gas reaction interface with a lower gibbs free energy, facilitating TiO2 to generate H2 by photocatalytic reaction without the requirement of noble metal-based co-catalyst. Except that, Gao et al. demonstrated the simultaneous generation of Water and $H_2$ using a photothermal catalytic gel [62]. The application of ISSG in hybrid system is very vast and therefore, the importance of photothermal materials is increasing. Hybrid systems are comparatively complex and different hybrid system has different working mechanisms; therefore, in this section, only the usual applications of ISSG-based devices are discussed.

### *7.1. Seawater desalination*

Solar evaporators are designed mainly to perform desalination by which usable or drinkable water can be produced from sea water. Salt contents of sea water near the surface are mostly the same all over the world and $Na^+$, $K^+$, $Mg^{2+}$ and $Ca^{2+}$ ions are the four major constituents [376]. The presence of excessive Sodium ion makes the water undrinkable, and the amount of Magnesium and Calcium ion determines the hardness of water. Hard water (high amount of $Mg^{2+}$ and $Ca^{2+}$) is responsible for sedimentation inside the water supply line. Therefore, the concentration of these ions in the desalinated water is commonly used as an indicator to prove the purity of water obtained after the desalination process. According to the standard set by World Health Organization (WHO), the concentrations of $Na^+$, $Ca^{2+,}$ and $Mg^{2+}$ in pure drinking water should be less than 200, 100, and 25 mg $L^{-1}$ respectively [377]. This benchmark is generally followed to verify the drinkability of the desalinated water produced by solar evaporators. The concentration of ions in water is generally measured by inductively coupled plasma mass spectroscopy (ICP-MS). Wu et al. designed a thick single-surface solar evaporator using carbonized sawdust for seawater (Bohai Sea) desalination [291]. This evaporator showed excellent desalination performance by reducing the concentrations of $Na^+$, $Mg^{2+}$, $K^{+,}$ and $Ca^{2+}$ in seawater from 15000, 7000, 900, and 900 mg $L^{-1}$ to 1.1, 0.99, 0.28, and 0.15 mg $L^{-1}$ respectively in the desalinated water with an ion removal rate of >99.9%. Li et al. successfully produced drinkable water (as per WHO standards) from seawater by using $WO_{3\_x}$ nanorod-decorated wood evaporator [193]. They demonstrated that salt ion concentrations in seawater before desalination ($Na^+$ = 9800, $Mg^{2+}$ = 980, $K^{2+}$ = 360, and $Ca^{2+}$ = 350 mg $L^{-1}$) were significantly reduced in desalinated pure water ($Na^+$ = 5.12, $Mg^{2+}$ = 0.43, $K^{2+}$ = 2.33 and $Ca^{2+}$ = 3.1 mg $L^{-1}$) produced by vapor condensation [193]. Han et al. demonstrated that after solar desalination of natural sea water (collected from Bo Sea, China) the concentration of $B^{3+}$ ion also reduced as shown in **Fig. 12a** [378] .

The quality of water can also be assessed by checking the electrical conductivity/resistivity. The conductivity of seawater is higher than purified water due to the presence of salts.

Therefore, its resistivity is less than that of the water obtained from evaporation-condensation process. The higher the resistivity of the purified water as compared to seawater, the better is the quality of the water. Li et al. verified the quality of the evaporated water by comparing the electrical resistance of seawater and the evaporated water [244]. The resistance of seawater and desalinated water was measured using a multi-meter by maintaining the same distance between electrodes. The resistance of seawater and desalinated water was measured as 175.1 kΩ and 1.53 MΩ respectively. Almost a nine-fold increment in resistance of condensed water indicates a significant reduction of salts from seawater after desalination.

Researchers also estimate total dissolved solids (TDS) to verify the quality of desalinated water. TDS mainly determines the palatability of water and according to WHO standards, water is said to have superb palatability if TDS is less than 300 ppm [114]. Except that, salinity, pH value, and conductivity of the purified water are also checked. TDS (ppm), salinity (%), pH, and conductivity (µS/cm) of seawater and purified water can be tested by water quality tester EZ-9909 SP to verify the quality of water before and after desalination [114]. As per WHO standards, the pH value of drinking water should be in between 6.5 and 8.5 [51]. Tsang's group measured the TDS, conductivity, salinity, and pH value of seawater as 29,950 ppm, 52.3 mS/cm, 3.14%, and 6.97 respectively before desalination whereas after desalination, the TDS, conductivity, salinity, and pH value of the purified water were measured as 26 ppm, 57 µS/cm, 0% and 7.63 respectively, which indicates the production of high-quality water [51].

### *7.2. Wastewater purification*

ISSG systems can also be used for industrial wastewater purification. Industries like paper, printing, spinning, textiles, dyeing, food processing etc. use different types of organic dyes/colors. Hence industrial wastewater contains various types of dyes. To check the effectiveness of solar evaporators in wastewater purification, different dye aqueous solutions such as Methyl Orange (MO) [305,379], Methyl Blue (MB) [36,196,355,380], Rhodamine B (RhB) [36], Reactive Black 5 (RB5) [380], Congo Red (CR) [196,350], Eriochrome Black T (EBT) [196] etc. are used as simulated industrial wastewater. Normally the dye aqueous

solution has a specific color due to the presence of a specific dye. After evaporation, if the condensed water becomes transparent, then it may be concluded that the wastewater purification is achieved. Moreover, UV-vis absorbance spectra for both dye-contaminated solution and purified water are observed and compared to verify the absence of dye in purified water as shown in **Fig. 12c**. Industrial wastewater also contains heavy metal ions like $Ni^{2+}$, $Cu^{2+}$, $Zn^{2+}$, $Pb^{2+}$, $Cd^{2+}$, $Cr^{6+}$, $Fe^{2+}$, $Hg^{2+}$ etc., and hence simulated wastewater containing these ions is often used to check the capability of the ISSG system to remove these ions from simulated wastewater [257,305,355,380]. Concentration of these ions in purified water is compared with WHO standards [381] to verify the effectiveness of ISSG system in wastewater purification. The inductively coupled plasma mass spectrometry (ICPMS) is commonly used to estimate the concentration of ions. Mehrkhah and the group prepared 1000 mg $L^{-1}$ simulated wastewater solutions of $Ni^{2+}$, $Zn^{2+}$, $Pb^{2+}$, $Cd^{2+}$, $Cr^{6+,}$ and $Fe^{2+}$ to check wastewater purification performance [380]. After testing their designed solar evaporator in the simulated wastewater, they found that the concentration of heavy metal ions reduced considerably ($Cd^{2+}$ = 0.007, $Cr^{6+}$ = 0.1, $Fe^{2+}$ = 0.003, $Ni^{2+}$ = 0.01, $Pb^{2+}$ = 0.003 and $Zn^{2+}$ = 0.01 mg $L^{-1}$) which indicates good quality of water as per WHO standards. Han et al. demonstrated that after purifying artificial wastewater by their solar evaporator, the concentration of heavy metal ions (i.e. $Cu^{2+}$, $Cr^{3+}$, $Pb^{2+}$ and $Zn^{2+}$) goes below 0.1 mg $L^{-1}$ in treated water as shown in **Fig. 12b** [378]. Except that, Sewage water can contain $NO_3^-$ which is very water soluble and may cause diseases like diabetes at high concentrations. The carbonized pinecone multiple surface evaporator fabricated by Shafaee et al. can reduce the concentration of $NO_3^-$ in sewage water from 12 mg $L^{-1}$ to 2.5 mg $L^{-1}$ [379].

### *7.3. Oil-water separation*

For evaluating the oil-water separation capability as well as anti-oil fouling capability of the solar evaporator, researchers have mainly investigated the performance of the evaporator in oily solutions like various oil emulsified water [141,226,253,351,368,371] and n-hexadecane [224,254,369]. The verification of oil separation capability of the evaporator is normally done

by wettability and oleophobic tests [224,254,369]. Except that digital image of oil contaminated water and purified water can be used to demonstrate the oil removal capability of solar evaporator. However, this observation method is not sufficient to quantify the performance of the evaporator in purifying oil contaminated water. Oily water contains organic compounds which should not be present in the purified water. Hence to quantify the performance of the evaporator in separating oil from water, total organic carbon measurement (TOC) is conducted by TOC analyzer for oil contaminated water and purified water found from vapor condensation [368,371]. Earwood et al. demonstrated that the TOC values of oily water and collected purified water (from vapor condensation) were 13.4 mg $L^{-1}$ and 1.62 mg $L^{-1}$ respectively, indicating that $TiO_2$ coated evaporator can remove 88% organic compounds from oily water [368]. The ISSG system proposed by Wu et al. achieved oil removal efficiency of 99.8 % and 98.8% for soybean oil and n-decane emulsions respectively. For both cases the TOC of purified water by solar distillation was found to be less than 30 mg $L^{-1}$ as shown in **Fig. 12d(ii)** [371]. The image of soybean oil emulsion before and after purification is also demonstrated in **Fig. 12d(i)**. Oil separation is a key performance defining factor for ISSG devices considering practical implications. Therefore, further research is required focusing on making the evaporators effective in separating oil from water.

### *7.4. Sterilization*

Researchers have also demonstrated the potential of ISSG technique in sterilizing surgical tools, medical equipment etc. effectively. Conventional medical sterilization process, which is known as autoclaving, normally uses saturated steam at high temperature (>121$^{o}$C) and pressure (>205 kPa) [382]. But these traditional sterilization devices available in the market need electricity for their operation. Moreover, they cannot be regarded as low-cost devices. High temperature steam generation is the key to use the solar evaporators as cost-effective sterilization device without the need of electricity to kill bacteria and other microorganisms [382–384].

Several studies demonstrated super-heated (>100$^{o}$C) solar steam generation with the aid of bulky and expensive optical concentrators for sterilization.[384] Solar driven sterilization with high temperature steam is generally limited to low solar conversion efficiency. Zhao et al. utilized a solar sterilization system to generate superheated steam of 100$^{o}$C for sterilization purposes. They used an ultra-transparent silica aerogel for efficient thermal concentration in their system and with 0.7 sun illumination achieved conversion efficiency of only 56% [382]. The solar sterilizer based on ISSG, with tunable steam temperature, designed by Chang et al. can produce superheated steam of temperature between 102 to 165 ºC but suffers from low solar conversion efficiency between 26 to 49% only [383]. The effectiveness of sterilization process was verified using *Geobacillus stearothermophilus* biological indicator and photograph of *Escherichia coli* bacteria on agar plate as shown in Fig. **12e (iii)** and **12e(iv)** respectively.

Designing a solar driven super-heated steam generating device with high solar conversion efficiency remains challenging and further studies are required. Tsang's group designed a solar driven, low-cost sterilization device using 1D–2D metallic MWCNTs and $HfTe_2$ van der Waals heterostructure as photothermal material [384]. Under 1.5 sun illumination, the device can increase the steam temperature up to 132 ºC within 20 minutes and maintain a higher evaporation efficiency of 87.43% without the need of expensive optical concentrators. Furthermore, they demonstrated that this sterilization device can reduce 88.24 % and 99.04% E. coli bacteria after 15 mins and 30 mins of sterilization respectively, which is well beyond the requirements of WHO. To demonstrate the sterilization performance a control bacterial solution is used. A bacterial solution filled tube is placed inside the ISSG device in such a way so that the solution can be exposed to superheated steam generated by the evaporator. The sterilized and control bacterial solutions are then used to culture bacteria on two separate agar plates in a controlled environment. The number of bacterial colonies are counted to show the effectiveness of the ISSG device in sterilizing bacteria. Zhang et al. built a sterilizing device based on solar-driven interfacial evaporation (SDIE) that can generate high temperature

(>132$^{o}$C) steam [385]. This device uses rGO/PTFE composite membrane as solar absorber. To verify the sterilization process, they put the biological indicator (EZTest Self-Contained Biological Indicator Strips; SGMBiotech) inside a glass vial in a tube in the superheated steam environment and measured the temperature using a thermocouple. When the temperature reached beyond 132 $^{o}$C, the colour of the indicator changed from purple to brown. The tube was then placed inside an oven set at 60°C for 24 hours after breaking the inner glass vial containing the culture medium and mixing it with the bacteria (*Geobacillus Stearothermophilus*) paper inside. Because the microorganisms were killed during sterilization, the medium's color remained brown which proved the sterilization success.

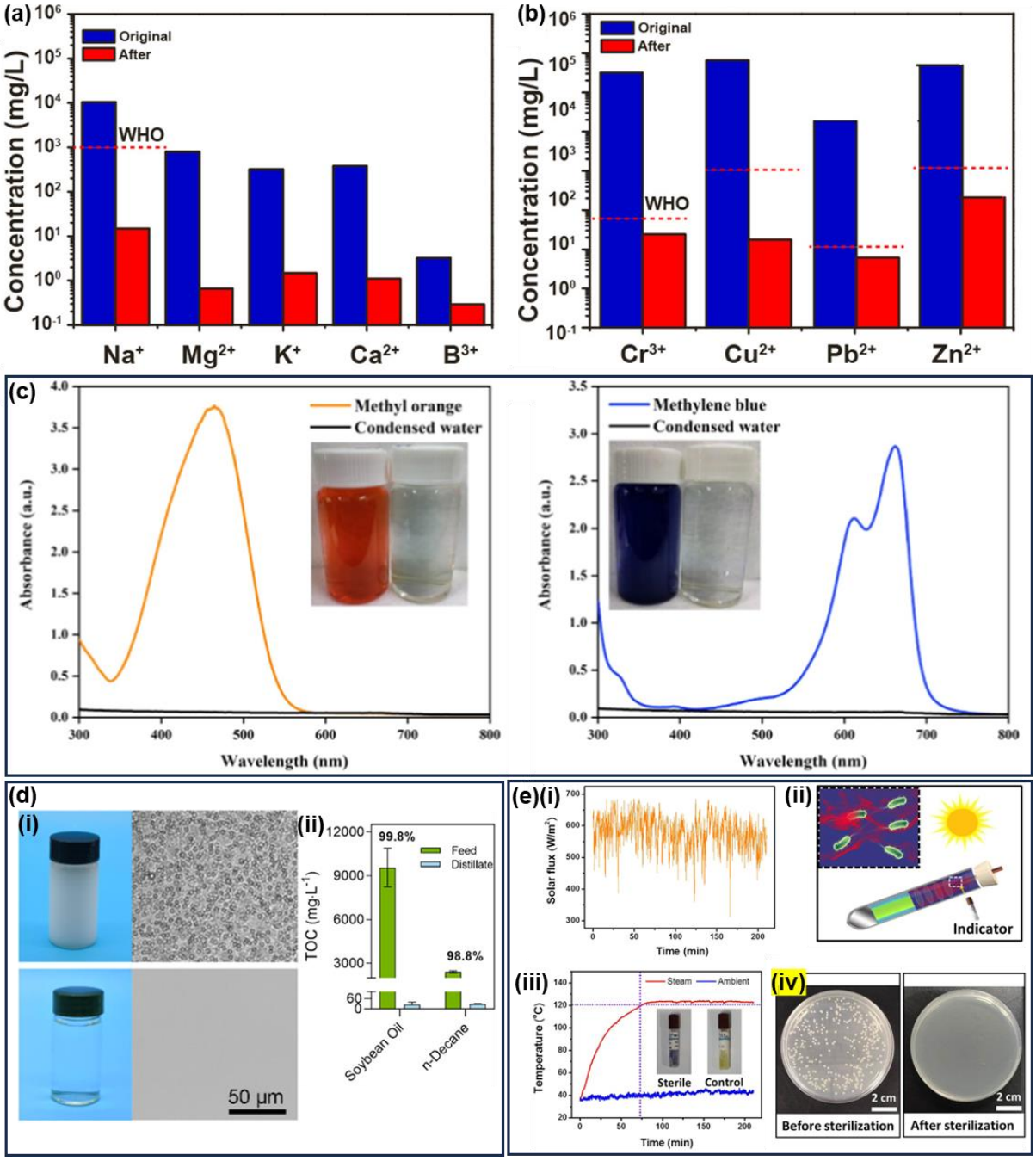


**Fig. 12.** Application: Ion concentration of (a) seawater before and after purification (b) heavy metal contaminated wastewater before and after purification [378]. Copyright 2020 American Chemical Society. (c) absorbance of dye contaminated water (Methyl orange and Methylene blue) before and after purification [386]. Copyright 2021 American Chemical Society. (d) (i) Image of soybean oil emulsion before and after purification and (ii) TOC of oil (Soybean Oil and n-Decane) contaminated water before and after purification [371]. Copyright 2021 American Chemical Society. (e) (i) Solar flux of outdoor solar irradiation (ii) Schematic of Sterilization using solar steam generator (iii) Steam temperature under ambient solar illumination and appearance of *G. stearothermophilus* biological indicator before and after sterilization (iv) Photographs of *E. coli* on agar plate before and after solar steam sterilization [383]. Copyright 2019 American Chemical Society.

Li et al. made a SIDE based sterilization system autoclave, capable of producing 121°C steam in 122 secs [387]. They verified sterilization process using different bacteria samples and log removal efficiency (LRE) of samples were calculated approx. 8 (≈99.999999% sterilization efficiency). Log removal efficiency (LRE) can be determined using the following equation [387]

$$LRE = -\log(\frac{C_t}{C_0}) \quad (23)$$

Here, $C_0$ and $C_t$ are the concentrations of microorganism at time zero and surviving microorganism after a sterilization time interval, t respectively.

Till now, there is still a scope to debate on the effectiveness of solar evaporators as low-cost, environment friendly and renewable energy driven sterilization device as an alternate solution for available sterilization devices. But recent studies have shown good prospects in this field and more prominent results are required to establish the idea of sterilizing medical equipment using ISSG devices.

## 8. Conclusion

In conclusion, this comprehensive review has navigated through the intricate landscape of solar-powered water desalination and purification, shedding light on innovative approaches to mitigate the escalating water scarcity crisis. With a deep appreciation for the historical context and an acute focus on contemporary advancements, this article encapsulates the dynamic evolution of desalination methods and accentuates the pressing need for sustainable solutions in the face of burgeoning global water demand. Throughout this review, the following pivotal aspects have been explored:

- **Mechanism and Photothermal Behavior:** A meticulous exploration of the inner workings of Interfacial Solar Steam Generation (ISSG) has been undertaken, unraveling the intricate mechanisms driving its efficiency. The photothermal behavior of diverse materials has been dissected, revealing the unique attributes that influence solar energy conversion.

- **Substrate's Role in Efficiency Enhancement:** The profound impact of substrate shape and type on solar evaporation efficiency has been elucidated, while the potential for environmental energy gain through multi-surface evaporators has been emphasized.

  Multiple surface evaporators provide higher evaporation rate as they have the capability of harvesting energy from the environment and have higher area for releasing vapor. However, if several multiple surface evaporators are placed side by side to cover a large area, the evaporation capability of single unit may get reduced for not getting sufficient environmental energy from the surroundings. A minimum distance is required to be maintained between two multiple surface evaporators to get better results which may increase the area of the overall system. Therefore, when a large system with many multiple surface evaporators is concerned, the way of calculating the evaporation rate and efficiency have to be changed.
- **Thermal Management Strategies:** Strategies for effective thermal management have been thoroughly discussed, including the exploration of various water transport paths that optimize heat distribution, ensuring sustained and proficient vapor generation.
- **Mitigating Challenges:** Solutions to critical challenges faced by ISSG systems, including salt accumulation, antibiofouling, anti-corrosion, and anti-oil fouling, have been presented. These insights pave the way for enhanced system durability and longevity.

Janus evaporators have better resistance against salt growth, but the evaporation rate and efficiency may get lower due to hydrophobic solar absorbing surface. On the other hand, evaporator with salt ion diffusion mechanism may have higher evaporation rate (due to hydrophilic solar absorbing surface) but may not give stable performance in highly salt concentrated water for longer time period. Therefore, both have their own disadvantages. Marangoni driven salt removal may become a good solution to remove salt from multiple surface solar evaporator as creating temperature gradient in multiple surface evaporator

is easy. However, the structure of evaporator plays an important role to make Marangoni driven salt removal successful. Therefore, more research on "Marangoni driven salt removal technique" is required to be done to find the best possible shape and structure of multiple surface evaporator.

- **Diverse Applications:** The review has underscored the versatile applications of ISSG, ranging from its pivotal role in seawater desalination to wastewater purification scenarios involving dye and heavy metal removal. Furthermore, its prowess in oil-water separation and sterilization bolsters its relevance across diverse industrial and healthcare contexts. Except for these, ISSG based hybrid system has shown a great potential in combining the photothermal and photocatalytic performance of different materials for application like simultaneous generation of water and electricity, water and hydrogen etc.

As with any comprehensive endeavor, this review article presents certain limitations:

- **Dilemma of Low dimensional and biomass derived photothermal materials**:
- Both low dimensional and biomass-derived photothermal materials provide satisfactory performances as the efficiency and evaporation rate of water depends not only on photothermal materials, but also on the structure, shape and type of substrate as well as the other factors like salt rejection capability, antifouling capability etc. The low dimensional materials are comparatively expensive whereas biomass-derived materials are more prone to decomposition due to the presence of microorganisms in natural seawater and wastewater. Metallic substrates also increase the fabrication cost of evaporator. The lifetime of a low dimensional material-based evaporator is also important as secondary contamination by nanoparticles from evaporator to water may occur due to aging and improper management of such system may release large number of nanoparticles to the environment which may cause harm to the aquatic organisms and microorganisms. Therefore, considering the lifetime and cost which also determine the commercial feasibility of solar evaporator, it's very difficult to give a verdict on selecting one specific type of evaporator as best for commercialization.
- **Scope and Economic Analysis:** Notably, this review has concentrated on the fundamental aspects and intricacies of solar evaporator technology, omitting an in-

depth economic analysis and the exploration of life-cycle considerations.

In closing, this comprehensive exploration of solar evaporator technology, with a spotlight on Interfacial Solar Steam Generation, stands as a beacon of hope amidst the challenges posed by water scarcity. By delving into the mechanisms, substrates, efficiency enhancement strategies, and diverse applications of ISSG, this review has propelled the discourse on sustainable and energy-efficient water desalination and purification to new heights. As we forge ahead, the collective insights presented herein offer a roadmap toward a more secure and water-abundant future.

**Conflicts of interest**

There is no conflict to declare.

**Acknowledgments**

M.N.A.S.I. and S.S. contributed equally to this work. This work is financially supported by the Innovation and Technology Fund, Hong Kong, China (GHP/040/19SZ), the Hong Kong Polytechnic University (Project number: 1-ZE14), Photonic Research Institute, The Hong Kong Polytechnic University (Project number: 1-CD6V), and the Hong Kong Polytechnic University Shenzhen Research Institute, Shenzhen, China (Grant Code: the science and technology innovation commission of Shenzhen (JCYJ20210324141206017)).

## References

[1] T. Ma, S. Sun, G. Fu, J.W. Hall, Y. Ni, L. He, J. Yi, N. Zhao, Y. Du, T. Pei, W. Cheng, C. Song, C. Fang, C. Zhou, Pollution exacerbates China's water scarcity and its regional inequality, Nat Commun. (n.d.) 1–9. https://doi.org/10.1038/s41467-020-14532-5.

[2] M. Salehi, Global water shortage and potable water safety; Today's concern and tomorrow's crisis, Environ Int. 158 (2022) 106936. https://doi.org/10.1016/j.envint.2021.106936.

[3] J. Lund Schlamovitz, P. Becker, Differentiated vulnerabilities and capacities for adaptation to water shortage in Gaborone, Botswana, Int J Water Resour Dev. 37 (2021) 278–299. https://doi.org/10.1080/07900627.2020.1756752.

[4] Z. Hussain, Z. Wang, J. Wang, H. Yang, M. Arfan, D. Hassan, W. Wang, M.I. Azam, M. Faisal, A comparative Appraisal of Classical and Holistic Water Scarcity Indicators, Water Resources Management. 36 (2022) 931–950. https://doi.org/10.1007/s11269-022-03061-z.

[5] J. Liu, H. Yang, S.N. Gosling, M. Kummu, M. Flörke, S. Pfister, N. Hanasaki, Y. Wada, X. Zhang, C. Zheng, J. Alcamo, T. Oki, Water scarcity assessments in the past, present, and future, Earths Future. 5 (2017) 545–559. https://doi.org/10.1002/2016EF000518.

[6] S. KALOGIROU, Seawater desalination using renewable energy sources, Prog Energy Combust Sci. 31 (2005) 242–281. https://doi.org/10.1016/j.pecs.2005.03.001.

[7] B. Van der Bruggen, Desalination by distillation and by reverse osmosis — trends towards the future, Membrane Technology. 2003 (2003) 6–9. https://doi.org/10.1016/S0958-2118(03)02018-4.

[8] A.W. Veenman, A review of new developments in desalination by distillation processes, Desalination. 27 (1978) 21–39. https://doi.org/10.1016/S0011-9164(00)82210-9.

[9] M. Wakeel, B. Chen, T. Hayat, A. Alsaedi, B. Ahmad, Energy consumption for water use cycles in different countries: A review, Appl Energy. 178 (2016) 868–885. https://doi.org/10.1016/j.apenergy.2016.06.114.

[10] D. Cohen-Tanugi, J.C. Grossman, Water Desalination across Nanoporous Graphene, Nano Lett. 12 (2012) 3602–3608. https://doi.org/10.1021/nl3012853.

[11] L. Zhou, X. Li, G.W. Ni, S. Zhu, J. Zhu, The revival of thermal utilization from the Sun: Interfacial solar vapor generation, Natl Sci Rev. 6 (2019) 562–578. https://doi.org/10.1093/nsr/nwz030.

[12] L. Zhou, X. Li, G.W. Ni, S. Zhu, J. Zhu, The revival of thermal utilization from the Sun: interfacial solar vapor generation, Natl Sci Rev. 6 (2019) 562–578. https://doi.org/10.1093/nsr/nwz030.

[13] D. Dsilva Winfred Rufuss, S. Iniyan, L. Suganthi, P.A. Davies, Solar stills: A comprehensive review of designs, performance and material advances, Renewable and Sustainable Energy Reviews. 63 (2016) 464–496. https://doi.org/10.1016/j.rser.2016.05.068.

[14] X. Luo, J. Shi, C. Zhao, Z. Luo, X. Gu, H. Bao, The energy efficiency of interfacial solar desalination, Appl Energy. 302 (2021) 117581. https://doi.org/10.1016/j.apenergy.2021.117581.

[15] P. Tao, G. Ni, C. Song, W. Shang, J. Wu, J. Zhu, G. Chen, T. Deng, Solar-driven interfacial evaporation, Nat Energy. 3 (2018) 1031–1041. https://doi.org/10.1038/s41560-018-0260-7.

[16] H. Wang, L. Miao, S. Tanemura, Morphology Control of Ag Polyhedron Nanoparticles for Cost-Effective and Fast Solar Steam Generation, Solar RRL. 1 (2017). https://doi.org/10.1002/solr.201600023.

[17] O. Neumann, A.S. Urban, J. Day, S. Lal, P. Nordlander, N.J. Halas, Solar Vapor Generation Enabled by Nanoparticles, ACS Nano. 7 (2013) 42–49. https://doi.org/10.1021/nn304948h.

[18] M.S. Zielinski, J.-W. Choi, T. La Grange, M. Modestino, S.M.H. Hashemi, Y. Pu, S. Birkhold, J.A. Hubbell, D. Psaltis, Hollow Mesoporous Plasmonic Nanoshells for Enhanced Solar Vapor Generation, Nano Lett. 16 (2016) 2159–2167. https://doi.org/10.1021/acs.nanolett.5b03901.

[19] H. Jin, G. Lin, L. Bai, A. Zeiny, D. Wen, Steam generation in a nanoparticle-based solar receiver, Nano Energy. 28 (2016) 397–406. https://doi.org/10.1016/j.nanoen.2016.08.011.

[20] G. Ni, N. Miljkovic, H. Ghasemi, X. Huang, S. V. Boriskina, C.-T. Lin, J. Wang, Y. Xu, Md.M. Rahman, T. Zhang, G. Chen, Volumetric solar heating of nanofluids for direct vapor generation, Nano Energy. 17 (2015) 290–301. https://doi.org/10.1016/j.nanoen.2015.08.021.

[21] Y. Fu, T. Mei, G. Wang, A. Guo, G. Dai, S. Wang, J. Wang, J. Li, X. Wang, Investigation on enhancing effects of Au nanoparticles on solar steam generation in graphene oxide nanofluids, Appl Therm Eng. 114 (2017) 961–968. https://doi.org/10.1016/j.applthermaleng.2016.12.054.

[22] H. Li, Y. He, Z. Liu, Y. Huang, B. Jiang, Synchronous steam generation and heat collection in a broadband Ag@TiO 2 core–shell nanoparticle-based receiver, Appl Therm Eng. 121 (2017) 617–627. https://doi.org/10.1016/j.applthermaleng.2017.04.102.

[23] X. Wang, Y. He, G. Cheng, L. Shi, X. Liu, J. Zhu, Direct vapor generation through localized solar heating via carbon-nanotube nanofluid, Energy Convers Manag. 130 (2016) 176–183. https://doi.org/10.1016/j.enconman.2016.10.049.

[24] S. Baral, A.J. Green, M.Y. Livshits, A.O. Govorov, H.H. Richardson, Comparison of Vapor Formation of Water at the Solid/Water Interface to Colloidal Solutions Using Optically Excited Gold Nanostructures, ACS Nano. 8 (2014) 1439–1448. https://doi.org/10.1021/nn405267r.

[25] N.J. Hogan, A.S. Urban, C. Ayala-Orozco, A. Pimpinelli, P. Nordlander, N.J. Halas, Nanoparticles Heat through Light Localization, Nano Lett. 14 (2014) 4640–4645. https://doi.org/10.1021/nl5016975.

[26] Z. Fang, Y.-R. Zhen, O. Neumann, A. Polman, F.J. García de Abajo, P. Nordlander, N.J. Halas, Evolution of Light-Induced Vapor Generation at a Liquid-Immersed Metallic Nanoparticle, Nano Lett. 13 (2013) 1736–1742. https://doi.org/10.1021/nl4003238.

[27] O. Neumann, C. Feronti, A.D. Neumann, A. Dong, K. Schell, B. Lu, E. Kim, M. Quinn, S. Thompson, N. Grady, P. Nordlander, M. Oden, N.J. Halas, Compact solar autoclave based on steam generation using broadband light-harvesting nanoparticles, Proceedings of the National Academy of Sciences. 110 (2013) 11677–11681. https://doi.org/10.1073/pnas.1310131110.

[28] D. Zhao, H. Duan, S. Yu, Y. Zhang, J. He, X. Quan, P. Tao, W. Shang, J. Wu, C. Song, T. Deng, Enhancing Localized Evaporation through Separated Light Absorbing Centers and Scattering Centers, Sci Rep. 5 (2015) 17276. https://doi.org/10.1038/srep17276.

[29] Y. Pang, J. Zhang, R. Ma, Z. Qu, E. Lee, T. Luo, Solar–Thermal Water Evaporation: A Review, ACS Energy Lett. 5 (2020) 437–456. https://doi.org/10.1021/acsenergylett.9b02611.

[30] F. Zhao, Y. Guo, X. Zhou, W. Shi, G. Yu, Materials for solar-powered water evaporation, Nat Rev Mater. 5 (2020) 388–401. https://doi.org/10.1038/s41578-020-0182-4.

[31] I. Ibrahim, V. Bhoopal, D.H. Seo, M. Afsari, H.K. Shon, L.D. Tijing, Biomass-based photothermal materials for interfacial solar steam generation: a review, Mater Today Energy. 21 (2021) 100716. https://doi.org/10.1016/j.mtener.2021.100716.

[32] A.M. Saleque, N. Nowshin, Md.N.A.S. Ivan, S. Ahmed, Y.H. Tsang, Natural Porous Materials for Interfacial Solar Steam Generation toward Clean Water Production, Solar RRL. 6 (2022). https://doi.org/10.1002/solr.202100986.

[33] S.W. Sharshir, A.M. Algazzar, K.A. Elmaadawy, A.W. Kandeal, M.R. Elkadeem, T. Arunkumar, J. Zang, N. Yang, New hydrogel materials for improving solar water evaporation, desalination and wastewater treatment: A review, Desalination. 491 (2020) 114564. https://doi.org/10.1016/j.desal.2020.114564.

[34] K. Xu, C. Wang, Z. Li, S. Wu, J. Wang, Salt Mitigation Strategies of Solar-Driven Interfacial Desalination, Adv Funct Mater. 31 (2021). https://doi.org/10.1002/adfm.202007855.

[35] T. Ding, Y. Zhou, W.L. Ong, G.W. Ho, Hybrid solar-driven interfacial evaporation systems: Beyond water production towards high solar energy utilization, Materials Today. 42 (2021) 178–191. https://doi.org/10.1016/j.mattod.2020.10.022.

[36] B. Yuan, C. Zhang, Y. Liang, L. Yang, H. Yang, L. Bai, D. Wei, W. Wang, Q. Wang, H. Chen, A Low-Cost 3D Spherical Evaporator with Unique Surface Topology and Inner Structure for Solar Water Evaporation-Assisted Dye Wastewater Treatment, Adv Sustain Syst. 5 (2021) 2000245. https://doi.org/10.1002/adsu.202000245.

[37] T. Gao, X. Wu, Y. Wang, G. Owens, H. Xu, A Hollow and Compressible 3D Photothermal Evaporator for Highly Efficient Solar Steam Generation without Energy Loss, Solar RRL. 5 (2021) 2100053. https://doi.org/https://doi.org/10.1002/solr.202100053.

[38] Y. Lu, D. Fan, H. Xu, H. Min, C. Lu, Z. Lin, X. Yang, Implementing Hybrid Energy Harvesting in 3D Spherical Evaporator for Solar Steam Generation and Synergic Water Purification, Solar RRL. 4 (2020) 1–11. https://doi.org/10.1002/solr.202000232.

[39] W. He, L. Zhou, M. Wang, Y. Cao, X. Chen, X. Hou, Structure development of carbon-based solar-driven water evaporation systems, Sci Bull (Beijing). 66 (2021) 1472–1483. https://doi.org/https://doi.org/10.1016/j.scib.2021.02.014.

[40] D. Xu, Z. Li, L. Li, J. Wang, Insights into the Photothermal Conversion of 2D MXene Nanomaterials: Synthesis, Mechanism, and Applications, Adv Funct Mater. 30 (2020) 2000712. https://doi.org/https://doi.org/10.1002/adfm.202000712.

[41] A. Allahbakhsh, Nitrogen-doped graphene quantum dots hydrogels for highly efficient solar steam generation, Desalination. 517 (2021) 115264. https://doi.org/10.1016/j.desal.2021.115264.

[42] H. Zhou, C. Xue, Q. Chang, J. Yang, S. Hu, Assembling carbon dots on vertically aligned acetate fibers as ideal salt-rejecting evaporators for solar water purification, Chemical Engineering Journal. 421 (2021) 129822. https://doi.org/10.1016/j.cej.2021.129822.

[43] Q. Hou, C. Xue, N. Li, H. Wang, Q. Chang, H. Liu, J. Yang, S. Hu, Self-assembly carbon dots for powerful solar water evaporation, Carbon N Y. 149 (2019) 556–563. https://doi.org/10.1016/j.carbon.2019.04.083.

[44] C. Wang, S. Zhou, C. Wu, Z. Yang, X. Zhang, Janus carbon nanotube sponges for highly efficient solar-driven vapor generation, Chemical Engineering Journal. 454 (2023) 140501. https://doi.org/10.1016/j.cej.2022.140501.

[45] C. Onggowarsito, A. Feng, S. Mao, S. Zhang, I. Ibrahim, L. Tijing, Q. Fu, H.H. Ngo, Development of an innovative MnO2 nanorod for efficient solar vapor generator, Environmental Functional Materials. 1 (2022) 196–203. https://doi.org/10.1016/j.efmat.2022.08.001.

[46] M. Kumarihamy, H.F. Wu, A rapid, cost-free, and disposable solar steam generator for sea/wastewater purification based on 2D titanium oxide nanosheets via ultrasound synthesis, Materials Today Sustainability. 22 (2023) 100377. https://doi.org/10.1016/j.mtsust.2023.100377.

[47] X. Hu, N. Xue, H. Wang, N. Wei, Y. Zhang, H. Cui, Design of stability and cost-effective Ti3C2/cotton architecture for solar steam generation, Mater Today Commun. 37 (2023) 107202. https://doi.org/10.1016/j.mtcomm.2023.107202.

[48] M.S. Irshad, X. Wang, A. Abbas, F. Yu, J. Li, J. Wang, T. Mei, J. Qian, S. Wu, M.Q. Javed, Salt-resistant carbon dots modified solar steam system enhanced by chemical advection, Carbon N Y. 176 (2021) 313–326. https://doi.org/10.1016/j.carbon.2021.01.140.

[49] W. Li, W. Feng, S. Wu, W. Wang, D. Yu, Synergy of photothermal effect in integrated 0D Ti2O3 nanoparticles/1D carboxylated carbon nanotubes for multifunctional water purification, Sep Purif Technol. 292 (2022) 120989. https://doi.org/10.1016/j.seppur.2022.120989.

[50] X. Ma, N. Tian, G. Wang, W. Wang, J. Miao, T. Fan, Biomimetic vertically aligned aerogel with synergistic photothermal effect enables efficient solar-driven desalination, Desalination. 550 (2023) 116397. https://doi.org/10.1016/j.desal.2023.116397.

[51] A.M. Saleque, S. Saha, M.N.A.S. Ivan, S. Ahmed, T.I. Alam, S.U. Hani, Y.H. Tsang, Reduced graphene oxide/TiTe2 quantum dot coated waste face mask recycled for highly efficient solar steam generation, Solar Energy Materials and Solar Cells. 253 (2023) 112232. https://doi.org/10.1016/j.solmat.2023.112232.

[52] D. Fan, Y. Lu, H. Zhang, H. Xu, C. Lu, Y. Tang, X. Yang, Synergy of photocatalysis and photothermal effect in integrated 0D perovskite oxide/2D MXene heterostructures for simultaneous water purification and solar steam generation, Appl Catal B. 295 (2021) 120285. https://doi.org/https://doi.org/10.1016/j.apcatb.2021.120285.

[53] M. Gao, C.K. Peh, L. Zhu, G. Yilmaz, G.W. Ho, Photothermal Catalytic Gel Featuring Spectral and Thermal Management for Parallel Freshwater and Hydrogen Production, Adv Energy Mater. 10 (2020) 1–9. https://doi.org/10.1002/aenm.202000925.

[54] Z. Ai, Y. Zhao, L. Chen, T. Wen, S. Song, T. Zhang, Floating MMT/MXene janus membrane for solar steam generation and mechanism of improving water transportation by DFT calculation, Sep Purif Technol. 300 (2022). https://doi.org/10.1016/j.seppur.2022.121918.

[55] M.M. Ghafurian, M.R. Malmir, Z. Akbari, M. Vafaei, H. Niazmand, E.K. Goharshadi, A. Ebrahimi, O. Mahian, Interfacial solar steam generation by sawdust coated with W doped VO2, Energy. 244 (2022). https://doi.org/10.1016/j.energy.2022.123146.

[56] C. Gao, J. Zhu, J. Li, B. Zhou, X. Liu, Y. Chen, Z. Zhang, J. Guo, Honeycomb-structured fabric with enhanced photothermal management and site-specific salt crystallization enables sustainable solar steam generation, J Colloid Interface Sci. 619 (2022) 322–330. https://doi.org/10.1016/j.jcis.2022.03.122.

[57] H. Jiang, H. Fang, D. Wang, J. Sun, Spray-Coated Commercial PTFE Membrane from MoS2/LaF3/PDMS Ink as Solar Absorber for Efficient Solar Steam Generation, Solar RRL. 4 (2020). https://doi.org/10.1002/solr.202000126.

[58] K. Goharshadi, S.A. Sajjadi, E.K. Goharshadi, R. Mehrkhah, Highly efficient plasmonic wood/Ag/Pd photoabsorber in interfacial solar steam generation, Mater Res Bull. 154 (2022) 111916. https://doi.org/10.1016/j.materresbull.2022.111916.

[59] Y. Pan, E. Li, Y. Wang, C. Liu, C. Shen, X. Liu, Simple Design of a Porous Solar Evaporator for Salt-Free Desalination and Rapid Evaporation, Environ Sci Technol. 56 (2022) 11818–11826. https://doi.org/10.1021/acs.est.2c03240.

[60] J. Xu, Y. Chen, M. Cao, C. Wang, P. Guo, Highly efficient solar steam generation of polyamide 6 membrane modified with graphene oxide and Au nanoparticles, J Mater Res. 37 (2022) 1475–1485. https://doi.org/10.1557/s43578-022-00552-y.

[61] M. Zhu, Y. Li, F. Chen, X. Zhu, J. Dai, Y. Li, Z. Yang, X. Yan, J. Song, Y. Wang, E. Hitz, W. Luo, M. Lu, B. Yang, L. Hu, Plasmonic Wood for High-Efficiency Solar Steam Generation, Adv Energy Mater. 8 (2018) 1–7. https://doi.org/10.1002/aenm.201701028.

[62] S. Chen, Z. Sun, W. Xiang, C. Shen, Z. Wang, X. Jia, J. Sun, C.J. Liu, Plasmonic wooden flower for highly efficient solar vapor generation, Nano Energy. 76 (2020) 104998. https://doi.org/10.1016/j.nanoen.2020.104998.

[63] Q. Li, S. Zhang, N. Wei, R. Xu, X. Li, L. Gong, H. Cui, Porous Ni/CNTs composite membrane as solar absorber for highly efficient solar steam generation, Solar Energy Materials and Solar Cells. 243 (2022). https://doi.org/10.1016/j.solmat.2022.111815.

[64] K. Sun, H. Cui, R. Xu, L. Wang, M. Li, Z. Yang, M. Zhao, N. Wei, Constructing of 3D porous composite materials of NiAl/CNTs for highly efficient solar steam generation, Solar Energy Materials and Solar Cells. 240 (2022) 111722. https://doi.org/10.1016/j.solmat.2022.111722.

[65] Y. Chen, J. Yang, J. Guo, F. Fang, A 3D photothermal bar for efficient steam generation, J Environ Chem Eng. 11 (2023) 109179. https://doi.org/10.1016/j.jece.2022.109179.

[66] C. Tian, C. Li, D. Chen, Y. Li, L. Xing, X. Tian, Y. Cao, W. Huang, Z. Liu, Y. Shen, Sandwich hydrogel with confined plasmonic Cu/carbon cells for efficient solar water purification, J Mater Chem A Mater. 9 (2021) 15462–15471. https://doi.org/10.1039/d1ta02927d.

[67] Z. Sun, J. Wang, Q. Wu, Z. Wang, Z. Wang, J. Sun, Plasmon Based Double-Layer Hydrogel Device for a Highly Efficient Solar Vapor Generation, 1901312 (2019) 1–7. https://doi.org/10.1002/adfm.201901312.

[68] G. Xue, K. Liu, Q. Chen, P. Yang, J. Li, T. Ding, J. Duan, B. Qi, J. Zhou, Robust and Low-Cost Flame-Treated Wood for High-Performance Solar Steam Generation, ACS Appl Mater Interfaces. 9 (2017) 15052–15057. https://doi.org/10.1021/acsami.7b01992.

[69] H. Jang, J. Choi, H. Lee, S. Jeon, Corrugated Wood Fabricated Using Laser-Induced Graphitization for Salt-Resistant Solar Steam Generation, ACS Appl Mater Interfaces. 12 (2020) 30320–30327. https://doi.org/10.1021/acsami.0c05138.

[70] C. Jia, Y. Li, Z. Yang, G. Chen, Y. Yao, F. Jiang, Y. Kuang, G. Pastel, H. Xie, B. Yang, S. Das, L. Hu, Rich Mesostructures Derived from Natural Woods for Solar Steam Generation, Joule. 1 (2017) 588–599. https://doi.org/10.1016/j.joule.2017.09.011.

[71] C. Wang, Y. Wang, M. Yan, W. Zhang, P. Wang, W. Guan, S. Zhang, L. Yu, J. Feng, Z. Gan, L. Dong, Highly efficient self-floating jellyfish-like solar steam generators based on the partially carbonized Enteromorpha aerogel, J Colloid Interface Sci. 630 (2023) 297–305. https://doi.org/10.1016/j.jcis.2022.09.133.

[72] Y. Sun, Z. Zhao, G. Zhao, L. Wang, D. Jia, Y. Yang, X. Liu, X. Wang, J. Qiu, High performance carbonized corncob-based 3D solar vapor steam generator enhanced by environmental energy, Carbon N Y. 179 (2021) 337–347. https://doi.org/10.1016/j.carbon.2021.04.037.

[73] B. Yuan, C. Zhang, Y. Liang, L. Yang, H. Yang, L. Bai, D. Wei, W. Wang, Q. Wang, H. Chen, A Low-Cost 3D Spherical Evaporator with Unique Surface Topology and Inner Structure for Solar Water Evaporation-Assisted Dye Wastewater Treatment, Adv Sustain Syst. 5 (2021) 2000245. https://doi.org/https://doi.org/10.1002/adsu.202000245.

[74] Z. Zhou, J. Gong, C. Zhang, W. Tang, B. Wei, J. Wang, Z. Fu, L. Li, W. Li, L. Xia, Hierarchically porous carbonized Pleurotus eryngii based solar steam generator for efficient wastewater purification, Renew Energy. 216 (2023). https://doi.org/10.1016/j.renene.2023.118987.

[75] X. Chen, Z. Wu, D. Lai, M. Zheng, L. Xu, J. Huo, Z. Chen, B. Yuan, M.L. Fu, Resilient biomass-derived hydrogel with tailored topography for highly efficient and long-term solar evaporation of high-salinity brine, J Mater Chem A Mater. 8 (2020) 22645–22656. https://doi.org/10.1039/d0ta07040h.

[76] Q. Fang, T. Li, Z. Chen, H. Lin, P. Wang, F. Liu, Full Biomass-Derived Solar Stills for Robust and Stable Evaporation to Collect Clean Water from Various Water-Bearing Media, ACS Appl Mater Interfaces. 11 (2019) 10672–10679. https://doi.org/10.1021/acsami.9b00291.

[77] X. Liu, Y. Tian, Y. Wu, A. Caratenuto, F. Chen, S. Cui, J.A. DeGiorgis, Y. Wan, Y. Zheng, Seawater desalination derived entirely from ocean biomass, J Mater Chem A Mater. 9 (2021) 22313–22324. https://doi.org/10.1039/d1ta05068k.

[78] X. Liu, Y. Tian, Y. Wu, F. Chen, Y. Mu, M.L. Minus, Y. Zheng, Fully Biomass-Based Hybrid Hydrogel for Efficient Solar Desalination with Salt Self-Cleaning Property, ACS Appl Mater Interfaces. 13 (2021) 42832–42842. https://doi.org/10.1021/acsami.1c11636.

[79] Z. Li, J. Zhang, S. Zang, C. Yang, Y. Liu, F. Jing, H. Jing, J. Hu, C. Wang, Y. Zhou, Engineering controllable water transport of biosafety cuttlefish juice solar absorber toward remarkably enhanced solar-driven gas-liquid interfacial evaporation, Nano Energy. 73 (2020). https://doi.org/10.1016/j.nanoen.2020.104834.

[80] E.Y. Krysanov, D.S. Pavlov, T.B. Demidova, Y.Y. Dgebuadze, Effect of nanoparticles on aquatic organisms, Biology Bulletin. 37 (2010) 406–412. https://doi.org/10.1134/S1062359010040114.

[81] M. Kumar, S. Sabu, V. Sangela, M. Meena, V.D. Rajput, T. Minkina, V. Vinayak, Harish, The mechanism of nanoparticle toxicity to cyanobacteria, Arch Microbiol. 205 (2023). https://doi.org/10.1007/s00203-022-03370-2.

[82] L. Zhu, M. Gao, C.K.N. Peh, G.W. Ho, Recent progress in solar-driven interfacial water evaporation: Advanced designs and applications, Nano Energy. 57 (2019) 507–518. https://doi.org/10.1016/j.nanoen.2018.12.046.

[83] Z.W. Seh, S. Liu, M. Low, S.-Y. Zhang, Z. Liu, A. Mlayah, M.-Y. Han, Janus Au-TiO2 Photocatalysts with Strong Localization of Plasmonic Near-Fields for Efficient Visible-Light Hydrogen Generation, Advanced Materials. 24 (2012) 2310–2314. https://doi.org/https://doi.org/10.1002/adma.201104241.

[84] U. Das, R. Biswas, N. Mazumder, Elucidating thermal effects in plasmonic metal nanostructures: a tutorial review, Eur Phys J Plus. 137 (2022) 1–18. https://doi.org/10.1140/epjp/s13360-022-03449-1.

[85] G. Baffou, R. Quidant, Thermo-plasmonics: using metallic nanostructures as nano-sources of heat, Laser Photon Rev. 7 (2013) 171–187. https://doi.org/10.1002/lpor.201200003.

[86] X. Luo, J. Shi, C. Zhao, Z. Luo, X. Gu, H. Bao, The energy efficiency of interfacial solar desalination, Appl Energy. 302 (2021) 117581. https://doi.org/10.1016/j.apenergy.2021.117581.

[87] Z. Lin, T. Yingling, J. Dengxin, Z. Bin, Z. Pei, X. Jun, G. Qiaoqiang, Y. Zongfu, Z. Jia, L. Zhou, Y. Tan, D. Ji, B. Zhu, P. Zhang, J. Xu, Q. Gan, Z. Yu, J. Zhu, Z. Lin, T. Yingling, J. Dengxin, Z. Bin, Z. Pei, X. Jun, G. Qiaoqiang, Y. Zongfu, Z. Jia, Self-assembly of highly efficient, broadband plasmonic absorbers for solar steam generation, Sci Adv. 2 (2016) e1501227. https://doi.org/10.1126/sciadv.1501227.

[88] Y. Shi, C. Zhang, Y. Wang, Y. Cui, Q. Wang, G. Liu, S. Gao, Y. Yuan, Plasmonic silver nanoparticles embedded in flexible three-dimensional carbonized melamine foam with enhanced solar-driven water evaporation, Desalination. 507 (2021) 115038. https://doi.org/10.1016/j.desal.2021.115038.

[89] K. Goharshadi, S.A. Sajjadi, E.K. Goharshadi, R. Mehrkhah, Highly efficient plasmonic wood/Ag/Pd photoabsorber in interfacial solar steam generation, Mater Res Bull. 154 (2022) 111916. https://doi.org/10.1016/j.materresbull.2022.111916.

[90] M. Ji, H. Liu, M. Cheng, L. Huang, G. Yang, F. Bao, G. Huang, Y. Huang, Y. Hu, G. Cong, J. Yu, C. Zhu, J. Xu, Plasmonic Metal Nanoparticle Loading to Enhance the Photothermal Conversion of Carbon Fibers, Journal of Physical Chemistry C. 126 (2022) 2454–2462. https://doi.org/10.1021/acs.jpcc.1c10792.

[91] A.G. Saad, A. Gebreil, D.A. Kospa, S.A. El-Hakam, A.A. Ibrahim, Integrated solar seawater desalination and power generation via plasmonic sawdust-derived biochar: Waste to wealth, Desalination. 535 (2022) 115824. https://doi.org/10.1016/j.desal.2022.115824.

[92] B. Soo Joo, I. Soo Kim, I. Ki Han, H. Ko, J. Gu Kang, G. Kang, Plasmonic silicon nanowires for enhanced heat localization and interfacial solar steam generation, Appl Surf Sci. 583 (2022) 152563. https://doi.org/10.1016/j.apsusc.2022.152563.

[93] M.J. Margeson, M. Dasog, Plasmonic metal nitrides for solar-driven water evaporation, Environ Sci (Camb). 6 (2020) 3169–3177.

[94] P.L. Wang, W. Zhang, Q. Yuan, T. Mai, M.Y. Qi, M.G. Ma, 3D Janus structure MXene/cellulose nanofibers/luffa aerogels with superb mechanical strength and high-efficiency desalination for solar-driven interfacial evaporation, J Colloid Interface Sci. 645 (2023) 306–318. https://doi.org/10.1016/j.jcis.2023.04.081.

[95] X. Fan, L. Liu, X. Jin, W. Wang, S. Zhang, B. Tang, MXene Ti3C2Tx for phase change composite with superior photothermal storage capability, J Mater Chem A Mater. 7 (2019) 14319–14327. https://doi.org/10.1039/c9ta03962g.

[96] I. Ibrahim, D.H. Seo, A.M. McDonagh, H.K. Shon, L. Tijing, Semiconductor photothermal materials enabling efficient solar steam generation toward desalination and wastewater treatment, Desalination. 500 (2021) 114853. https://doi.org/10.1016/j.desal.2020.114853.

[97] W. Li, H. Jian, W. Wang, D. Yu, Highly efficient solar vapour generation via self-floating three-dimensional Ti2O3-based aerogels, Colloids Surf A Physicochem Eng Asp. 634 (2022) 128031. https://doi.org/10.1016/j.colsurfa.2021.128031.

[98] H. Liu, C. Chen, H. Wen, R. Guo, N.A. Williams, B. Wang, F. Chen, L. Hu, Narrow bandgap semiconductor decorated wood membrane for high-efficiency solar-assisted water purification, J Mater Chem A Mater. 6 (2018) 18839–18846. https://doi.org/10.1039/c8ta05924a.

[99] M.Q. Yang, C.F. Tan, W. Lu, K. Zeng, G.W. Ho, Spectrum Tailored Defective 2D Semiconductor Nanosheets Aerogel for Full-Spectrum-Driven Photothermal Water Evaporation and Photochemical Degradation, Adv Funct Mater. 30 (2020). https://doi.org/10.1002/adfm.202004460.

[100] X. Yang, Y. Yang, L. Fu, M. Zou, Z. Li, A. Cao, Q. Yuan, An Ultrathin Flexible 2D Membrane Based on Single-Walled Nanotube-MoS 2 Hybrid Film for High-Performance Solar Steam Generation, Adv Funct Mater. 28 (2018) 1704505. https://doi.org/10.1002/adfm.201704505.

[101] D. Ghim, Q. Jiang, S.S. Cao, S. Singamaneni, Y.S. Jun, Mechanically interlocked 1T/2H phases of MoS2 nanosheets for solar thermal water purification, Nano Energy. (2018). https://doi.org/10.1016/j.nanoen.2018.09.038.

[102] X. Zhang, G. Wu, X.-C. Yang, MoS 2 Nanosheet–Carbon Foam Composites for Solar Steam Generation, ACS Appl Nano Mater. 3 (2020) 9706–9714. https://doi.org/10.1021/acsanm.0c01712.

[103] H. Zhang, Y. Wang, Y. Liu, M. Zhao, C. Liu, Y. Wang, M.K. Albolkany, N. Wu, M. Wang, L. Yang, B. Liu, Efficient Solar Evaporation by [Ni(Phen)3][V14O34Cl]Cl Hybrid Semiconductor Confined in Mesoporous Glass, ChemSusChem. 13 (2020) 2945–2951. https://doi.org/https://doi.org/10.1002/cssc.202000356.

[104] J. Huang, Y. He, L. Wang, Y. Huang, B. Jiang, Bifunctional Au@TiO2 core–shell nanoparticle films for clean water generation by photocatalysis and solar evaporation, Energy Convers Manag. 132 (2017) 452–459. https://doi.org/10.1016/j.enconman.2016.11.053.

[105] P. Sun, W. Wang, W. Zhang, S. Zhang, J. Gu, L. Yang, D. Pantelić, B. Jelenković, D. Zhang, 3D Interconnected Gyroid Au–CuS Materials for Efficient Solar Steam Generation, ACS Appl Mater Interfaces. 12 (2020) 34837–34847. https://doi.org/10.1021/acsami.0c06701.

[106] L. Song, X.F. Zhang, Z. Wang, T. Zheng, J. Yao, Fe3O4/polyvinyl alcohol decorated delignified wood evaporator for continuous solar steam generation, Desalination. 507 (2021) 115024. https://doi.org/10.1016/j.desal.2021.115024.

[107] B.B. Zahmatkesh, H. Niazmand, E.K. Goharshadi, Synergistic effect of Fe3O4 nanoparticles and Au nanolayer in enhancement of interfacial solar steam generation, Mater Res Bull. 162 (2023) 112178. https://doi.org/10.1016/j.materresbull.2023.112178.

[108] J.R. Vélez-Cordero, J. Hernández-Cordero, Heat generation and conduction in PDMS-carbon nanoparticle membranes irradiated with optical fibers, International Journal of Thermal Sciences. 96 (2015) 12–22. https://doi.org/10.1016/j.ijthermalsci.2015.04.009.

[109] P. Zhang, J. Li, L. Lv, Y. Zhao, L. Qu, Vertically Aligned Graphene Sheets Membrane for Highly Efficient Solar Thermal Generation of Clean Water, ACS Nano. 11 (2017) 5087–5093. https://doi.org/10.1021/acsnano.7b01965.

[110] K.K. Liu, Q. Jiang, S. Tadepalli, R. Raliya, P. Biswas, R.R. Naik, S. Singamaneni, Wood-Graphene Oxide Composite for Highly Efficient Solar Steam Generation and Desalination, ACS Appl Mater Interfaces. 9 (2017) 7675–7681. https://doi.org/10.1021/acsami.7b01307.

[111] Q. Jiang, L. Tian, K.-K. Liu, S. Tadepalli, R. Raliya, P. Biswas, R.R. Naik, S. Singamaneni, Bilayered Biofoam for Highly Efficient Solar Steam Generation, Advanced Materials. 28 (2016) 9400–9407. https://doi.org/https://doi.org/10.1002/adma.201601819.

[112] Z. Liu, H. Song, D. Ji, C. Li, A. Cheney, Y. Liu, N. Zhang, X. Zeng, B. Chen, J. Gao, Y. Li, X. Liu, D. Aga, S. Jiang, Z. Yu, Q. Gan, Extremely Cost-Effective and Efficient Solar Vapor Generation under Nonconcentrated Illumination Using Thermally Isolated Black Paper, Global Challenges. 1 (2017) 1600003. https://doi.org/10.1002/gch2.201600003.

[113] Y. Liu, J. Chen, D. Guo, M. Cao, L. Jiang, Floatable, Self-Cleaning, and Carbon-Black-Based Superhydrophobic Gauze for the Solar Evaporation Enhancement at the Air-Water Interface, ACS Appl Mater Interfaces. 7 (2015) 13645–13652. https://doi.org/10.1021/acsami.5b03435.

[114] M.N.A.S. Ivan, A.M. Saleque, S. Ahmed, P.K. Cheng, J. Qiao, T.I. Alam, Y.H. Tsang, Waste Egg Tray and Toner-Derived Highly Efficient 3D Solar Evaporator for Freshwater Generation, ACS Appl Mater Interfaces. 14 (2022) 7936–7948. https://doi.org/10.1021/acsami.1c22215.

[115] Y. Wang, L. Zhang, P. Wang, Self-Floating Carbon Nanotube Membrane on Macroporous Silica Substrate for Highly Efficient Solar-Driven Interfacial Water Evaporation, ACS Sustain Chem Eng. 4 (2016) 1223–1230. https://doi.org/10.1021/acssuschemeng.5b01274.

[116] H. Ren, M. Tang, B. Guan, K. Wang, J. Yang, F. Wang, M. Wang, J. Shan, Z. Chen, D. Wei, H. Peng, Z. Liu, Hierarchical Graphene Foam for Efficient Omnidirectional Solar–Thermal Energy Conversion, Advanced Materials. 29 (2017) 1–7. https://doi.org/10.1002/adma.201702590.

[117] P. Zhang, F. Liu, Q. Liao, H. Yao, H. Geng, H. Cheng, C. Li, L. Qu, A Microstructured Graphene/Poly(N-isopropylacrylamide) Membrane for Intelligent Solar Water

Evaporation, Angewandte Chemie International Edition. 57 (2018) 16343–16347. https://doi.org/https://doi.org/10.1002/anie.201810345.

[118] G. Xue, Y. Xu, T. Ding, J. Li, J. Yin, W. Fei, Y. Cao, J. Yu, L. Yuan, L. Gong, J. Chen, S. Deng, J. Zhou, W. Guo, Water-evaporation-induced electricity with nanostructured carbon materials, Nat Nanotechnol. 12 (2017) 317–321. https://doi.org/10.1038/nnano.2016.300.

[119] S. Zhang, H. Ma, D. Guo, P. Guo, J. Wang, M. Liu, S. Wu, C. Bao, Multiscale Preparation of Graphene Oxide/Carbon Nanotube-Based Membrane Evaporators by a Spray Method for Efficient Solar Steam Generation, ACS Appl Nano Mater. 5 (2022) 7198–7207. https://doi.org/10.1021/acsanm.2c01122.

[120] W. Li, X. Li, J. Liu, M.J. Zeng, X. Feng, X. Jia, Z.Z. Yu, Coating of Wood with Fe2O3-Decorated Carbon Nanotubes by One-Step Combustion for Efficient Solar Steam Generation, ACS Appl Mater Interfaces. 13 (2021) 22845–22854. https://doi.org/10.1021/acsami.1c03388.

[121] S. Ge-Zhang, H. Yang, H. Mu, Interfacial solar steam generator by MWCNTs/carbon black nanoparticles coated wood, Alexandria Engineering Journal. 63 (2023) 1–10. https://doi.org/10.1016/j.aej.2022.08.002.

[122] J. Wang, Z. Guo, B. Xiao, X. Xiong, G. Liu, X. Wang, Reduced graphene oxide/Cu7·2S4 composite hydrogels for highly efficient solar steam generation, Materials Today Sustainability. 18 (2022). https://doi.org/10.1016/j.mtsust.2022.100121.

[123] A. Guo, X. Ming, Y. Fu, G. Wang, X. Wang, Fiber-Based, Double-Sided, Reduced Graphene Oxide Films for Efficient Solar Vapor Generation, ACS Appl Mater Interfaces. 9 (2017) 29958–29964. https://doi.org/10.1021/acsami.7b07759.

[124] S. Meng, X. Zhao, C.-Y. Tang, P. Yu, R.-Y. Bao, Z.-Y. Liu, M.-B. Yang, W. Yang, A bridge-arched and layer-structured hollow melamine foam/reduced graphene oxide composite with an enlarged evaporation area and superior thermal insulation for high-performance solar steam generation, J Mater Chem A Mater. 8 (2020) 2701–2711. https://doi.org/10.1039/C9TA12802F.

[125] T. Gao, X. Wu, G. Owens, H.L. Xu, A cobalt oxide@polydopamine-reduced graphene oxide-based 3D photothermal evaporator for highly efficient solar steam generation, Tungsten. 2 (2020) 423–432. https://doi.org/10.1007/s42864-020-00062-6.

[126] R. Mehrkhah, E.K. Goharshadi, M.M. Ghafurian, M. Mohammadi, O. Mahian, Clean water production by non-noble metal/reduced graphene oxide nanocomposite coated on wood: Scalable interfacial solar steam generation and heavy metal sorption, Solar Energy. 224 (2021) 440–454. https://doi.org/10.1016/j.solener.2021.06.004.

[127] G. Cheng, X. Wang, X. Liu, Y. He, B. V. Balakin, Enhanced interfacial solar steam generation with composite reduced graphene oxide membrane, Solar Energy. 194 (2019) 415–430. https://doi.org/10.1016/j.solener.2019.10.065.

[128] G. Wang, Y. Fu, A. Guo, T. Mei, J. Wang, J. Li, X. Wang, Reduced Graphene Oxide-Polyurethane Nanocomposite Foam as a Reusable Photoreceiver for Efficient Solar Steam Generation, Chemistry of Materials. 29 (2017) 5629–5635. https://doi.org/10.1021/acs.chemmater.7b01280.

[129] E.A. Hussein, M.M. Zagho, G.K. Nasrallah, A.A. Elzatahry, Recent advances in functional nanostructures as cancer photothermal therapy, Int J Nanomedicine. 13 (2018) 2897–2906. https://doi.org/10.2147/IJN.S161031.

[130] A. Kumar, A. Kumar, V. Krishnan, Perovskite Oxide Based Materials for Energy and Environment-Oriented Photocatalysis, ACS Catal. 10 (2020) 10253–10315. https://doi.org/10.1021/acscatal.0c02947.

[131] P. Sun, W. Zhang, I. Zada, Y. Zhang, J. Gu, Q. Liu, H. Su, D. Pantelić, B. Jelenković, D. Zhang, 3D-Structured Carbonized Sunflower Heads for Improved Energy Efficiency in Solar Steam Generation, ACS Appl Mater Interfaces. 12 (2020) 2171–2179. https://doi.org/10.1021/acsami.9b11738.

[132] G. Xue, K. Liu, Q. Chen, P. Yang, J. Li, T. Ding, J. Duan, B. Qi, J. Zhou, Robust and Low-Cost Flame-Treated Wood for High-Performance Solar Steam Generation, ACS Appl Mater Interfaces. 9 (2017) 15052–15057. https://doi.org/10.1021/acsami.7b01992.

[133] H. Jang, J. Choi, H. Lee, S. Jeon, Corrugated Wood Fabricated Using Laser-Induced Graphitization for Salt-Resistant Solar Steam Generation, ACS Appl Mater Interfaces. 12 (2020) 30320–30327. https://doi.org/10.1021/acsami.0c05138.

[134] Z. Yu, S. Cheng, C. Li, Y. Sun, B. Li, Enhancing efficiency of carbonized wood based solar steam generator for wastewater treatment by optimizing the thickness, Solar Energy. 193 (2019) 434–441. https://doi.org/10.1016/j.solener.2019.09.080.

[135] N. Xu, X. Hu, W. Xu, X. Li, L. Zhou, S. Zhu, J. Zhu, Mushrooms as Efficient Solar Steam-Generation Devices, Advanced Materials. 29 (2017) 1–5. https://doi.org/10.1002/adma.201606762.

[136] M. Zhu, J. Yu, C. Ma, C. Zhang, D. Wu, H. Zhu, Carbonized daikon for high efficient solar steam generation, Solar Energy Materials and Solar Cells. 191 (2019) 83–90. https://doi.org/10.1016/j.solmat.2018.11.015.

[137] Y. Long, S. Huang, H. Yi, J. Chen, J. Wu, Q. Liao, H. Liang, H. Cui, S. Ruan, Y.J. Zeng, Carrot-inspired solar thermal evaporator, J Mater Chem A Mater. 7 (2019) 26911–26916. https://doi.org/10.1039/c9ta08754k.

[138] Y. Sun, Z. Zhao, G. Zhao, L. Wang, D. Jia, Y. Yang, X. Liu, X. Wang, J. Qiu, High performance carbonized corncob-based 3D solar vapor steam generator enhanced by environmental energy, Carbon N Y. 179 (2021) 337–347. https://doi.org/10.1016/j.carbon.2021.04.037.

[139] L. Yang, G. Chen, N. Zhang, Y. Xu, X. Xu, Sustainable Biochar-Based Solar Absorbers for High-Performance Solar-Driven Steam Generation and Water Purification, ACS Sustain Chem Eng. 7 (2019) 19311–19320. https://doi.org/10.1021/acssuschemeng.9b06169.

[140] A.K. Menon, I. Haechler, S. Kaur, S. Lubner, R.S. Prasher, Enhanced solar evaporation using a photo-thermal umbrella for wastewater management, Nat Sustain. 3 (2020) 144–151. https://doi.org/10.1038/s41893-019-0445-5.

[141] X. Su, D. Hao, M. Sun, T. Wei, D. Xu, X. Ai, X. Guo, T. Zhao, L. Jiang, Nature Sunflower Stalk Pith with Zwitterionic Hydrogel Coating for Highly Efficient and Sustainable Solar Evaporation, Adv Funct Mater. 32 (2022). https://doi.org/10.1002/adfm.202108135.

[142] C. Chen, Y. Kuang, L. Hu, Challenges and Opportunities for Solar Evaporation, Joule. 3 (2019) 683–718. https://doi.org/10.1016/j.joule.2018.12.023.

[143] D. Tong, B. Song, A high-efficient and ultra-strong interfacial solar evaporator based on carbon-fiber fabric for seawater and wastewater purification, Desalination. 527 (2022). https://doi.org/10.1016/j.desal.2022.115586.

[144] Y. Zhang, T. Xiong, D.K. Nandakumar, S.C. Tan, Structure Architecting for Salt-Rejecting Solar Interfacial Desalination to Achieve High-Performance Evaporation With In Situ Energy Generation, Advanced Science. 7 (2020) 1903478. https://doi.org/10.1002/advs.201903478.

[145] H. Fan, A. Gao, G. Zhang, S. Zhao, J. Cui, Y. Yan, A design of bifunctional photothermal layer on polysulfone membrane with enclosed cellular-like structure for efficient solar steam generation, Chemical Engineering Journal. 415 (2021) 128798. https://doi.org/10.1016/j.cej.2021.128798.

[146] Y. Chang, Z. Wang, Y.E. Shi, X. Ma, L. Ma, Y. Zhang, J. Zhan, Hydrophobic W18O49 mesocrystal on hydrophilic PTFE membrane as an efficient solar steam generation device under one sun, J Mater Chem A Mater. 6 (2018) 10939–10946. https://doi.org/10.1039/c8ta02700e.

[147] R. Du, H. Zhu, H. Zhao, H. Lu, C. Dong, M. Liu, F. Yang, J. Yang, J. Wang, J. Pan, Coupling ultrafine plasmonic Co3O4 with thin-layer carbon over SiO2 nanosphere for dual-functional PMS activation and solar interfacial water evaporation, 940 (2023). https://doi.org/10.1016/j.jallcom.2023.168816.

[148] H. Li, L. Li, L. Xiong, B. Wang, G. Wang, S. Ma, X. Han, SiO2/MXene/Poly(tetrafluoroethylene)-Based Janus Membranes as Solar Absorbers for Solar Steam Generation, ACS Appl Nano Mater. 4 (2021) 14274–14284. https://doi.org/10.1021/acsanm.1c03873.

[149] A.H. Elsheikh, S.W. Sharshir, M.K.A. Ali, J. Shaibo, E.M.A. Edreis, T. Abdelhamid, C. Du, Z. Haiou, Thin film technology for solar steam generation: A new dawn, Solar Energy. 177 (2019) 561–575. https://doi.org/10.1016/j.solener.2018.11.058.

[150] C.L. Guo, E.D. Miao, J.X. Zhao, L. Liang, Q. Liu, Paper-based integrated evaporation device for efficient solar steam generation through localized heating, Solar Energy. 188 (2019) 1283–1291. https://doi.org/10.1016/j.solener.2019.07.023.

[151] Q. Qi, Y. Wang, W. Wang, D. Yu, Surface self-assembled multi-layer MWCNTs-COOH/BN-PDA/CF for flexible and efficient solar steam generator, J Clean Prod. 279 (2021) 123626. https://doi.org/10.1016/j.jclepro.2020.123626.

[152] Y. Chen, S. Fang, L. Sun, F. Xu, M. Wang, J. Zhang, X. Mu, X. Wang, P. Wang, J. Liu, Z. Sun, H. Yao, J. Zhou, L. Miao, Hierarchical NiFe2O4-NiAl-LDH arrays immobilized on activated carbon cloth for bifunctional application on high-performance supercapacitors and solar steam generation, Sustainable Materials and Technologies. 33 (2022) e00500. https://doi.org/10.1016/j.susmat.2022.e00500.

[153] Y. Li, X. Jin, Y. Zheng, W. Li, F. Zheng, W. Wang, T. Lin, Z. Zhu, Tunable Water Delivery in Carbon-Coated Fabrics for High-Efficiency Solar Vapor Generation, ACS Appl Mater Interfaces. 11 (2019) 46938–46946. https://doi.org/10.1021/acsami.9b17360.

[154] Y. Li, R. Zan, Y. Wang, L. Shang, R. Wu, Y. Liu, Z. Rao, K. Yao, Y. Liu, L. Fei, Simultaneous engineering on absorption window and transportation geometry of

graphene-based foams toward high-performance solar steam generator, Appl Surf Sci. 599 (2022). https://doi.org/10.1016/j.apsusc.2022.154021.

[155] Q. Chen, Z. Pei, Y. Xu, Z. Li, Y. Yang, Y. Wei, Y. Ji, A durable monolithic polymer foam for efficient solar steam generation, Chem Sci. 9 (2018) 623–628. https://doi.org/10.1039/c7sc02967e.

[156] M. Zhu, X. Liu, Y. Tian, A. Caratenuto, F. Chen, Y. Zheng, Dome-arrayed chitosan/PVA hydrogel-based solar evaporator for steam generation, Sci Rep. 12 (2022). https://doi.org/10.1038/s41598-022-08589-z.

[157] Y. Gu, X. Mu, P. Wang, X. Wang, J. Liu, J. Shi, A. Wei, Y. Tian, G. Zhu, H. Xu, J. Zhou, L. Miao, Integrated photothermal aerogels with ultrahigh-performance solar steam generation, Nano Energy. 74 (2020) 104857. https://doi.org/10.1016/j.nanoen.2020.104857.

[158] F. Tao, M. Green, A.V. Garcia, T. Xiao, A.T. Van Tran, Y. Zhang, Y. Yin, X. Chen, Recent progress of nanostructured interfacial solar vapor generators, Appl Mater Today. 17 (2019) 45–84. https://doi.org/10.1016/j.apmt.2019.07.011.

[159] Y. Chang, X. Ma, P. Zhao, Flexible MoO2 coated PTEF membrane for stable solar steam generation in harsh environments, Solar Energy Materials and Solar Cells. 254 (2023). https://doi.org/10.1016/j.solmat.2023.112240.

[160] H. Jiang, H. Fang, D. Wang, J. Sun, Spray-Coated Commercial PTFE Membrane from MoS2/LaF3/PDMS Ink as Solar Absorber for Efficient Solar Steam Generation, Solar RRL. 4 (2020). https://doi.org/10.1002/solr.202000126.

[161] Q. Lu, Y. Yang, J. Feng, X. Wang, Oxygen-Defected Molybdenum Oxides Hierarchical Nanostructure Constructed by Atomic-Level Thickness Nanosheets as an Efficient Absorber for Solar Steam Generation, Solar RRL. 3 (2019) 1–8. https://doi.org/10.1002/solr.201800277.

[162] L. Huang, J. Pei, H. Jiang, X. Hu, Water desalination under one sun using graphene-based material modified PTFE membrane, Desalination. 442 (2018) 1–7. https://doi.org/10.1016/j.desal.2018.05.006.

[163] B. Bai, X. Yang, R. Tian, X.X. Wang, H. Wang, A high efficiency solar steam generation system with using residual heat to enhance steam escape, Desalination. 491 (2020) 114382. https://doi.org/10.1016/j.desal.2020.114382.

[164] X. Zhao, X.J. Zha, L.S. Tang, J.H. Pu, K. Ke, R.Y. Bao, Z. ying Liu, M.B. Yang, W. Yang, Self-assembled core-shell polydopamine@MXene with synergistic solar absorption capability for highly efficient solar-to-vapor generation, Nano Res. 13 (2020) 255–264. https://doi.org/10.1007/s12274-019-2608-0.

[165] J. Ji, F. Liu, N.A. Hashim, M.R.M. Abed, K. Li, Poly(vinylidene fluoride) (PVDF) membranes for fluid separation, React Funct Polym. 86 (2015) 134–153. https://doi.org/10.1016/j.reactfunctpolym.2014.09.023.

[166] N. Wei, Z. Li, Q. Li, E. Yang, R. Xu, X. Song, J. Sun, C. Dou, J. Tian, H. Cui, Scalable and low-cost fabrication of hydrophobic PVDF/WS2 porous membrane for highly efficient solar steam generation, J Colloid Interface Sci. 588 (2021) 369–377. https://doi.org/10.1016/j.jcis.2020.12.084.

[167] M. Xia, J. Wei, Z. Han, Q. Tian, C. Xiao, Q.M. Hasi, Y. Zhang, L. Chen, An integrated solar absorber with salt-resistant and oleophobic based on PVDF composite membrane for solar steam generation, Mater Today Energy. 25 (2022) 100959. https://doi.org/10.1016/j.mtener.2022.100959.

[168] Z. Chen, J. Li, J. Zhou, X. Chen, Photothermal Janus PPy-SiO2@PAN/F-SiO2@PVDF-HFP membrane for high-efficient, low energy and stable desalination through solar membrane distillation, Chemical Engineering Journal. 451 (2023) 138473. https://doi.org/10.1016/j.cej.2022.138473.

[169] J. Huang, Y. Hu, Y. Bai, Y. He, J. Zhu, Novel solar membrane distillation enabled by a PDMS/CNT/PVDF membrane with localized heating, Desalination. 489 (2020) 114529. https://doi.org/10.1016/j.desal.2020.114529.

[170] A.A. Tessema, C.M. Wu, K.G. Motora, S. Naseem, Highly-efficient and salt-resistant CsxWO3@g-C3N4/PVDF fiber membranes for interfacial water evaporation, desalination, and sewage treatment, Compos Sci Technol. 211 (2021) 108865. https://doi.org/10.1016/j.compscitech.2021.108865.

[171] C.H. Huang, J.X. Huang, Y.H. Chiao, C.M. Chang, W.S. Hung, S.J. Lue, C.F. Wang, C.C. Hu, K.R. Lee, H.H. Pan, J.Y. Lai, Tailoring of a Piezo-Photo-Thermal Solar Evaporator for Simultaneous Steam and Power Generation, Adv Funct Mater. 31 (2021). https://doi.org/10.1002/adfm.202010422.

[172] Y. Zhang, S. Cao, Z. Qiu, K. Yin, Y. Lei, K. Sun, X. Chang, X. Li, R. Fan, In situ chemo-polymerized polypyrrole-coated filter paper for high-efficient solar vapor generation, Int J Energy Res. 44 (2020) 1191–1204. https://doi.org/10.1002/er.5012.

[173] X. Shan, A. Zhao, Y. Lin, Y. Hu, Y. Di, C. Liu, Z. Gan, Low-Cost, Scalable, and Reusable Photothermal Layers for Highly Efficient Solar Steam Generation and Versatile Energy Conversion, Adv Sustain Syst. 4 (2020) 1–8. https://doi.org/10.1002/adsu.201900153.

[174] Q. Qi, Y. Wang, W. Wang, X. Ding, D. Yu, High-efficiency solar evaporator prepared by one-step carbon nanotubes loading on cotton fabric toward water purification, Science of the Total Environment. 698 (2020) 134136. https://doi.org/10.1016/j.scitotenv.2019.134136.

[175] J. Xiong, Z. Zhang, J. Yi, B. Li, X. Wang, Y. Wang, W. Wang, S. Peng, X. Min, M. Li, J. Peng, Hierarchical MnO2 Nanosheets Grown on Cotton Fabric as a Flexible and Washable Solar Evaporator for Seawater Desalination, ACS Appl Nano Mater. 4 (2021) 13724–13733. https://doi.org/10.1021/acsanm.1c03089.

[176] R. Meng, J. Lyu, L. Zou, Q. Zhong, Z. Liu, B. Zhu, M. Chen, L. Zhang, Z. Chen, CNT-based gel-coated cotton fabrics for constructing symmetrical evaporator with up/down inversion property for efficient continuous solar desalination, Desalination. 554 (2023) 116494. https://doi.org/https://doi.org/10.1016/j.desal.2023.116494.

[177] Y. Wang, Q. Qi, J. Fan, W. Wang, D. Yu, Simple and robust MXene/carbon nanotubes/cotton fabrics for textile wastewater purification via solar-driven interfacial water evaporation, Sep Purif Technol. 254 (2021). https://doi.org/10.1016/j.seppur.2020.117615.

[178] Z. Qin, H. Sun, Y. Tang, S. Yin, L. Yang, M. Xu, Z. Liu, Bioinspired Hydrophilic-Hydrophobic Janus Composites for Highly Efficient Solar Steam Generation, ACS Appl Mater Interfaces. 13 (2021) 19467–19475. https://doi.org/10.1021/acsami.1c02026.

[179] S. Gao, X. Dong, J. Huang, J. Dong, F. Di Maggio, S. Wang, F. Guo, T. Zhu, Z. Chen, Y. Lai, Bioinspired Soot-Deposited Janus Fabrics for Sustainable Solar Steam Generation with Salt-Rejection, Global Challenges. 3 (2019) 1800117. https://doi.org/10.1002/gch2.201800117.

[180] J. Wang, R. Wang, Y. Geng, Y. Li, J. Li, J. Qiu, M. Li, Activated pulverized coal membrane for effective solar-driven interfacial evaporation and desalination, Chem Eng Sci. 265 (2023) 118248. https://doi.org/10.1016/j.ces.2022.118248.

[181] R. Chen, K. Zhu, Q. Gan, Y. Yu, T. Zhang, X. Liu, M. Ye, Y. Yin, Interfacial solar heating by self-assembled Fe3O4@C film for steam generation, Mater Chem Front. 1 (2017) 2620–2626. https://doi.org/10.1039/c7qm00374a.

[182] Y. Dong, Y. Tan, K. Wang, Y. Cai, J. Li, C. Sonne, C. Li, Reviewing wood-based solar-driven interfacial evaporators for desalination, Water Res. 223 (2022). https://doi.org/10.1016/j.watres.2022.119011.

[183] J. Yang, Y. Chen, X. Jia, Y. Li, S. Wang, H. Song, Wood-Based Solar Interface Evaporation Device with Self-Desalting and High Antibacterial Activity for Efficient Solar Steam Generation, ACS Appl Mater Interfaces. 12 (2020) 47029–47037. https://doi.org/10.1021/acsami.0c14068.

[184] R. Mehrkhah, E.K. Goharshadi, E. Lichtfouse, H.S. Ahn, S. Wongwises, W. Yu, O. Mahian, Interfacial solar steam generation by wood-based devices to produce drinking water: a review, Environ Chem Lett. (2022). https://doi.org/10.1007/s10311-022-01501-1.

[185] C. Jia, Y. Li, Z. Yang, G. Chen, Y. Yao, F. Jiang, Y. Kuang, G. Pastel, H. Xie, B. Yang, S. Das, L. Hu, Rich Mesostructures Derived from Natural Woods for Solar Steam Generation, Joule. 1 (2017) 588–599. https://doi.org/10.1016/j.joule.2017.09.011.

[186] Y. Kuang, C. Chen, S. He, E.M. Hitz, Y. Wang, W. Gan, R. Mi, L. Hu, A High-Performance Self-Regenerating Solar Evaporator for Continuous Water Desalination, Advanced Materials. 31 (2019) 1900498. https://doi.org/10.1002/adma.201900498.

[187] H. Liu, C. Chen, G. Chen, Y. Kuang, X. Zhao, J. Song, C. Jia, X. Xu, E. Hitz, H. Xie, S. Wang, F. Jiang, T. Li, Y. Li, A. Gong, R. Yang, S. Das, L. Hu, High-Performance Solar Steam Device with Layered Channels: Artificial Tree with a Reversed Design, Adv Energy Mater. 8 (2018) 1–8. https://doi.org/10.1002/aenm.201701616.

[188] X. Luo, C. Huang, S. Liu, J. Zhong, High performance of carbon-particle/bulk-wood bi-layer system for solar steam generation, Int J Energy Res. 42 (2018) 4830–4839. https://doi.org/10.1002/er.4239.

[189] M.M. Ghafurian, H. Niazmand, E. Ebrahimnia-Bajestan, R.A. Taylor, Wood surface treatment techniques for enhanced solar steam generation, Renew Energy. 146 (2020) 2308–2315. https://doi.org/10.1016/j.renene.2019.08.036.

[190] L. Huang, L. Ling, J. Su, Y. Song, Z. Wang, B.Z. Tang, P. Westerhoff, R. Ye, Laser-Engineered Graphene on Wood Enables Efficient Antibacterial, Anti-Salt-Fouling, and Lipophilic-Matter-Rejection Solar Evaporation, ACS Appl Mater Interfaces. 12 (2020) 51864–51872. https://doi.org/10.1021/acsami.0c16596.

[191] M. Zhu, Y. Li, F. Chen, X. Zhu, J. Dai, Y. Li, Z. Yang, X. Yan, J. Song, Y. Wang, E. Hitz, W. Luo, M. Lu, B. Yang, L. Hu, Plasmonic Wood for High-Efficiency Solar Steam Generation, Adv Energy Mater. 8 (2018) 1–7. https://doi.org/10.1002/aenm.201701028.

[192] M. Wang, P. Wang, J. Zhang, C. Li, Y. Jin, A Ternary Pt/Au/TiO 2 -Decorated Plasmonic Wood Carbon for High-Efficiency Interfacial Solar Steam Generation and Photodegradation of Tetracycline, ChemSusChem. 12 (2019) 467–472. https://doi.org/10.1002/cssc.201802485.

[193] Z. Li, M. Zheng, N. Wei, Y. Lin, W. Chu, R. Xu, H. Wang, J. Tian, H. Cui, Broadband-absorbing WO3-x nanorod-decorated wood evaporator for highly efficient solar-driven interfacial steam generation, Solar Energy Materials and Solar Cells. 205 (2020) 110254. https://doi.org/10.1016/j.solmat.2019.110254.

[194] Y. Bian, Q. Du, K. Tang, Y. Shen, L. Hao, D. Zhou, X. Wang, Z. Xu, H. Zhang, L. Zhao, S. Zhu, J. Ye, H. Lu, Y. Yang, R. Zhang, Y. Zheng, S. Gu, Carbonized Bamboos as Excellent 3D Solar Vapor-Generation Devices, Adv Mater Technol. 4 (2019) 1800593. https://doi.org/https://doi.org/10.1002/admt.201800593.

[195] C. Sheng, N. Yang, Y. Yan, X. Shen, C. Jin, Z. Wang, Q. Sun, Bamboo decorated with plasmonic nanoparticles for efficient solar steam generation, Appl Therm Eng. 167 (2020) 114712. https://doi.org/10.1016/j.applthermaleng.2019.114712.

[196] Md.N.A.S. Ivan, A.M. Saleque, S. Ahmed, Z.L. Guo, D. Zu, L. Xu, T.I. Alam, S.U. Hani, Y.H. Tsang, Jute stick derived self-regenerating sustainable solar evaporators with different salt mitigation mechanisms for highly efficient solar desalination, J Mater Chem A Mater. 11 (2023) 3961–3974. https://doi.org/10.1039/D2TA08237C.

[197] Q. Wang, L. Wang, S. Song, Y. Li, F. Jia, T. Feng, N. Hu, Flexible 2D@ 3D Janus evaporators for high-performance and continuous solar desalination, Desalination. 525 (2022) 115483.

[198] Y. Shi, N. Meng, Y. Wang, Z. Cheng, W. Zhang, Y. Liao, Scalable Fabrication of Conjugated Microporous Polymer Sponges for Efficient Solar Steam Generation, ACS Appl Mater Interfaces. 14 (2022) 4522–4531. https://doi.org/10.1021/acsami.1c21693.

[199] Y. Cai, Y. Dong, K. Wang, D. Tian, J. Qu, J. Hu, J. Lee, J. Li, K.H. Kim, A polydimethylsiloxane-based sponge for water purification and interfacial solar steam generation, J Colloid Interface Sci. 629 (2023) 895–907. https://doi.org/10.1016/j.jcis.2022.09.045.

[200] B. Shao, Y. Wang, X. Wu, Y. Lu, X. Yang, G.Y. Chen, G. Owens, H. Xu, Stackable nickel-cobalt@polydopamine nanosheet based photothermal sponges for highly efficient solar steam generation, J Mater Chem A Mater. 8 (2020) 11665–11673. https://doi.org/10.1039/d0ta03799k.

[201] F. (Frank) Gong, H. Li, W. Wang, J. Huang, D. (David) Xia, J. Liao, M. Wu, D. V. Papavassiliou, Scalable, eco-friendly and ultrafast solar steam generators based on one-step melamine-derived carbon sponges toward water purification, Nano Energy. 58 (2019) 322–330. https://doi.org/10.1016/j.nanoen.2019.01.044.

[202] H. Li, M. Yang, A. Chu, H. Yang, J. Chen, Z. Yang, Y. Qian, J. Fang, Sustainable Lignocellulose-Based Sponge Coated with Polypyrrole for Efficient Solar Steam Generation, ACS Appl Polym Mater. 4 (2022) 6572–6581. https://doi.org/10.1021/acsapm.2c00935.

[203] L. Ren, X. Yi, Z. Yang, D. Wang, L. Liu, J. Ye, Designing carbonized loofah sponge architectures with plasmonic Cu nanoparticles encapsulated in graphitic layers for

highly efficient solar vapor generation, Nano Lett. 21 (2021) 1709–1715. https://doi.org/10.1021/acs.nanolett.0c04511.

[204] C. Liu, K. Hong, X. Sun, A. Natan, P. Luan, Y. Yang, H. Zhu, An 'antifouling'porous loofah sponge with internal microchannels as solar absorbers and water pumpers for thermal desalination, J Mater Chem A Mater. 8 (2020) 12323–12333.

[205] X. Shan, Y. Lin, A. Zhao, Y. Di, Y. Hu, Y. Guo, Z. Gan, Porous reduced graphene oxide/nickel foam for highly efficient solar steam generation, Nanotechnology. 30 (2019). https://doi.org/10.1088/1361-6528/ab3127.

[206] X. Gao, H. Ren, J. Zhou, R. Du, C. Yin, R. Liu, H. Peng, L. Tong, Z. Liu, J. Zhang, Synthesis of Hierarchical Graphdiyne-Based Architecture for Efficient Solar Steam Generation, Chemistry of Materials. 29 (2017) 5777–5781. https://doi.org/10.1021/acs.chemmater.7b01838.

[207] J. He, G. Zhao, P. Mu, H. Wei, Y. Su, H. Sun, Z. Zhu, W. Liang, A. Li, Scalable fabrication of monolithic porous foam based on cross-linked aromatic polymers for efficient solar steam generation, Solar Energy Materials and Solar Cells. 201 (2019). https://doi.org/10.1016/j.solmat.2019.110111.

[208] J. He, Z. Zhang, C. Xiao, F. Liu, H. Sun, Z. Zhu, W. Liang, A. Li, High-Performance Salt-Rejecting and Cost-Effective Superhydrophilic Porous Monolithic Polymer Foam for Solar Steam Generation, ACS Appl Mater Interfaces. 12 (2020) 16308–16318. https://doi.org/10.1021/acsami.9b22832.

[209] J. He, G. Zhao, P. Mu, H. Wei, Y. Su, H. Sun, Z. Zhu, W. Liang, A. Li, Scalable fabrication of monolithic porous foam based on cross-linked aromatic polymers for efficient solar steam generation, Solar Energy Materials and Solar Cells. 201 (2019). https://doi.org/10.1016/j.solmat.2019.110111.

[210] C. Wang, J. Wang, Z. Li, K. Xu, T. Lei, W. Wang, Superhydrophilic porous carbon foam as a self-desalting monolithic solar steam generation device with high energy efficiency, J Mater Chem A Mater. 8 (2020) 9528–9535. https://doi.org/10.1039/d0ta01439g.

[211] W. Fang, L. Zhao, X. He, H. Chen, W. Li, X. Zeng, X. Chen, Y. Shen, W. Zhang, Carbonized rice husk foam constructed by surfactant foaming method for solar steam generation, Renew Energy. 151 (2020) 1067–1075. https://doi.org/10.1016/j.renene.2019.11.111.

[212] W. Zhang, W. Zhu, S. Shi, N. Hu, Y. Suo, J. Wang, Bioinspired foam with large 3D macropores for efficient solar steam generation, J Mater Chem A Mater. 6 (2018) 16220–16227. https://doi.org/10.1039/c8ta04296a.

[213] J. Zhou, Z. Sun, X. Mu, J. Zhang, P. Wang, Y. Chen, X. Wang, J. Gao, L. Miao, L. Sun, Highly efficient and long-term stable solar-driven water purification through a rechargeable hydrogel evaporator, Desalination. 537 (2022). https://doi.org/10.1016/j.desal.2022.115872.

[214] J. He, Y. Fan, C. Xiao, F. Liu, H. Sun, Z. Zhu, W. Liang, A. Li, Enhanced solar steam generation of hydrogel composite with aligned channel and shape memory behavior, Compos Sci Technol. 204 (2021) 108633. https://doi.org/https://doi.org/10.1016/j.compscitech.2020.108633.

[215] N. Hu, Y. Xu, Z. Liu, M. Liu, X. Shao, J. Wang, Double-layer cellulose hydrogel solar steam generation for high-efficiency desalination, Carbohydr Polym. 243 (2020). https://doi.org/10.1016/j.carbpol.2020.116480.

[216] X. Yin, Y. Zhang, Q. Guo, X. Cai, J. Xiao, Z. Ding, J. Yang, Macroporous Double-Network Hydrogel for High-Efficiency Solar Steam Generation under 1 sun Illumination, ACS Appl Mater Interfaces. 10 (2018) 10998–11007. https://doi.org/10.1021/acsami.8b01629.

[217] L. Li, N. He, B. Jiang, K. Yu, Q. Zhang, H. Zhang, D. Tang, Y. Song, Highly Salt-Resistant 3D Hydrogel Evaporator for Continuous Solar Desalination via Localized Crystallization, Adv Funct Mater. 2104380 (2021) 2104380. https://doi.org/10.1002/adfm.202104380.

[218] F. Jiang, H. Liu, Y. Li, Y. Kuang, X. Xu, C. Chen, H. Huang, C. Jia, X. Zhao, E. Hitz, Y. Zhou, R. Yang, L. Cui, L. Hu, Lightweight, Mesoporous, and Highly Absorptive All-Nanofiber Aerogel for Efficient Solar Steam Generation, ACS Appl Mater Interfaces. 10 (2018) 1104–1112. https://doi.org/10.1021/acsami.7b15125.

[219] S. Han, T.P. Ruoko, J. Gladisch, J. Erlandsson, L. Wågberg, X. Crispin, S. Fabiano, Cellulose-Conducting Polymer Aerogels for Efficient Solar Steam Generation, Adv Sustain Syst. 4 (2020). https://doi.org/10.1002/adsu.202000004.

[220] X. Hu, W. Xu, L. Zhou, Y. Tan, Y. Wang, S. Zhu, J. Zhu, Tailoring Graphene Oxide-Based Aerogels for Efficient Solar Steam Generation under One Sun, Advanced Materials. 29 (2017). https://doi.org/10.1002/adma.201604031.

[221] X. Han, S. Ding, L. Fan, Y. Zhou, S. Wang, Janus biocomposite aerogels constituted of cellulose nanofibrils and MXenes for application as single-module solar-driven interfacial evaporators, J Mater Chem A Mater. 9 (2021) 18614–18622. https://doi.org/10.1039/d1ta04991g.

[222] J. Ren, S. Yang, Z. Hu, H. Wang, Self-Propelled Aerogel Solar Evaporators for Efficient Solar Seawater Purification, Langmuir. 37 (2021) 9532–9539. https://doi.org/10.1021/acs.langmuir.1c01387.

[223] X. Lu, J. Tang, Z. Song, H. Wang, D. Yu, G. Li, W. Li, W. Liu, Hyperstable and compressible plant fibers/chitosan aerogel as portable solar evaporator, Solar Energy. 231 (2022) 828–836. https://doi.org/10.1016/j.solener.2021.12.036.

[224] L. Chen, J. Wei, Q. Tian, Z. Han, L. Li, S. Meng, Q.M. Hasi, Dual-Functional Graphene Oxide-Based Photothermal Materials with Aligned Channels and Oleophobicity for Efficient Solar Steam Generation, Langmuir. 37 (2021) 10191–10199. https://doi.org/10.1021/acs.langmuir.1c01647.

[225] J. Yuan, X. Lei, C. Yi, H. Jiang, F. Liu, G.J. Cheng, 3D-printed hierarchical porous cellulose/alginate/carbon black hydrogel for high-efficiency solar steam generation, Chemical Engineering Journal. 430 (2022). https://doi.org/10.1016/j.cej.2021.132765.

[226] M.S. Irshad, X. Wang, M.S. Abbasi, N. Arshad, Z. Chen, Z. Guo, L. Yu, J. Qian, J. You, T. Mei, Semiconductive, Flexible MnO2NWs/Chitosan Hydrogels for Efficient Solar Steam Generation, ACS Sustain Chem Eng. 9 (2021) 3887–3900. https://doi.org/10.1021/acssuschemeng.0c08981.

[227] Y. Sun, J. Gao, Y. Liu, H. Kang, M. Xie, F. Wu, H. Qiu, Copper sulfide-macroporous polyacrylamide hydrogel for solar steam generation, Chem Eng Sci. 207 (2019) 516–526. https://doi.org/10.1016/j.ces.2019.06.044.

[228] Z. Yu, P. Wu, Biomimetic MXene-Polyvinyl Alcohol Composite Hydrogel with Vertically Aligned Channels for Highly Efficient Solar Steam Generation, Adv Mater Technol. 5 (2020). https://doi.org/10.1002/admt.202000065.

[229] M.-Q. Yang, C.F. Tan, W. Lu, K. Zeng, G.W. Ho, Spectrum Tailored Defective 2D Semiconductor Nanosheets Aerogel for Full-Spectrum-Driven Photothermal Water Evaporation and Photochemical Degradation, Adv Funct Mater. 30 (2020) 2004460. https://doi.org/https://doi.org/10.1002/adfm.202004460.

[230] Y. Tian, X. Wang, Y. Gu, X. Mu, P. Wang, A. Wei, J. Zhang, Y. Chen, Z. Sun, L. Jia, Z. Zhao, J. Zhou, L. Miao, Versatile PVA/CS/CuO aerogel with superior hydrophilic and mechanical properties towards efficient solar steam generation, Nano Select. 2 (2021) 2380–2389. https://doi.org/10.1002/nano.202100125.

[231] X. Zhou, F. Zhao, Y. Guo, B. Rosenberger, G. Yu, Architecting highly hydratable polymer networks to tune the water state for solar water purification, Sci Adv. 5 (2019) 1–8. https://doi.org/10.1126/sciadv.aaw5484.

[232] F. Zhao, Y. Guo, X. Zhou, W. Shi, G. Yu, Materials for solar-powered water evaporation, Nat Rev Mater. 5 (2020) 388–401. https://doi.org/10.1038/s41578-020-0182-4.

[233] J. Ren, L. Chen, J. Gong, J. Qu, R. Niu, Hofmeister effect mediated hydrogel evaporator for simultaneous solar evaporation and thermoelectric power generation, Chemical Engineering Journal. 458 (2023) 141511. https://doi.org/10.1016/j.cej.2023.141511.

[234] X. Fan, Y. Peng, B. Lv, Y. Yang, Z. You, C. Song, Y. Xu, A siphon-based spatial evaporation device for efficient salt-free interfacial steam generation, Desalination. 552 (2023) 116442. https://doi.org/10.1016/j.desal.2023.116442.

[235] X. Zhou, Y. Guo, F. Zhao, W. Shi, G. Yu, Topology-Controlled Hydration of Polymer Network in Hydrogels for Solar-Driven Wastewater Treatment, Advanced Materials. 32 (2020) 1–7. https://doi.org/10.1002/adma.202007012.

[236] Y. Xu, B. Lv, Y. Yang, X. Fan, Y. Yu, C. Song, Y. Liu, Facile fabrication of low-cost starch-based biohydrogel evaporator for efficient solar steam generation, Desalination. 517 (2021) 115260. https://doi.org/10.1016/j.desal.2021.115260.

[237] Y. Guo, X. Zhou, F. Zhao, J. Bae, B. Rosenberger, G. Yu, Synergistic Energy Nanoconfinement and Water Activation in Hydrogels for Efficient Solar Water Desalination, ACS Nano. 13 (2019) 7913–7919. https://doi.org/10.1021/acsnano.9b02301.

[238] A.M. Saleque, M.N.A.S. Ivan, S. Ahmed, Y.H. Tsang, Light-trapping texture bio-hydrogel with anti-biofouling and antibacterial properties for efficient solar desalination, Chemical Engineering Journal. 458 (2023) 141430. https://doi.org/10.1016/j.cej.2023.141430.

[239] S. Mao, C. Onggowarsito, A. Feng, S. Zhang, Q. Fu, L.D. Nghiem, A cryogel solar vapor generator with rapid water replenishment and high intermediate water content for seawater desalination, J Mater Chem A Mater. 11 (2022) 858–867. https://doi.org/10.1039/d2ta08317e.

[240] B. Wen, X. Zhang, Y. Yan, Y. Huang, S. Lin, Y. Zhu, Z. Wang, B. Zhou, S. Yang, J. Liu, Tailoring polypyrrole-based Janus aerogel for efficient and stable solar steam generation, Desalination. 516 (2021) 115228.

[241] C.T.K. Finnerty, A.K. Menon, K.M. Conway, D. Lee, M. Nelson, J.J. Urban, D. Sedlak, B. Mi, Interfacial Solar Evaporation by a 3D Graphene Oxide Stalk for Highly Concentrated Brine Treatment, Environ Sci Technol. 55 (2021) 15435–15445. https://doi.org/10.1021/acs.est.1c04010.

[242] Y. Chen, J. Yang, J. Guo, F. Fang, A 3D photothermal bar for efficient steam generation, J Environ Chem Eng. 11 (2023) 109179. https://doi.org/10.1016/j.jece.2022.109179.

[243] D.N. Thoai, Q.T.H. Ta, T.T. Truong, H. Van Nam, G. Van Vo, Review on the recent development and applications of three dimensional (3D) photothermal materials for solar evaporators, J Clean Prod. 293 (2021). https://doi.org/10.1016/j.jclepro.2021.126122.

[244] C. Li, W. Li, H.Y. Zhao, X.Y. Feng, X. Li, Z.Z. Yu, Constructing central hollow cylindrical reduced graphene oxide foams with vertically and radially orientated porous channels for highly efficient solar-driven water evaporation and purification, Nano Res. (2023). https://doi.org/10.1007/s12274-022-5348-5.

[245] T.A. Wani, P. Garg, A. Bera, An environmental pollutant to an efficient solar vapor generator: An eco-friendly method for freshwater production, Mater Adv. 2 (2021) 3856–3861. https://doi.org/10.1039/d1ma00361e.

[246] Y. Xu, J. Xu, J. Zhang, X. Li, B. Fu, C. Song, W. Shang, P. Tao, T. Deng, All-in-one polymer sponge composite 3D evaporators for simultaneous high-flux solar-thermal desalination and electricity generation, Nano Energy. 93 (2022). https://doi.org/10.1016/j.nanoen.2021.106882.

[247] J. Tang, T. Zheng, Z. Song, Y. Shao, N. Li, K. Jia, Y. Tian, Q. Song, H. Liu, G. Xue, Realization of Low Latent Heat of a Solar Evaporator via Regulating the Water State in Wood Channels, ACS Appl Mater Interfaces. 12 (2020) 18504–18511. https://doi.org/10.1021/acsami.0c01261.

[248] X. Wang, Z. Li, Y. Wu, H. Guo, X. Zhang, Y. Yang, H. Mu, J. Duan, Construction of a Three-Dimensional Interpenetrating Network Sponge for High-Efficiency and Cavity-Enhanced Solar-Driven Wastewater Treatment, ACS Appl Mater Interfaces. 13 (2021) 10902–10915. https://doi.org/10.1021/acsami.0c21690.

[249] J. Wu, T. Zhang, J. Qu, F.Z. Jiao, C. Hu, H.Y. Zhao, X. Li, Z.Z. Yu, Hydrothermally Modified 3D Porous Loofah Sponges with MoS2 Sheets and Carbon Particles for Efficient Solar Steam Generation and Seawater Desalination, ACS Appl Mater Interfaces. (2023). https://doi.org/10.1021/acsami.3c05198.

[250] P. Anukunwithaya, J.J. Koh, J.C.C. Yeo, S. Liu, X. Hou, N. Liu, C. He, A self-regenerating 3D sponge evaporator with a tunable porous structure for efficient solar desalination, J Mater Chem A Mater. 10 (2022) 15743–15751. https://doi.org/10.1039/d2ta03452b.

[251] T.A. Wani, P. Garg, S. Bera, S. Bhattacharya, S. Dutta, H. Kumar, A. Bera, Narrow-Bandgap LaMO3 (M = Ni, Co) nanomaterials for efficient interfacial solar steam generation, J Colloid Interface Sci. 612 (2022) 203–212. https://doi.org/10.1016/j.jcis.2021.12.158.

[252] R.T. Ginting, H. Abdullah, V. Fauzia, Facile preparation of MXene and protonated-g-C3N4 on natural latex foam for highly efficient solar steam generation, Mater Lett. 313 (2022). https://doi.org/10.1016/j.matlet.2022.131779.

[253] X. Ming, A. Guo, Q. Zhang, Z. Guo, F. Yu, B. Hou, Y. Wang, K.P. Homewood, X. Wang, 3D macroscopic graphene oxide/MXene architectures for multifunctional water purification, Carbon N Y. 167 (2020) 285–295. https://doi.org/10.1016/j.carbon.2020.06.023.

[254] L. Chen, X. Mu, Y. Guo, H. Lu, Y. Yang, C. Xiao, Q. Hasi, MXene-doped kapok fiber aerogels with oleophobicity for efficient interfacial solar steam generation, J Colloid Interface Sci. 626 (2022) 35–46. https://doi.org/10.1016/j.jcis.2022.06.143.

[255] H. Liu, Y. Liu, L. Wang, X. Qin, J. Yu, Nanofiber based origami evaporator for multifunctional and omnidirectional solar steam generation, Carbon N Y. 177 (2021) 199–206. https://doi.org/10.1016/j.carbon.2021.02.081.

[256] W. Li, X. Tian, X. Li, J. Liu, C. Li, X. Feng, C. Shu, Z.Z. Yu, An environmental energy-enhanced solar steam evaporator derived from MXene-decorated cellulose acetate cigarette filter with ultrahigh solar steam generation efficiency, J Colloid Interface Sci. 606 (2022) 748–757. https://doi.org/10.1016/j.jcis.2021.08.043.

[257] Z. Ai, Y. Zhao, R. Gao, L. Chen, T. Wen, W. Wang, T. Zhang, W. Ge, S. Song, Self-assembly hierarchical binary gel based on MXene and montmorillonite nanosheets for efficient and stable solar steam generation, J Clean Prod. 357 (2022) 132000. https://doi.org/10.1016/j.jclepro.2022.132000.

[258] Z. Ai, Y. Zhao, L. Chen, T. Wen, S. Song, T. Zhang, Floating MMT/MXene janus membrane for solar steam generation and mechanism of improving water transportation by DFT calculation, Sep Purif Technol. 300 (2022). https://doi.org/10.1016/j.seppur.2022.121918.

[259] L. Pu, H. Ma, J. Dong, C. Zhang, F. Lai, G. He, P. Ma, W. Dong, Y. Huang, T. Liu, Xylem-Inspired Polyimide/MXene Aerogels with Radial Lamellar Architectures for Highly Sensitive Strain Detection and Efficient Solar Steam Generation, Nano Lett. 22 (2022) 4560–4568. https://doi.org/10.1021/acs.nanolett.2c01486.

[260] X.J. Zha, X. Zhao, J.H. Pu, L.S. Tang, K. Ke, R.Y. Bao, L. Bai, Z.Y. Liu, M.B. Yang, W. Yang, Flexible Anti-Biofouling MXene/Cellulose Fibrous Membrane for Sustainable Solar-Driven Water Purification, ACS Appl Mater Interfaces. 11 (2019) 36589–36597. https://doi.org/10.1021/acsami.9b10606.

[261] K. Li, T. Chang, Z. Li, H. Yang, F. Fu, T. Li, J.S. Ho, P. Chen, Biomimetic MXene Textures with Enhanced Light-to-Heat Conversion for Solar Steam Generation and Wearable Thermal Management, Adv Energy Mater. 9 (2019) 1901687. https://doi.org/10.1002/aenm.201901687.

[262] J. Fei, S.W. Koh, W. Tu, J. Ge, H. Rezaeyan, S. Hou, H. Duan, Y.C. Lam, H. Li, Functionalized MXene Enabled Sustainable Water Harvesting and Desalination, Adv Sustain Syst. 4 (2020) 2000102. https://doi.org/10.1002/adsu.202000102.

[263] X.P. Li, X. Li, H. Li, Y. Zhao, W. Li, S. Yan, Z.Z. Yu, 2D Ferrous Ion-Crosslinked Ti3C2Tx MXene Aerogel Evaporators for Efficient Solar Steam Generation, Adv Sustain Syst. 5 (2021). https://doi.org/10.1002/adsu.202100263.

[264] X. Zhao, L.M. Peng, C.Y. Tang, J.H. Pu, X.J. Zha, K. Ke, R.Y. Bao, M.B. Yang, W. Yang, All-weather-available, continuous steam generation based on the synergistic photo-thermal and electro-thermal conversion by MXene-based aerogels, Mater Horiz. 7 (2020) 855–865. https://doi.org/10.1039/c9mh01443h.

[265] T. Wang, S. Gao, G. Wang, H. Wang, J. Bai, S. Ma, B. Wang, Three-dimensional hierarchical oxygen vacancy-rich WO3-decorated Ni foam evaporator for high-efficiency solar-driven interfacial steam generation, J Colloid Interface Sci. 602 (2021) 767–777. https://doi.org/10.1016/j.jcis.2021.06.065.

[266] M. Aziznezhad, E. Goharshadi, M. Namayandeh-Jorabchi, Surfactant-mediated prepared VO2 (M) nanoparticles for efficient solar steam generation, Solar Energy Materials and Solar Cells. (2020). https://doi.org/10.1016/j.solmat.2020.110515.

[267] I. Ibrahim, D.H. Seo, A. Angeloski, A. McDonagh, H.K. Shon, L.D. Tijing, 3D microflowers CuS/Sn2S3 heterostructure for highly efficient solar steam generation and water purification, Solar Energy Materials and Solar Cells. 232 (2021). https://doi.org/10.1016/j.solmat.2021.111377.

[268] I. Zada, W. Zhang, P. Sun, M. Imtiaz, N. Iqbal, U. Ghani, R. Naz, Y. Zhang, Y. Li, J. Gu, Q. Liu, D. Pantelić, B. Jelenković, D. Zhang, Superior photothermal black TiO2 with random size distribution as flexible film for efficient solar steam generation, Appl Mater Today. 20 (2020) 100669. https://doi.org/10.1016/j.apmt.2020.100669.

[269] Y. Shi, R. Li, Y. Jin, S. Zhuo, L. Shi, J. Chang, S. Hong, K.C. Ng, P. Wang, A 3D Photothermal Structure toward Improved Energy Efficiency in Solar Steam Generation, Joule. 2 (2018) 1171–1186. https://doi.org/10.1016/j.joule.2018.03.013.

[270] T. Chen, Z. Wu, Z. Liu, J.T. Aladejana, X. (Alice) Wang, M. Niu, Q. Wei, Y. Xie, Hierarchical Porous Aluminophosphate-Treated Wood for High-Efficiency Solar Steam Generation, ACS Appl Mater Interfaces. 12 (2020) 19511–19518. https://doi.org/10.1021/acsami.0c01815.

[271] J. Wang, Y. Li, L. Deng, N. Wei, Y. Weng, S. Dong, D. Qi, J. Qiu, X. Chen, T. Wu, High-Performance Photothermal Conversion of Narrow-Bandgap Ti2O3Nanoparticles, Advanced Materials. 29 (2017) 1–6. https://doi.org/10.1002/adma.201603730.

[272] Z. Guo, X. Ming, G. Wang, B. Hou, X. Liu, T. Mei, J. Li, J. Wang, X. Wang, Super-hydrophilic copper sulfide films as light absorbers for efficient solar steam generation under one sun illumination, Semicond Sci Technol. 33 (2018). https://doi.org/10.1088/1361-6641/aaa323.

[273] G. Wang, Y. Fu, X. Ma, W. Pi, D. Liu, X. Wang, Reusable reduced graphene oxide based double-layer system modified by polyethylenimine for solar steam generation, Carbon N Y. 114 (2017) 117–124. https://doi.org/10.1016/j.carbon.2016.11.071.

[274] X.F. Zhang, Z. Wang, L. Song, Y. Feng, J. Yao, Chinese ink enabled wood evaporator for continuous water desalination, Desalination. 496 (2020) 114727. https://doi.org/10.1016/j.desal.2020.114727.

[275] L. Noureen, Z. Xie, M. Hussain, M. Li, Q. Lyu, K. Wang, L. Zhang, J. Zhu, BiVO4 and reduced graphene oxide composite hydrogels for solar-driven steam generation and decontamination of polluted water, Solar Energy Materials and Solar Cells. 222 (2021). https://doi.org/10.1016/j.solmat.2020.110952.

[276] M. Yang, T. Chu, J. Shi, J. Zhang, Y. Zhang, L. Wang, Synergy of photothermal effect in integrated 0D natural melanin /2D reduced graphene oxide for effective solar steam generation and water purification, Colloids Surf A Physicochem Eng Asp. 632 (2022). https://doi.org/10.1016/j.colsurfa.2021.127786.

[277] S. Sun, B. Sun, Y. Wang, M.F. Antwi-Afari, H.Y. Mi, Z. Guo, C. Liu, C. Shen, Carbon black and polydopamine modified non-woven fabric enabling efficient solar steam generation towards seawater desalination and wastewater purification, Sep Purif Technol. 278 (2022). https://doi.org/10.1016/j.seppur.2021.119621.

[278] C. Xiao, W. Liang, Q.M. Hasi, F. Wang, L. Chen, J. He, F. Liu, H. Sun, Z. Zhu, A. Li, Efficient solar steam generation of carbon black incorporated hyper-cross-linked polymer composites, ACS Appl Energy Mater. 3 (2020) 11350–11358. https://doi.org/10.1021/acsaem.0c02290.

[279] L. Wang, C. Liu, H. Wang, Y. Xu, S. Ma, Y. Zhuang, W. Xu, W. Cui, H. Yang, Three-Dimensional Wood-Inspired Bilayer Membrane Device Containing Microchannels for Highly Efficient Solar Steam Generation, ACS Appl Mater Interfaces. 12 (2020) 24328–24338. https://doi.org/10.1021/acsami.0c04740.

[280] S. Wang, Y. Niu, C. Wang, F. Wang, Z. Zhu, H. Sun, W. Liang, A. Li, Modified Hollow Glass Microspheres/Reduced Graphene Oxide Composite Aerogels with Low Thermal Conductivity for Highly Efficient Solar Steam Generation, ACS Appl Mater Interfaces. 13 (2021) 42803–42812. https://doi.org/10.1021/acsami.1c11291.

[281] H.C. Yang, Z. Chen, Y. Xie, J. Wang, J.W. Elam, W. Li, S.B. Darling, Chinese Ink: A Powerful Photothermal Material for Solar Steam Generation, Adv Mater Interfaces. 6 (2019) 1–7. https://doi.org/10.1002/admi.201801252.

[282] R. Zhang, Y. Zhou, B. Xiang, X. Zeng, Y. Luo, X. Meng, S. Tang, Scalable Carbon Black Enhanced Nanofiber Network Films for High-Efficiency Solar Steam Generation, Adv Mater Interfaces. 8 (2021) 1–9. https://doi.org/10.1002/admi.202101160.

[283] Y. Jin, J. Chang, Y. Shi, L. Shi, S. Hong, P. Wang, A highly flexible and washable nonwoven photothermal cloth for efficient and practical solar steam generation, J Mater Chem A Mater. 6 (2018) 7942–7949. https://doi.org/10.1039/c8ta00187a.

[284] T. Chen, S. Wang, Z. Wu, X. (Alice) Wang, J. Peng, B. Wu, J. Cui, X. Fang, Y. Xie, N. Zheng, A cake making strategy to prepare reduced graphene oxide wrapped plant fiber sponges for high-efficiency solar steam generation, J Mater Chem A Mater. 6 (2018) 14571–14576. https://doi.org/10.1039/C8TA04420A.

[285] Z. Zhang, P. Mu, J. Han, J. He, Z. Zhu, H. Sun, W. Liang, A. Li, Superwetting and mechanically robust MnO2 nanowire-reduced graphene oxide monolithic aerogels for efficient solar vapor generation, J Mater Chem A Mater. 7 (2019) 18092–18099. https://doi.org/10.1039/c9ta04509k.

[286] F. Wang, D. Wei, Y. Li, T. Chen, P. Mu, H. Sun, Z. Zhu, W. Liang, A. Li, Chitosan/reduced graphene oxide-modified spacer fabric as a salt-resistant solar absorber for efficient solar steam generation, J Mater Chem A Mater. 7 (2019) 18311–18317. https://doi.org/10.1039/c9ta05859a.

[287] F. Wang, P. Mu, Z. Zhang, T. Chen, Y. Li, H. Sun, Z. Zhu, W. Liang, A. Li, Reduced Graphene Oxide Coated Hollow Polyester Fibers for Efficient Solar Steam Generation, Energy Technology. 7 (2019). https://doi.org/10.1002/ente.201900265.

[288] Z. Deng, P.F. Liu, J. Zhou, L. Miao, Y. Peng, H. Su, P. Wang, X. Wang, W. Cao, F. Jiang, L. Sun, S. Tanemura, A Novel Ink-Stained Paper for Solar Heavy Metal Treatment and Desalination, Solar RRL. 2 (2018). https://doi.org/10.1002/solr.201800073.

[289] Y. Lin, W. Zhou, Y. Di, X. Zhang, L. Yang, Z. Gan, Low-cost carbonized kelp for highly efficient solar steam generation, AIP Adv. 9 (2019). https://doi.org/10.1063/1.5096295.

[290] J. Feng, B. Bai, L. Yang, N. Hu, H. Wang, Low-cost and facile hydrophilic amplification of raw corn straws for the applications of highly efficient interfacial solar steam generation, Mater Chem Phys. 271 (2021). https://doi.org/10.1016/j.matchemphys.2021.124904.

[291] D. Wu, C. Du, C. Huang, Combining carbonized sawdust beds with preheating water design for efficient solar steam generation, Appl Therm Eng. 195 (2021). https://doi.org/10.1016/j.applthermaleng.2021.117238.

[292] S. Lal, S.K. Batabyal, Potato-based microporous carbon cake: Solar radiation induced water treatment, J Environ Chem Eng. 10 (2022). https://doi.org/10.1016/j.jece.2022.108502.

[293] J. Fang, J. Liu, J. Gu, Q. Liu, W. Zhang, H. Su, D. Zhang, Hierarchical porous carbonized lotus seedpods for highly efficient solar steam generation, Chemistry of Materials. 30 (2018) 6217–6221. https://doi.org/10.1021/acs.chemmater.8b01702.

[294] Y. Lu, X. Wang, D. Fan, H. Yang, H. Xu, H. Min, X. Yang, Biomass derived Janus solar evaporator for synergic water evaporation and purification, Sustainable Materials and Technologies. 25 (2020). https://doi.org/10.1016/j.susmat.2020.e00180.

[295] Y. Geng, W. Sun, P. Ying, Y. Zheng, J. Ding, K. Sun, L. Li, M. Li, Bioinspired Fractal Design of Waste Biomass-Derived Solar–Thermal Materials for Highly Efficient Solar Evaporation, Adv Funct Mater. 31 (2021). https://doi.org/10.1002/adfm.202007648.

[296] Q. Fang, T. Li, Z. Chen, H. Lin, P. Wang, F. Liu, Full Biomass-Derived Solar Stills for Robust and Stable Evaporation to Collect Clean Water from Various Water-Bearing Media, ACS Appl Mater Interfaces. 11 (2019) 10672–10679. https://doi.org/10.1021/acsami.9b00291.

[297] X. Chen, Z. Wu, D. Lai, M. Zheng, L. Xu, J. Huo, Z. Chen, B. Yuan, M.L. Fu, Resilient biomass-derived hydrogel with tailored topography for highly efficient and long-term solar evaporation of high-salinity brine, J Mater Chem A Mater. 8 (2020) 22645–22656. https://doi.org/10.1039/d0ta07040h.

[298] Y. Wu, R. Kong, C. Ma, L. Li, Y. Zheng, Y. Lu, L. Liang, Y. Pang, Q. Wu, Z. Shen, H. Chen, Simulation-Guided Design of Bamboo Leaf-Derived Carbon-Based High-Efficiency Evaporator for Solar-Driven Interface Water Evaporation, Energy and Environmental Materials. 5 (2022) 1323–1331. https://doi.org/10.1002/eem2.12251.

[299] M.S. Zafar, M. Zahid, A. Athanassiou, D. Fragouli, Biowaste-Derived Carbonized Bone for Solar Steam Generation and Seawater Desalination, Adv Sustain Syst. 5 (2021). https://doi.org/10.1002/adsu.202100031.

[300] J. Li, X. Zhou, G. Chen, F. Wang, J. Mao, Y. Long, H. Sun, Z. Zhu, W. Liang, A. Li, Evaporation efficiency monitoring device based on biomass photothermal material for salt-resistant solar-driven interfacial evaporation, Solar Energy Materials and Solar Cells. 222 (2021). https://doi.org/10.1016/j.solmat.2020.110941.

[301] Y. Pang, J. Zhang, R. Ma, Z. Qu, E. Lee, T. Luo, Solar–Thermal Water Evaporation: A Review, ACS Energy Lett. 5 (2020) 437–456. https://doi.org/10.1021/acsenergylett.9b02611.

[302] H. Ghasemi, G. Ni, A.M. Marconnet, J. Loomis, S. Yerci, N. Miljkovic, G. Chen, Solar steam generation by heat localization, Nat Commun. 5 (2014) 4449. https://doi.org/10.1038/ncomms5449.

[303] G. Ni, S.H. Zandavi, S.M. Javid, S. V Boriskina, T.A. Cooper, G. Chen, A salt-rejecting floating solar still for low-cost desalination, Energy Environ Sci. 11 (2018) 1510–1519. https://doi.org/10.1039/c8ee00220g.

[304] Z. Liu, B. Wu, B. Zhu, Z. Chen, M. Zhu, X. Liu, Continuously Producing Watersteam and Concentrated Brine from Seawater by Hanging Photothermal Fabrics under Sunlight, Adv Funct Mater. 29 (2019) 1905485. https://doi.org/10.1002/adfm.201905485.

[305] F. Peng, J. Xu, X. Bai, G. Feng, X. Zeng, M.R. Ibn Raihan, H. Bao, M.R.I. Raihan, H. Bao, A janus solar evaporator with 2D water path for highly efficient salt-resisting solar steam generation, Solar Energy Materials and Solar Cells. 221 (2021) 110910. https://doi.org/10.1016/j.solmat.2020.110910.

[306] X. Mu, Y. Gu, P. Wang, A. Wei, Y. Tian, J. Zhou, Y. Chen, J. Zhang, Z. Sun, J. Liu, L. Sun, S. Tanemura, L. Miao, Strategies for breaking theoretical evaporation limitation in direct solar steam generation, Solar Energy Materials and Solar Cells. 220 (2021). https://doi.org/10.1016/j.solmat.2020.110842.

[307] X. Min, B. Zhu, B. Li, J. Li, J. Zhu, Interfacial Solar Vapor Generation: Materials and Structural Design, Acc Mater Res. 2 (2021) 198–209. https://doi.org/10.1021/accountsmr.0c00104.

[308] X. Li, R. Lin, G. Ni, N. Xu, X. Hu, B. Zhu, G. Lv, J. Li, S. Zhu, J. Zhu, Three-dimensional artificial transpiration for efficient solar waste-water treatment, Natl Sci Rev. 5 (2018) 70–77. https://doi.org/10.1093/nsr/nwx051.

[309] X. Li, W. Xu, M. Tang, L. Zhou, B. Zhu, S. Zhu, J. Zhu, Graphene oxide-based efficient and scalable solar desalination under one sun with a confined 2D water path, Proc Natl Acad Sci U S A. 113 (2016) 13953–13958. https://doi.org/10.1073/pnas.1613031113.

[310] F. Liu, L. Xia, L. Zhang, F. Guo, X. Zhang, Y. Yu, R. Yang, Sunflower-Stalk-Based Solar-Driven Evaporator with a Confined 2D Water Channel and an Enclosed Thermal-Insulating Cellular Structure for Stable and Efficient Steam Generation, ACS Appl Mater Interfaces. 13 (2021) 55299–55306. https://doi.org/10.1021/acsami.1c20747.

[311] Y. Sui, D. Hao, Y. Guo, Z. Cai, B. Xu, A flowerlike sponge coated with carbon black nanoparticles for enhanced solar vapor generation, J Mater Sci. 55 (2020) 298–308. https://doi.org/10.1007/s10853-019-03977-9.

[312] X. Li, W. Xu, M. Tang, L. Zhou, B. Zhu, S. Zhu, J. Zhu, Graphene oxide-based efficient and scalable solar desalination under one sun with a confined 2D water path, Proc Natl Acad Sci U S A. 113 (2016) 13953–13958. https://doi.org/10.1073/pnas.1613031113.

[313] P.F. Liu, L. Miao, Z. Deng, J. Zhou, Y. Gu, S. Chen, H. Cai, L. Sun, S. Tanemura, Flame-treated and fast-assembled foam system for direct solar steam generation and non-plugging high salinity desalination with self-cleaning effect, Appl Energy. 241 (2019) 652–659. https://doi.org/10.1016/j.apenergy.2019.02.030.

[314] S. Liu, C. Huang, Q. Huang, F. Wang, C. Guo, A new carbon-black/cellulose-sponge system with water supplied by injection for enhancing solar vapor generation, J Mater Chem A Mater. 7 (2019) 17954–17965. https://doi.org/10.1039/c9ta02913c.

[315] H. Liang, Q. Liao, N. Chen, Y. Liang, G. Lv, P. Zhang, B. Lu, L. Qu, Thermal Efficiency of Solar Steam Generation Approaching 100 % through Capillary Water Transport, Angewandte Chemie - International Edition. 58 (2019) 19041–19046. https://doi.org/10.1002/anie.201911457.

[316] T. Li, H. Liu, X. Zhao, G. Chen, J. Dai, G. Pastel, C. Jia, C. Chen, E. Hitz, D. Siddhartha, R. Yang, L. Hu, Scalable and Highly Efficient Mesoporous Wood-Based Solar Steam Generation Device: Localized Heat, Rapid Water Transport, Adv Funct Mater. 28 (2018). https://doi.org/10.1002/adfm.201707134.

[317] H. Li, Y. He, Y. Hu, X. Wang, Commercially Available Activated Carbon Fiber Felt Enables Efficient Solar Steam Generation, ACS Appl Mater Interfaces. 10 (2018) 9362–9368. https://doi.org/10.1021/acsami.7b18071.

[318] W. Huang, G. Hu, C. Tian, X. Wang, J. Tu, Y. Cao, K. Zhang, Nature-inspired salt resistant polypyrrole-wood for highly efficient solar steam generation, Sustain Energy Fuels. 3 (2019) 3000–3008. https://doi.org/10.1039/c9se00163h.

[319] M. Hu, D. Yu, J. Wei, Thermal conductivity determination of small polymer samples by differential scanning calorimetry, Polym Test. 26 (2007) 333–337. https://doi.org/https://doi.org/10.1016/j.polymertesting.2006.11.003.

[320] K. Xu, C. Wang, Z. Li, S. Wu, J. Wang, Salt mitigation strategies of solar-driven interfacial desalination, Adv Funct Mater. 31 (2021) 2007855. https://doi.org/10.1002/adfm.202007855.

[321] M. Sheng, Y. Yang, X. Bin, S. Zhao, C. Pan, F. Nawaz, W. Que, Recent advanced self-propelling salt-blocking technologies for passive solar-driven interfacial evaporation desalination systems, Nano Energy. 89 (2021) 106468. https://doi.org/10.1016/j.nanoen.2021.106468.

[322] Y. Bian, Q. Du, K. Tang, Y. Shen, L. Hao, D. Zhou, X. Wang, Z. Xu, H. Zhang, L. Zhao, S. Zhu, J. Ye, H. Lu, Y. Yang, R. Zhang, Y. Zheng, S. Gu, Carbonized Bamboos as Excellent 3D Solar Vapor-Generation Devices, Adv Mater Technol. 4 (2019) 1800593. https://doi.org/https://doi.org/10.1002/admt.201800593.

[323] R. Zhang, Y. Zhou, B. Xiang, X. Zeng, Y. Luo, X. Meng, S. Tang, Scalable Carbon Black Enhanced Nanofiber Network Films for High-Efficiency Solar Steam Generation, Adv Mater Interfaces. 8 (2021) 1–9. https://doi.org/10.1002/admi.202101160.

[324] A.J. McElrone, W.T. Pockman, J. Martínez-Vilalta, R.B. Jackson, Variation in xylem structure and function in stems and roots of trees to 20 m depth, New Phytologist. 163 (2004) 507–517. https://doi.org/10.1111/j.1469-8137.2004.01127.x.

[325] A. Ebrahimi, E.K. Goharshadi, M. Mohammadi, Reduced graphene oxide/silver/wood as a salt-resistant photoabsorber in solar steam generation and a strong antibacterial agent, Mater Chem Phys. 275 (2022) 125258. https://doi.org/10.1016/j.matchemphys.2021.125258.

[326] Q. Zhang, G. Yi, Z. Fu, H. Yu, S. Chen, X. Quan, Vertically Aligned Janus MXene-Based Aerogels for Solar Desalination with High Efficiency and Salt Resistance, ACS Nano. 13 (2019) 13196–13207. https://doi.org/10.1021/acsnano.9b06180.

[327] B. Lv, C. Gao, Y. Xu, X. Fan, J. Xiao, Y. Liu, C. Song, A self-floating, salt-resistant 3D Janus radish-based evaporator for highly efficient solar desalination, Desalination. 510 (2021) 115093. https://doi.org/10.1016/j.desal.2021.115093.

[328] Q. Wang, L. Wang, S. Song, Y. Li, F. Jia, T. Feng, N. Hu, Flexible 2D@3D Janus evaporators for high-performance and continuous solar desalination, Desalination. 525 (2022) 115483. https://doi.org/10.1016/j.desal.2021.115483.

[329] R. Gu, Z. Yu, Y. Sun, P. Xie, Y. Li, S. Cheng, Enhancing stability of interfacial solar evaporator in high-salinity solutions by managing salt precipitation with Janus-based directional salt transfer structure, Desalination. 524 (2022) 115470. https://doi.org/10.1016/j.desal.2021.115470.

[330] K.-Y. Law, Definitions for Hydrophilicity, Hydrophobicity, and Superhydrophobicity: Getting the Basics Right, J Phys Chem Lett. 5 (2014) 686–688. https://doi.org/10.1021/jz402762h.

[331] J. Chen, J.L. Yin, B. Li, Z. Ye, D. Liu, D. Ding, F. Qian, N.V. Myung, Q. Zhang, Y. Yin, Janus Evaporators with Self-Recovering Hydrophobicity for Salt-Rejecting Interfacial Solar Desalination, ACS Nano. 14 (2020) 17419–17427. https://doi.org/10.1021/acsnano.0c07677.

[332] C. Shi, Z. Wu, Y. Li, X. Zhang, Y. Xu, A. Chen, C. Yan, Y. Shi, T. Wang, B. Su, Superhydrophobic/Superhydrophilic Janus Evaporator for Extreme High Salt-Resistance Solar Desalination by an Integrated 3D Printing Method, ACS Appl Mater Interfaces. 15 (2023) 23971–23979. https://doi.org/10.1021/acsami.3c03320.

[333] Y. Xia, Q. Hou, H. Jubaer, Y. Li, Y. Kang, S. Yuan, H. Liu, M.W. Woo, L. Zhang, L. Gao, H. Wang, X. Zhang, Spatially isolating salt crystallisation from water evaporation for continuous solar steam generation and salt harvesting, Energy Environ Sci. 12 (2019) 1840–1847. https://doi.org/10.1039/c9ee00692c.

[334] Y. Shao, J. Tang, N. Li, T. Sun, L. Yang, D. Chen, H. Zhi, D. Wang, H. Liu, G. Xue, Designing a bioinspired synthetic tree by unidirectional freezing for simultaneous solar steam generation and salt collection, EcoMat. 2 (2020) 1–8. https://doi.org/10.1002/eom2.12018.

[335] Y. Shi, C. Zhang, R. Li, S. Zhuo, Y. Jin, L. Shi, S. Hong, J. Chang, C. Ong, P. Wang, Solar Evaporator with Controlled Salt Precipitation for Zero Liquid Discharge Desalination, Environ Sci Technol. 52 (2018) 11822–11830. https://doi.org/10.1021/acs.est.8b03300.

[336] J. Xiao, Y. Guo, W. Luo, D. Wang, S. Zhong, Y. Yue, C. Han, R. Lv, J. Feng, J. Wang, W. Huang, X. Tian, W. Xiao, Y. Shen, A scalable, cost-effective and salt-rejecting MoS2/SA@melamine foam for continuous solar steam generation, Nano Energy. 87 (2021) 106213. https://doi.org/10.1016/j.nanoen.2021.106213.

[337] M. Zou, Y. Zhang, Z. Cai, C. Li, Z. Sun, C. Yu, Z. Dong, L. Wu, Y. Song, 3D Printing a Biomimetic Bridge-Arch Solar Evaporator for Eliminating Salt Accumulation with Desalination and Agricultural Applications, Advanced Materials. 33 (2021) 2102443. https://doi.org/10.1002/adma.202102443.

[338] L. Wu, Z. Dong, Z. Cai, T. Ganapathy, N.X. Fang, C. Li, C. Yu, Y. Zhang, Y. Song, Highly efficient three-dimensional solar evaporator for high salinity desalination by

localized crystallization, Nat Commun. 11 (2020) 1–12. https://doi.org/10.1038/s41467-020-14366-1.

[339] Y. Shao, A. Shen, N. Li, L. Yang, J. Tang, H. Zhi, D. Wang, G. Xue, Marangoni Effect Drives Salt Crystallization Away from the Distillation Zone for Large-Scale Continuous Solar Passive Desalination, ACS Appl Mater Interfaces. 14 (2022) 30324–30331. https://doi.org/10.1021/acsami.2c04572.

[340] M. Morciano, M. Fasano, S. V. Boriskina, E. Chiavazzo, P. Asinari, Solar passive distiller with high productivity and Marangoni effect-driven salt rejection, Energy Environ Sci. 13 (2020) 3646–3655. https://doi.org/10.1039/d0ee01440k.

[341] Y. Chen, J. Yang, L. Zhu, S. Wang, X. Jia, Y. Li, D. Shao, L. Feng, H. Song, Marangoni-driven biomimetic salt secretion evaporator, Desalination. 548 (2023) 116287. https://doi.org/10.1016/j.desal.2022.116287.

[342] Y. Xia, Y. Li, S. Yuan, Y. Kang, M. Jian, Q. Hou, L. Gao, H. Wang, X. Zhang, A self-rotating solar evaporator for continuous and efficient desalination of hypersaline brine, J Mater Chem A Mater. 8 (2020) 16212–16217. https://doi.org/10.1039/d0ta04677a.

[343] S. Luo, Z. Li, X. Cui, Y. Ge, An anti-salt accumulation 2.5D arch solar-driven evaporator based on Marangoni effect for seawater desalination, Chemical Engineering Journal. 454 (2023) 140286. https://doi.org/10.1016/j.cej.2022.140286.

[344] Y. Dong, Y. Lin, C. Du, C. Zhou, S. Yang, Manipulating hydropathicity/hydrophobicity properties to achieve anti-corrosion copper-based membrane toward high-efficient solar water purification, Colloids Surf A Physicochem Eng Asp. 643 (2022) 128755. https://doi.org/10.1016/j.colsurfa.2022.128755.

[345] Q. Li, S. Zhang, N. Wei, R. Xu, X. Li, L. Gong, H. Cui, Porous Ni/CNTs composite membrane as solar absorber for highly efficient solar steam generation, Solar Energy Materials and Solar Cells. 243 (2022). https://doi.org/10.1016/j.solmat.2022.111815.

[346] K. Sun, H. Cui, R. Xu, L. Wang, M. Li, Z. Yang, M. Zhao, N. Wei, Constructing of 3D porous composite materials of NiAl/CNTs for highly efficient solar steam generation, Solar Energy Materials and Solar Cells. 240 (2022) 111722. https://doi.org/10.1016/j.solmat.2022.111722.

[347] J. Fu, Z. Li, X. Li, F. Sun, L. Li, H. Li, J. Zhao, J. Ma, Hierarchical porous metallic glass with strong broadband absorption and photothermal conversion performance for solar steam generation, Nano Energy. 106 (2023) 108019. https://doi.org/10.1016/j.nanoen.2022.108019.

[348] W. Li, K. Han, Y. Zhang, Y. Li, J. Hu, L. Ma, M. Yue, Preparation of graphitized carbon-coated glass fiber cloth materials with high mechanical strength, corrosion resistance, and solar-driven water evaporation performance, Solar Energy Materials and Solar Cells. 248 (2022) 112015.

[349] L. Zhang, A. Yasin, M. Li, B. Hao, P.-C. Ma, Silicate based solar evaporator with self-cleaning and corrosion resistant properties for durable seawater desalination, Sustainable Materials and Technologies. 30 (2021) e00362. https://doi.org/https://doi.org/10.1016/j.susmat.2021.e00362.

[350] J. Xu, Y. Chen, M. Cao, C. Wang, P. Guo, Highly efficient solar steam generation of polyamide 6 membrane modified with graphene oxide and Au nanoparticles, J Mater Res. 37 (2022) 1475–1485. https://doi.org/10.1557/s43578-022-00552-y.

[351] F. He, M. Han, J. Zhang, Z. Wang, X. Wu, Y. Zhou, L. Jiang, S. Peng, Y. Li, A simple, mild and versatile method for preparation of photothermal woods toward highly efficient solar steam generation, Nano Energy. 71 (2020) 104650. https://doi.org/10.1016/j.nanoen.2020.104650.

[352] J. Yan, W. Xiao, L. Chen, Z. Wu, J. Gao, H. Xue, Superhydrophilic carbon nanofiber membrane with a hierarchically macro/meso porous structure for high performance solar steam generators, Desalination. 516 (2021) 115224. https://doi.org/10.1016/j.desal.2021.115224.

[353] B. Peng, Q. Lyu, Y. Gao, M. Li, G. Xie, Z. Xie, H. Zhang, J. Ren, J. Zhu, L. Zhang, P. Wang, Composite Polyelectrolyte Photothermal Hydrogel with Anti-biofouling and Antibacterial Properties for the Real-World Application of Solar Steam Generation, ACS Appl Mater Interfaces. 14 (2022) 16546–16557. https://doi.org/10.1021/acsami.2c02464.

[354] H. Li, J. Wu, X. Gao, T. Li, M. Zhang, X. Niu, D. Zhang, Y. Wang, H. Fan, K. Wang, Preparation and Performance Study of Antibacterial Materials Based on GO−TiO2, ChemistrySelect. 6 (2021) 7880–7886. https://doi.org/10.1002/slct.202101404.

[355] R. Mehrkhah, M. Mohammadi, A. Zenhari, M. Baghayeri, M.R. Roknabadi, Antibacterial Evaporator Based on Wood-Reduced Graphene Oxide/Titanium Oxide Nanocomposite for Long-Term and Highly Efficient Solar-Driven Wastewater Treatment, Ind Eng Chem Res. (2022). https://doi.org/10.1021/acs.iecr.2c02528.

[356] X.Y. Wang, J. Xue, C. Ma, T. He, H. Qian, B. Wang, J. Liu, Y. Lu, Anti-biofouling double-layered unidirectional scaffold for long-term solar-driven water evaporation, J Mater Chem A Mater. 7 (2019) 16696–16703. https://doi.org/10.1039/c9ta02210d.

[357] V. Lakshmi Prasanna, R. Vijayaraghavan, Insight into the Mechanism of Antibacterial Activity of ZnO: Surface Defects Mediated Reactive Oxygen Species even in the Dark, Langmuir. 31 (2015) 9155–9162. https://doi.org/10.1021/acs.langmuir.5b02266.

[358] H. Li, W. Zhu, M. Li, Y. Li, R.T.K. Kwok, J.W.Y. Lam, L. Wang, D. Wang, B.Z. Tang, Side Area-Assisted 3D Evaporator with Antibiofouling Function for Ultra-Efficient Solar Steam Generation, 2102258 (2021) 1–8. https://doi.org/10.1002/adma.202102258.

[359] M.J. Hajipour, K.M. Fromm, A.A. Ashkarran, D.J. De Aberasturi, I.R. De Larramendi, T. Rojo, Antibacterial properties of nanoparticles, Trends Biotechnol. 30 (2012) 499–511. https://doi.org/10.1016/j.tibtech.2012.06.004.

[360] Y. Xu, J. Ma, Y. Han, J. Zhang, F. Cui, Y. Zhao, X. Li, W. Wang, Multifunctional CuO Nanowire Mesh for Highly Efficient Solar Evaporation and Water Purification, ACS Sustain Chem Eng. 7 (2019) 5476–5485. https://doi.org/10.1021/acssuschemeng.8b06679.

[361] Y. Li, T. Wu, H. Shen, S. Yang, Y. Qin, Z. Zhu, L. Zheng, X. Wen, M. Xia, X. Yin, Flexible MXene-based Janus porous fibrous membranes for sustainable solar-driven desalination and emulsions separation, J Clean Prod. 347 (2022) 131324. https://doi.org/10.1016/j.jclepro.2022.131324.

[362] Y. Xu, J. Ma, Y. Han, H. Xu, Y. Wang, D. Qi, W. Wang, A simple and universal strategy to deposit Ag/polypyrrole on various substrates for enhanced interfacial solar evaporation and antibacterial activity, Chemical Engineering Journal. 384 (2020) 123379. https://doi.org/10.1016/j.cej.2019.123379.

[363] X. Fan, H. Mu, Y. Xu, C. Song, Y. Liu, Silver nanoparticles-polydopamine-wax gourd: An antimicrobial solar evaporator with enhanced steam generation, Int J Energy Res. 46 (2022) 8949–8961. https://doi.org/10.1002/er.7773.

[364] J. Yang, Y. Chen, X. Jia, Y. Li, S. Wang, H. Song, Wood-Based Solar Interface Evaporation Device with Self-Desalting and High Antibacterial Activity for Efficient Solar Steam Generation, ACS Appl Mater Interfaces. 12 (2020) 47029–47037. https://doi.org/10.1021/acsami.0c14068.

[365] L. Hao, N. Liu, H. Bai, P. He, R. Niu, J. Gong, High-performance solar-driven interfacial evaporation through molecular design of antibacterial, biomass-derived hydrogels, J Colloid Interface Sci. 608 (2022) 840–852. https://doi.org/10.1016/j.jcis.2021.10.035.

[366] C. Wen, H. Guo, J. Yang, Q. Li, X. Zhang, X. Sui, M. Cao, L. Zhang, Zwitterionic hydrogel coated superhydrophilic hierarchical antifouling floater enables unimpeded interfacial steam generation and multi-contamination resistance in complex conditions, Chemical Engineering Journal. 421 (2021) 130344. https://doi.org/10.1016/j.cej.2021.130344.

[367] M. Xia, S. Zhao, Q.-M. Hasi, Y. Zhang, L. Li, L. Chen, Superhydrophilic and oil-repellent porous material based on halloysite nanotubes and wood fibers for efficient solar steam generation, Mater Today Energy. 21 (2021) 100726. https://doi.org/https://doi.org/10.1016/j.mtener.2021.100726.

[368] J. Earwood, G. Xu, Y. Xing, B. Deng, Surface modified basalt membrane as a photothermal material for improved oily wastewater solar evaporation, Sep Sci Technol. 58 (2023) 1121–1132. https://doi.org/10.1080/01496395.2022.2119149.

[369] L. Chen, M. Xia, J. Du, X. Luo, L. Zhang, A. Li, Superhydrophilic and Oleophobic Porous Architectures Based on Basalt Fibers as Oil-Repellent Photothermal Materials for Solar Steam Generation, ChemSusChem. 13 (2020) 493–500. https://doi.org/https://doi.org/10.1002/cssc.201902775.

[370] S. Yang, Z. Xu, T. Zhao, T. Zhang, Y. Zhao, Emulsion-templated, hydrophilic and underwater oleophobic PVA aerogels with enhanced mechanical property, Colloids Surf A Physicochem Eng Asp. 653 (2022) 129979. https://doi.org/https://doi.org/10.1016/j.colsurfa.2022.129979.

[371] S.-L. Wu, L.-N. Quan, Y.-T. Huang, Y.-T. Li, H.-C. Yang, S.B. Darling, Suspended Membrane Evaporators Integrating Environmental and Solar Evaporation for Oily Wastewater Purification, ACS Appl Mater Interfaces. 13 (2021) 39513–39522. https://doi.org/10.1021/acsami.1c12120.

[372] T. Ding, Y. Zhou, W.L. Ong, G.W. Ho, Hybrid solar-driven interfacial evaporation systems: Beyond water production towards high solar energy utilization, Materials Today. 42 (2021) 178–191. https://doi.org/10.1016/j.mattod.2020.10.022.

[373] H. Wang, W. Xie, B. Yu, B. Qi, R. Liu, X. Zhuang, S. Liu, P. Liu, J. Duan, J. Zhou, Simultaneous Solar Steam and Electricity Generation from Synergistic Salinity-Temperature Gradient, Adv Energy Mater. 11 (2021). https://doi.org/10.1002/aenm.202100481.

[374] J. Ren, Y. Ding, J. Gong, J. Qu, R. Niu, Simultaneous Solar-driven Steam and Electricity Generation by Cost-effective, Easy Scale-up MnO2-based Flexible Membranes, Energy and Environmental Materials. 6 (2023). https://doi.org/10.1002/eem2.12376.

[375] L. Zhu, T. Ding, M. Gao, C.K.N. Peh, G.W. Ho, Shape Conformal and Thermal Insulative Organic Solar Absorber Sponge for Photothermal Water Evaporation and Thermoelectric Power Generation, Adv Energy Mater. 9 (2019). https://doi.org/10.1002/aenm.201900250.

[376] F.J. Millero, R. Feistel, D.G. Wright, T.J. McDougall, The composition of Standard Seawater and the definition of the Reference-Composition Salinity Scale, Deep Sea Research Part I: Oceanographic Research Papers. 55 (2008) 50–72. https://doi.org/https://doi.org/10.1016/j.dsr.2007.10.001.

[377] B. Gong, H. Yang, S. Wu, Y. Tian, X. Guo, C. Xu, W. Kuang, J. Yan, K. Cen, Z. Bo, K. (Ken) Ostrikov, Multifunctional solar bamboo straw: Multiscale 3D membrane for self-sustained solar-thermal water desalination and purification and thermoelectric waste heat recovery and storage, Carbon N Y. 171 (2021) 359–367. https://doi.org/https://doi.org/10.1016/j.carbon.2020.09.033.

[378] S. Han, J. Yang, X. Li, W. Li, X. Zhang, N. Koratkar, Z.Z. Yu, Flame Synthesis of Superhydrophilic Carbon Nanotubes/Ni Foam Decorated with Fe2O3 Nanoparticles for Water Purification via Solar Steam Generation, ACS Appl Mater Interfaces. 12 (2020) 13229–13238. https://doi.org/10.1021/acsami.0c00606.

[379] M. Shafaee, E.K. Goharshadi, M.M. Ghafurian, M. Mohammadi, H. Behnejad, A highly efficient and sustainable photoabsorber in solar-driven seawater desalination and wastewater purification, RSC Adv. 13 (2023) 17935–17946. https://doi.org/10.1039/d3ra01938a.

[380] R. Mehrkhah, K. Goharshadi, E.K. Goharshadi, H.-S. Sajjadizadeh, Multifunctional Photoabsorber for Highly Efficient Interfacial Solar Steam Generation and Wastewater Treatment, ChemistrySelect. 8 (2023) e202204386. https://doi.org/https://doi.org/10.1002/slct.202204386.

[381] W.H. Organization, Safe drinking-water from desalination, World Health Organization, 2011.

[382] L. Zhao, B. Bhatia, L. Zhang, E. Strobach, A. Leroy, M.K. Yadav, S. Yang, T.A. Cooper, L.A. Weinstein, A. Modi, S.B. Kedare, G. Chen, E.N. Wang, A Passive High-Temperature High-Pressure Solar Steam Generator for Medical Sterilization, Joule. 4 (2020) 2733–2745. https://doi.org/10.1016/j.joule.2020.10.007.

[383] C. Chang, P. Tao, J. Xu, B. Fu, C. Song, J. Wu, W. Shang, T. Deng, High-Efficiency Superheated Steam Generation for Portable Sterilization under Ambient Pressure and Low Solar Flux, ACS Appl Mater Interfaces. 11 (2019) 18466–18474. https://doi.org/10.1021/acsami.9b04535.

[384] A.M. Saleque, S. Ahmed, M.N.A.S. Ivan, M.I. Hossain, W. Qarony, P.K. Cheng, J. Qiao, Z.L. Guo, L. Zeng, Y.H. Tsang, High-temperature solar steam generation by MWCNT-HfTe2 van der Waals heterostructure for low-cost sterilization, Nano Energy. 94 (2022) 106916. https://doi.org/10.1016/j.nanoen.2022.106916.

[385] Y. Zhang, D. Zhao, F. Yu, C. Yang, J. Lou, Y. Liu, Y. Chen, Z. Wang, P. Tao, W. Shang, J. Wu, C. Song, T. Deng, Floating rGO-based black membranes for solar driven sterilization, Nanoscale. 9 (2017) 19384–19389. https://doi.org/10.1039/C7NR06861A.

[386] M. He, H. Dai, H. Liu, Q. Cai, Y. Liu, L. Wang, X. Qin, J. Yu, High-Performance Solar Steam Generator Based on Polypyrrole-Coated Fabric via 3D Macro- and

Microstructure Design, ACS Appl Mater Interfaces. 13 (2021) 40664–40672. https://doi.org/10.1021/acsami.1c11802.

[387] J. Li, M. Du, G. Lv, L. Zhou, X. Li, L. Bertoluzzi, C. Liu, S. Zhu, J. Zhu, Interfacial Solar Steam Generation Enables Fast-Responsive, Energy-Efficient, and Low-Cost Off-Grid Sterilization, Advanced Materials. 30 (2018) 1–7. https://doi.org/10.1002/adma.201805159.

**Table of Content (TOC) image**

**Authors' Biography:**

**Dr. Md. Nahian Al Subri Ivan** is a Research Associate in the Applied Physics Department at The Hong Kong Polytechnic University. He obtained his Ph.D. degree from the same University in 2023. He has completed his M.Sc. in Electrical Power Engineering from RWTH Aachen University, Germany, and B.Sc. in Electrical and Electronic Engineering (EEE) from American International University – Bangladesh (AIUB). He has worked as an Assistant Professor in the Dept. of EEE, AIUB. His main research focuses are Solar Steam Generation, Energy Storage Devices, 2D materials, Waste Materials, Renewable Energy Technologies, Reliability Analysis and Electric Vehicles.

**Mr. Shuvra Saha** is pursuing his PhD in the department of Applied Physics at The Hong Kong Polytechnic University. He has completed Bachelor of Engineering in Electronics and Telecommunications from University of Pune, India, and Master of Engineering in Telecommunication from American International University-Bangladesh (AIUB). He has worked as an Assistant Professor in the department of Electrical and Electronic Engineering, (AIUB). His research focuses are 2D materials, solar steam generation, desalination, and $NH_3$-$H_2$ driven power systems and electric vehicles.

**Dr. Ahmed Mortuza Saleque** is currently working as a Postdoctoral Scholar at the UC Davis, and Marvell Nanofabrication Laboratory, UC Berkeley. He completed his Ph.D. in Applied Physics at The Hong Kong Polytechnic University in 2022. Prior to this, he attained a joint Master's degree in Sustainable Transportation and Electrical Power Systems from the University of Nottingham, University of Oviedo, and University of Rome. He has an extensive academic background, having served as a Lecturer and later as an Assistant Professor at American International University-Bangladesh. Dr. Saleque's research spans nano-micro fabrication, photothermal energy conversion, 2D materials, optics, and photonics.

**Dr. Safayet Ahmed** is a Postdoctoral Fellow in the Applied Physics Department at The Hong Kong Polytechnic University. He received his PhD from the same university in 2022. Before starting his Ph.D., he completed his B.Sc. and M.Sc. degrees in Electrical and Electronics Engineering from AIUB, in 2015 and 2017, respectively. He worked as a Lecturer in the same department at AIUB from 2016 to 2018 and was later promoted to Senior Lecturer in 2019. Dr. Ahmed has published 24 SCI journal articles and attended 14 conference proceedings. His research interest lies in ultrafast photonics, nonlinear optics, 2D-Materials, and twistoptics.

**Dr. Amrit Kumar Thakur** obtained his Ph.D. in Solar-Thermal Technology, Mechanical Engineering from Anna University, Chennai, India in 2022. Presently, he is a Post Doctoral researcher in the Mechanical Engineering Department at the University of California, Merced, USA. He has been working in the fields of Desalination, Water and interface, Heat Transfer, Thermal Energy Storage, Battery management and Material science. He was awarded JSPS fellowship in 2023 and presently serving as editor and guest editor for several journals. He has about 10 years of research and teaching experience. He has published more than 30 papers in high-impact journals.

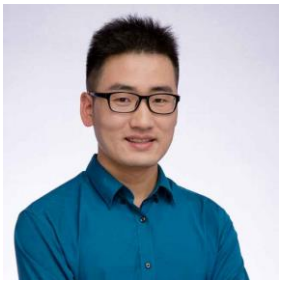

**Gongxun Bai** obtained his bachelor's degree from Huazhong University of Science and Technology, master's degree from Shanghai Institute of Optics and Fine Mechanics, Chinese Academy of Sciences, and PhD degree from the Hong Kong Polytechnic University. Now he is a professor at the Institute of Optoelectronic Materials and Devices, China Jiliang University. His research focuses on rare earth luminescent materials, mechanoluminescent materials, optoelectronic sensing materials, and devices.

**Dr. ZHANG Miao** obtained her Ph.D. degree from Beijing Jiaotong University in China. Subsequently, she was selected as a postdoctoral fellow at the Hong Kong Polytechnic University through the Hong Kong Scholars Program (2019). Currently, she holds the position of Research Assistant Professor in the Department of Applied Biology and Chemical Technology at PolyU. Her research interests focus on the development of novel organic/organometallic materials for photovoltaic and photothermal applications. To date, she has achieved more than 55 publications in SCI journals, and these works garnered more than 3800 citations.

**Prof. Saidur Rahman** is currently working as a Distinguished Research Professor and Head of the Research Centre for Nano-Materials and Energy Technology at the Sunway University. He is also working with the Lancaster University as a Full Professor and published almost 600 journal papers. He is working in the area of emerging nanomaterials (MXenes) and their applications in energy storage, heat transfer, solar energy harvesting, and environmental remediation.

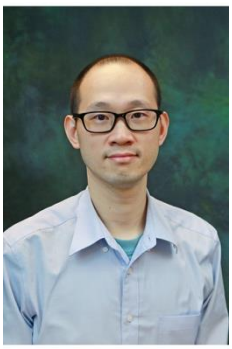

**Dr. Yuen Hong TSANG** received his B.Sc. and Ph.D. degrees in Physics from the University of Manchester, UK, in 2000 and 2004, respectively. He is currently working as a Professor in the Department of Applied Physics at The Hong Kong Polytechnic University. Dr. Tsang's academic research interests cover topics including novel 2D materials and nanostructure used for optics and photonic devices, laser materials, high power lasers, and novel materials for energy applications. He has published around 170 SCI journal articles and gathered over 8800 citations.